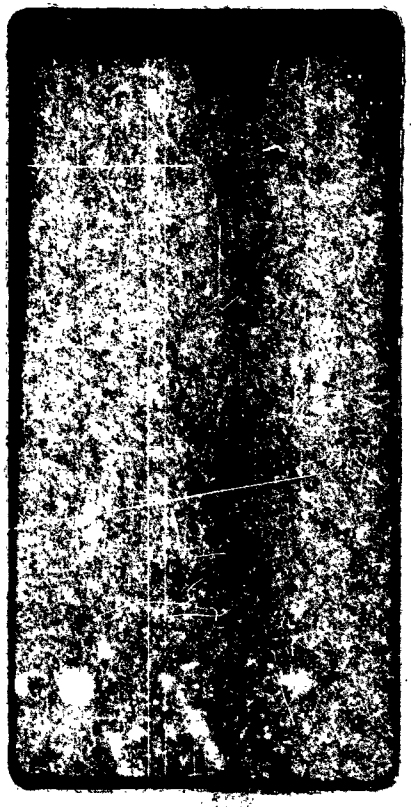

Abstract

The work presented here concerns microwave interaction with plasmas in gas discharges and semiconductors. The main aim of the investigations has been to get a basic understanding of some central problems in this field that have applications to plasma amplifiers.

The different sub-reports can be summarized as follows.

I. The excitation of waves in a waveguide partially filled with a cool isotropic plasma is studied. Special attention is paid to cases where backward waves exist and the influence of a drift motion of the plasma is considered.

II. A circular waveguide is filled with two concentric dielectrics and with an infinitely thin metal tube between the dielectrics from $z = 0$ to $z = +\infty$. The effect of the discontinuity at $z = 0$ on a dominant circularly symmetric TM-mode incident from $z = -\infty$ is investigated. The results have applications to plasma waveguides.

III. Wave propagation in plasma waveguides is studied theoretically and experimentally. Dispersion curves showing the existence of backward-waves are given for the surface-wave dipole modes. The quasi-static solutions have been compared to the exact ones. Experiments have been performed and show good agreement with the theory.

IV. Electron plasma resonance absorption is observed in an n-type crystal of Ge at 35,000 Mc/sec and liquid hydrogen temperature. The crystal, in the form of a rod, is placed across a rectangular waveguide parallel to the broad walls. No static magnetic field is applied. Microwave power absorption of a magnitude and temperature dependence closely agreeing with that predicted by an approximate theory developed by the author is measured using a suitably doped Ge specimen. Observation of plasma resonance absorption gives a direct method to determine the charge carrier density in semiconductors.

V. It is shown that the ordinary theory, which describes a magnetized plasma as an anisotropic dielectric, can be used to describe the magneto-plasma resonances observed in semiconductors and metals.

VI. The variation of plasma density and electron-temperature along the positive column of a low-pressure Hg-discharge is studied by means of a microwave cavity and Langmuir probes.

VII. The noise-radiation from a low-pressure Hg-discharge inside a waveguide has been measured. The scattering and absorption of a coherent signal has also been measured and compared with the noise-spectra.

VIII. Using Kirchhoff's law and a simple hydrodynamic model it is shown that thermally excited longitudinal waves give rise to noise emission in the microwave region from cylindrical gaseous discharges. The emitted radiation has a characteristic spectrum with several sharp peaks at the resonance frequencies of the longitudinal standing waves. The predicted spectrum seems to agree well with experiments.

Table of Contents

I. EXCITATION OF BACKWARD WAVE MODES IN PLASMA WAVEGUIDES

Introduction

It is known that in waveguides partially filled with a homogeneous medium that may either be isotropic or anisotropic there exist modes with negative dispersion (backward waves). This medium can be an ordinary dielectric (CLARRICOATS 1960), a plasma (TRIVELPIECE 1959), (OLINER 1962), or a ferrite (TRIVELPIECE 1961). In order to get more insight into the nature of these modes we will study the excitation of a circularly cylindrical waveguide containing a homogeneous, cool, isotropic plasma column (Fig. 1). The frequency of the exciting signal will be assumed to be so high that the motion of the ions can be neglected.

We will first consider under what conditions negative dispersion may exist in the system shown in Fig. 1 and discuss the general behaviour of the modes in this waveguide. The modes that exist in this system are in general hybrid modes with both E_z- and B_z-components. Only modes with no azimuthal field variations are pure TE- or TM-modes.

The power flow, P, in the z-direction through a cross-section of this waveguide can for one mode be written in the following form:

$$P = \frac{1}{\mu_o}\iint \mathrm{Re}(\bar{E}\times\bar{B}^*)_z\,dS = \iint \frac{\beta\beta_o}{Z_o(\varepsilon\beta_o^2-\beta^2)^2}\Big[c^2\Big\{\Big(\frac{\partial B_z}{\partial r}\Big)^2+\Big(\frac{n}{r}\Big)^2 B_z^2\Big\}+$$

$$+\varepsilon\Big\{\Big(\frac{\partial E_z}{\partial r}\Big)^2+\Big(\frac{n}{r}\Big)^2 E_z^2\Big\}-c\,\frac{\varepsilon\beta_o^2+\beta^2}{\beta_o^2}\,\frac{n}{r}\,\frac{\partial}{\partial r}\,(B_z E_z)\Big]\,dS \qquad (1)$$

where $E_z e^{j(\omega t-\beta z)}e^{jn\varphi}$ is the electric field component in the z-direction (the same relation holds for B_z and the magnetic field).

$$\beta_o = \frac{\omega}{c} \qquad\qquad Z_o = \sqrt{\frac{\mu_o}{\varepsilon_o}}$$

$$\varepsilon = 1 - \frac{\omega_p^2}{\omega^2}\,,\ \omega_p \text{ is the plasma frequency.}$$

For a lossless, passive, uniform waveguide one can deduce the following relation between the power flow, the group velocity $(\frac{\partial\omega}{\partial\beta})$, and the stored energy per unit length (W),

$$P = \frac{\partial\omega}{\partial\beta}\cdot W \qquad (2)$$

provided β is real (CHORNEY 1962). Backward waves occur when the phase velocity and the group velocity are opposite ($\beta \frac{\partial \omega}{\partial \beta} < 0$).

Equation (1) together with Eq. (2) shows that backward waves cannot exist for TE-modes. Nor can they exist for TM-modes if $\varepsilon > 0$. By performing the integration in Eq. (1) it can be shown that backward waves cannot exist for TM-modes even if $\varepsilon < 0$. Thus, it is only for hybrid modes that backward waves may occur in the system shown in Fig. 1.

The case where the fields vay as $e^{j\varphi}$ in the φ-direction will now be discussed. The characteristic equation for this case has been studied (ALFREDSSON 1963) and the dispersion curves have the general form shown in Fig. 2.

The dispersion curves I, II, ... correspond to modes which are very similar to those in the empty waveguide. These modes are infinite in number and have a phase velocity larger than the velocity of light. The waves associated with dispersion curve 1-2-3 can propagate with a phase velocity smaller than the velocity of light and are very similar to waves on a free plasma rod. At the points Q_1 and Q_2, where $\partial\omega/\partial\beta = 0$, the dispersion curve 1-2-3 will be connected with the dispersion curves 1', 2', 3' and 1", 2", 3", which are only schematically indicated in fhe figure. These dispersion curves correspond to complex values of the propagation constants and for one pair of branches, e.g. 1', 2', the β-values are complex conjugate for a given value of ω. If losses are introduced, branch 1 will no longer be connected with branches 2 and 2' but only with branch 1'. The situation will be the same for point Q_2. Thus the dispersion curve 1-2-3 breaks up into three different dispersion curves corresponding to three different modes, which for convenience will be called the plasma modes. In case of zero losses, the fields corresponding to the dashed dispersion curves carry no energy (CHORNEY 1962) and decrease exponentially from the source of excitation. The number of plasma modes may be one, two or three (as in the case above). Fig. 3 shows the dispersion curves for the plasma modes for three different values of the plasma frequency at given r_1/r_2. In the following we will primarily be interested in the excitation of the propagating plasma modes.

Excitation by a Gap

We will now determine the fields in the system shown in Fig. 1 when it is excited through the gap and the tangential E-fields at $r = r_2$ for $|z| \leq 1$ are given. In the Appendix it is shown that for $z > 0$ there will only exist waves with $\frac{\partial \omega}{\partial \beta} > 0$ and for $z < 0$ only waves with $\frac{\partial \omega}{\partial \beta} < 0$. Thus, for modes with negative dispersion the phase velocity will be directed towards the excitation gap.

The differential equation for E_z (and B_z) is

$$\frac{\partial^2 E_z}{\partial r^2} + \frac{1}{r}\frac{\partial E_z}{\partial r} + (\varepsilon\beta_o^2 - \frac{1}{r^2})E_z + \frac{\partial^2 E_z}{\partial z^2} = 0 \tag{3}$$

The Fourier transforms $\Psi_z(r,\beta)$ and $\Phi_z(r,\beta)$ are defined as

$$\Psi_z = \frac{1}{\sqrt{2\pi}} \int_{-\infty}^{+\infty} E_z(r,z)e^{-j\beta z}dz$$

$$\Phi_z = \frac{1}{\sqrt{2\pi}} \int_{-\infty}^{+\infty} B_z(r,z)e^{-j\beta z}dz \tag{4}$$

and Ψ_z (and Φ_z) will thus satisfy the equation

$$\frac{d^2\Psi_z}{dr^2} + \frac{1}{r}\frac{d\Psi_z}{dr} + (\varepsilon\beta_o^2 - \beta^2 - \frac{1}{r^2})\Psi_z = 0 \tag{5}$$

The Fourier transforms of the transverse components are given by

$$\bar{\Psi}_T = \frac{-j\omega}{\varepsilon\beta_o^2 - \beta^2}\left\{-\hat{z} \times \bar{\nabla}_T\Phi_z + \frac{\beta}{\beta_o c}\bar{\nabla}_T \Psi_z\right\} \tag{6}$$

$$\bar{\Phi}_T = \frac{-j\beta}{\varepsilon\beta_o^2 - \beta^2}\left\{\bar{\nabla}_T\Phi_z + \frac{\beta_o\varepsilon}{\beta c}\hat{z} \times \bar{\nabla}_T \Psi_z\right\} \tag{7}$$

In the plasma region, $r \leq a$, the solution of (5) is of the form

$$\Psi_z = AI_1(h_1 r)$$

$$\Phi_z = BI_1(h_1 r) \tag{8}$$

In the vacuum region $a \leq r \leq b$

$$\Psi_z = CI_1(h_2 r) + DK_1(h_2 r)$$

$$\Phi_z = EI_1(h_2 r) + FK_1(h_2 r) \tag{9}$$

where $h_1 = (\beta^2 - \varepsilon\beta_o^2)^{\frac{1}{2}}$ and $h_2 = (\beta^2 - \beta_o^2)^{\frac{1}{2}}$

The boundary conditions are

$$\Psi_z,\ \Phi_z,\ \Psi_\varphi,\ \Phi_\varphi \text{ continuous at } r = a \tag{10}$$

$$\Psi_z(\beta) = R(\beta);\quad \Psi_\varphi(\beta) = Q(\beta) \text{ at } r = b \tag{11}$$

where

$$R(\beta) = \frac{1}{\sqrt{2\pi}} \int_{-1}^{+1} E_{z_o}(z) e^{-j\beta z} dz \tag{12}$$

and

$$Q(\beta) = \frac{1}{\sqrt{2\pi}} \int_{-1}^{+1} E_{\varphi_o}(z) e^{-j\beta z} dz \tag{13}$$

Using the boundary conditions together with (8) and (9) we get the following equation for the coefficients A, B....:

$$\begin{vmatrix} -I_{11} & 0 & I_{21} & K_{21} & 0 & 0 \\ 0 & -I_{11} & 0 & 0 & I_{21} & K_{21} \\ -\frac{\beta}{r_1 h_1^2} I_{11} & -\frac{j\omega}{h_1} I'_{11} & \frac{\beta}{r_1 h_2^2} I_{21} & \frac{\beta}{r_1 h_2^2} K_{21} & \frac{j\omega}{h_2} I'_{21} & \frac{j\omega}{h_2} K'_{21} \\ \frac{j\varepsilon\beta_o}{h_1 c} I'_{11} & -\frac{\beta}{r_1 h_1^2} I_{11} & -\frac{j\beta_o}{h_2 c} I'_{21} & -\frac{j\beta_o}{h_2 c} K'_{21} & \frac{\beta}{r_1 h_2^2} I_{21} & \frac{\beta}{r_1 h_2^2} K_{21} \\ 0 & 0 & I_{22} & K_{22} & 0 & 0 \\ 0 & 0 & -\frac{\beta}{r_1 h_2^2} I_{22} & -\frac{\beta}{r_1 h_2^2} K_{22} & -\frac{j\omega}{h_2} I'_{22} & -\frac{j\omega}{h_2} K'_{22} \end{vmatrix} \begin{vmatrix} A \\ B \\ C \\ D \\ E \\ F \end{vmatrix} = \begin{vmatrix} 0 \\ 0 \\ 0 \\ 0 \\ P \\ Q \end{vmatrix} \tag{14}$$

where the following abbreviations have been used

$$I_{11} = I_1(h_1 r_1) \qquad I_{21} = I_1(h_2 r_1) \qquad I_{22} = I_1(h_2 r_2)$$

and similarly for K'_1, I'_1 and K_1.

Solving A in Eq. (14) and using the inverse Fourier transform on Eq. (8) we obtain the following expression for the E_z-field inside the plasma column:

$$E_z(r) = \frac{1}{\sqrt{2\pi}} \int_{-\infty}^{+\infty} \frac{F(\beta)R(\beta) + G(\beta)Q(\beta)}{\Lambda(\beta)} I_1(h_1 r) e^{+j\beta z} d\beta \tag{15}$$

where

$$\Delta(\beta) = h_2 \left\{ \varepsilon \frac{h_2}{h_1} \frac{I'_{11}}{I_{11}} (I_{22}K_{21} - K_{22}I_{21}) - (I_{22}K'_{21} - K_{22}I'_{21}) \right\} \cdot$$

$$\cdot \left\{ \frac{h_2}{h_1} \frac{I'_{11}}{I_{11}} (I'_{22}K_{21} - K'_{22}I_{21}) - (I'_{22}K'_{21} - K'_{22}I'_{21}) \right\} -$$

$$- \beta^2 \left(\frac{1}{h_1^2} - \frac{1}{h_2^2} \right) \frac{h_2^3}{(r_1\beta_o)^2} (I_{22}K_{21} - K_{22}I_{21})(I'_{22}K_{21} - K'_{22}I_{21})$$

$$F(\beta) = \frac{1}{r_1 I_{11}} \left\{ \frac{h_2}{h_1} \frac{I'_{11}}{I_{11}} (I'_{22}K_{21} - K'_{22}I_{21}) - (I'_{22}K'_{21} - K'_{22}I'_{21}) + \right.$$

$$\left. + \frac{\beta^2}{\beta_o^2} \frac{1}{r_1 r_2} \left(\frac{1}{h_1^2} - \frac{1}{h_2^2}\right) (I_{22}K_{21} - K_{22}I_{21}) \right\}$$

$$G(\beta) = \frac{-1}{r_1 I_{11}} \frac{\beta h_2^2}{r_1 \beta_o^2} \left(\frac{1}{h_1^2} - \frac{1}{h_2^2}\right)^2 (K_{21}I_{22} - I_{21}K_{22})$$

$\Delta(\beta) = 0$ is the characteristic equation for the plasma waveguide (AGDUR 1962).

The other field components can be obtained in an analogous way. For $z < 0$ this integral is evaluated by a contour integration along the contour shown in Fig. 4. The integral along the semicircle goes to zero when $R \to \infty$ and the value of the contour integral is equal to the integral (15). The integrand in (15) has no branch points (the branch point singularities from individual terms cancel) but an infinite number of poles which are indicated in Fig. 4. One can distinguish between three different types of poles: 1) poles on the imaginary axis which correspond to pure cut-off modes; 2) poles in the complex plane occurring in complex conjugate pairs which correspond to the dashed curves in Fig. 2 and which in analogy with the cut-off modes do not contribute to the energy flow; 3) poles on the real axis which correspond to propagating modes. If losses are introduced, the poles on the real axis will move either upwards or downwards in the β-plane depending on whether they correspond to waves with $\frac{\partial \omega}{\partial \beta} < 0$ or $\frac{\partial \omega}{\partial \beta} > 0$, as shown in the Appendix.

As an example we study the excitation of the waveguide at a frequency ω_o at which only plasma modes are propagating and have a dispersion characteristic as shown in Fig. 5. From the Appendix and the figure it is seen that

at β_1	$\frac{\partial \omega}{\partial \beta} > 0$	pole in lower halfplane
$-\beta_1$	$\frac{\partial \omega}{\partial \beta} < 0$	" " upper "
β_2	$\frac{\partial \omega}{\partial \beta} < 0$	" " upper "
$-\beta_2$	$\frac{\partial \omega}{\partial \beta} > 0$	" " lower "
β_3	$\frac{\partial \omega}{\partial \beta} > 0$	" " lower "
$-\beta_3$	$\frac{\partial \omega}{\partial \beta} < 0$	" " upper "

In the limiting case of no losses we therefore have to deform the contour as shown in Fig. 6.

The value of the integral in Eq. (15) is then obtained from

$$2\pi j \sum \text{Residues} = \frac{2\pi j}{\sqrt{2\pi}} \sum_{m=1}^{\infty} \frac{F(\beta_m)R(\beta_m) + G(\beta_m)Q(\beta_m)}{\left(\frac{\partial \Delta}{\partial \beta}\right)_{\beta=\beta_m}} I_1(h_{1m}r)e^{j\beta_m z} \quad (16)$$

assuming that all poles are simple. Double poles occur for points on the dispersion curve where

$$\frac{\partial \omega}{\partial \beta} = 0; \quad \left(\frac{\partial \Delta}{\partial \beta} = 0\right).$$

On the basis of the theory developed we will now study the excitation of plasma waves for a plasma waveguide where $\frac{r_2}{r_1} = 5$ and $\omega_p r_2/c = 1.7$. The dispersion curve for this case is given in Fig. 3. As seen from the figure it is possible to excite three different plasma modes in this case. The cut-off frequencies for the waveguide modes are well above the cut-off frequencies for the plasma modes for these parameter values, and for $\omega/\omega_p < \frac{1}{\sqrt{2}}$ the plasma modes will be the only propagating modes excited in the waveguide.

The excitation will be studied when the electric field in the gap is: $E_{z_o} = \delta(z - 0)$; $E_{r_o} = 0$, which corresponds to a unit voltage across an infinitely short gap and gives $R = \frac{1}{\sqrt{2}}$ and $Q = 0$. Far away from the gap the cut-off modes have a negligible amplitude and only the propagating plasma modes will contribute to the fields. Fig. 7 shows the E_z-field at the boundary of the plasma column for the plasma modes excited by the unit gap voltage. The power flow P_1 in a plasma mode when this mode has a given value of the E_z-field at the plasma boundary is shown for the three plasma modes in Fig. 8. The power flow has been computed from Eq. (1) and E_z at the boundary has the value $I_1(h_1 r_1)$. By combining the results shown in Fig. 7 and Fig. 8, Fig. 9 has been obtained which shows the power flow P in the different modes associated by the above excitation.

The asymtotes in these figures correspond to the two points on the dispersion curves that separate the different plasma modes. At these points E_z and $P \to \infty$. $P_1 \to 0$, which follows from Eq. (2) because W is finite while $\frac{\partial \omega}{\partial \beta} \to 0$. As pointed out above the character of the dispersion curve will change drastically around these points when losses are introduced and the same will hold for the curves shown in the last figures. When $\beta \to 0$, $E_z \to 0$ because the plasma mode becomes a pure TE-mode in the limit $\beta = 0$. For the same reason $P_1 \to \infty$ when $\beta \to 0$. $P_1 \to \infty$ when $\beta \to \infty$ simply because the given E_z-field at the plasma boundary approaches infinity.

The main conclusion that can be drawn from the results in Figs. 7 and 9 is that the power and electric field contributions from mode C are in general very small in comparison with the contributions from the two other plasma modes.

Excitation by a Given Transverse Field

For comparison with the results obtained above we will here study the power flow in the plasma modes for the same waveguide as above ($\frac{r_2}{r_1} = 5$; $\frac{\omega_p r_2}{c} = 1.7$) when the transverse field in the plane z = 0 is given by

$$\bar{E}_T^o = \left[\frac{-jr_2}{x'_{11} r} \cdot J_1\left(\frac{x'_{11} r}{r_2}\right) \hat{r} + J'\left(\frac{x'_{11} r}{r_2}\right) \hat{\varphi} \right] e^{j\varphi} \qquad (17)$$

where x'_{11} is the first root of $J'(x) = 0$. This is the same field as the transverse electric field for the TE_{11}-mode in an empty waveguide with radius r_2. Expanding the field in the plasma waveguide for $z = 0$ in the different modes and allowing only modes with $\frac{\partial \omega}{\partial \beta} > 0$ we put

$$\bar{E}_T^o = \sum_{n=1}^{\infty} a_n \bar{E}_{Tn} \qquad (18)$$

where $\bar{E}_{Tn} \cdot e^{j(\omega t - \beta_n z)}$ is the transverse field in the n:th mode. Using the orthogonality relation

$$\iint (\bar{E}_{Tn} \times \bar{H}^*_{Tm})_z dS = 0 \qquad (19)$$

we obtain from Eq.(18):

$$a_n = \frac{\iint (\bar{E}_T^o \times \bar{H}^*_{Tn})_z dS}{\iint (\bar{E}_{Tn} \times \bar{H}^*_{Tn})_z dS} \qquad (20)$$

The power flow in the n:th mode will then be:

$$P_2 = \frac{\{\iint (\bar{E}_T^o \times \bar{H}^*_{Tn})_z dS\}^2}{\iint (\bar{E}_{Tn} \times \bar{H}^*_{Tn})_z dS} \qquad (21)$$

P_2 has been computed for the plasma modes treated on page and the results are given in Fig. 10. Also in this case the power transported in the slowest plasma mode (C) is in general negligible in comparison with that transported in the other two modes.

Influence of a Drift Velocity on Dispersion Curves

If the plasma electrons in the plasma waveguide treated above are assumed to have a drift velocity the dispersion curves for the new system (ω', β') can be obtained by the following transformation of the ω,β-curves given above.

$$\omega' = \frac{1}{\sqrt{1 - (\frac{v_o}{c})^2}} \cdot (\omega + \beta v_o) \tag{22}$$

$$\beta' = \frac{1}{\sqrt{1 - (\frac{v_o}{c})^2}} \cdot \beta + \frac{\omega}{c} \cdot \frac{v_o}{c} \tag{23}$$

v_o is the drift velocity of the plasma electrons in the positive z-direction. The dispersion curves in the ω,β-system are not affected by a motion of the waveguide walls.

Fig. 11 illustrates the influence of a drift velocity of the electrons. The dashed curve corresponds to $v_o = 0$. In the case shown in this figure the group velocity in the ω',β'-system is always positive and we can therefore only excite propagating plasma modes in the positive z-direction. The group velocity for the plasma modes treated above may be very small and even a very small drift velocity may have a large effect on the dispersion characteristic of the system. This is shown by Fig. 12.

APPENDIX

The waveguide described above belongs to a class of waveguides which have a characteristic equation

$$F(\omega, \beta, j\nu) = 0 \tag{24}$$

where F is an even function of β and real for real values of ω, β and $j\nu$. ν is a loss parameter.

If ω_1, β_1 (both real) is a solution to Eq. (24) when $\nu = 0$ we can obtain the following two solutions when small losses are introduced ($\nu = \Delta\nu$)

$$\text{(I)} \quad \omega = \omega_1; \quad \beta = \beta_1 - \frac{(\frac{\partial F}{\partial (j\nu)})_1}{(\frac{\partial F}{\partial \beta})_1} \cdot j\Delta\nu \tag{25}$$

$$\text{(II)} \quad \omega = \omega_1 - \frac{(\frac{\partial F}{\partial (j\nu)})_1}{(\frac{\partial F}{\partial \omega})_1} \cdot j\Delta\nu; \quad \beta = \beta_1 \tag{26}$$

The second solution corresponds to a cavity making damped oscillations and we must therefore require

$$\frac{\left(\frac{\partial F}{\partial (j\nu)}\right)_1}{\left(\frac{\partial F}{\partial \omega}\right)_1} < 0 \tag{27}$$

Considering the behaviour of a wave $e^{-j\beta z}$, excited at $z = 0$, when $z \to +\infty$, it is necessary that $\mathrm{Im}(\beta) < 0$. For such a wave we therefore have the following condition

$$\frac{\left(\frac{\partial F}{\partial (j\nu)}\right)_1}{\left(\frac{\partial F}{\partial \beta}\right)_1} > 0 \tag{28}$$

We therefore finally obtain

$$\frac{\partial \omega}{\partial \beta} = - \frac{\frac{\partial F}{\partial \beta}}{\frac{\partial F}{\partial \omega}} > 0 \tag{29}$$

This means that only those waves which have the group velocity directed outwards from the place of excitation will be excited.

This result has been proved before using more sophisticated methods (BRESLER, 1959).

Bibliography

1. AGDUR, B & ENANDER, B.: Resonances of a Microwave Cavity Partially Filled with a Plasma. J. Appl. Phys. 33 (1962), pp. 575-581.

2. ALFREDSSON, L.: Investigations of Modes in a Plasma Waveguide (1963). To be published.

3. BRESLER, A.D.: The Far Fields Excited by a Point Source in a Passive Dissipationsless Anisotropic Uniform Waveguide. Trans. IRE on Microwave Theory and Techniques (1959), pp. 282-287.

4. CHORNEY, P.: Power and Energy Relations in Bidirectional Waveguides. Electromagnetics and Fluid Dynamics of Gaseous Plasma, pp. 195-210. Polytechnique Press 1962.

5. CLARRICOATS, P.J.B. & WALDRON, R.A.: Non-periodic Slow-wave and Backward-wave Structures. Electronics and Control 8 (1960), p. 455.

6. OLINER, A.A. & TAMIR, T.: Backward Waves on Isotropic Plasma Slabs. J. Appl. Phys. 33 (1962), p. 231.

7. TRIVELPIECE, A.W. & GOULD, R.W.: Space Charge Waves in Cylindrical Plasma Columns. J.Appl. Phys. 30 (1959), pp. 1784-1793.

8. TRIVELPIECE, A.W., IGNATIUS, A. & HOLSCHER, P.C.: Backward Waves in Longitudinally Magnetized Ferrite Rods. J. Appl. Phys. 32(1961), pp. 259-267.

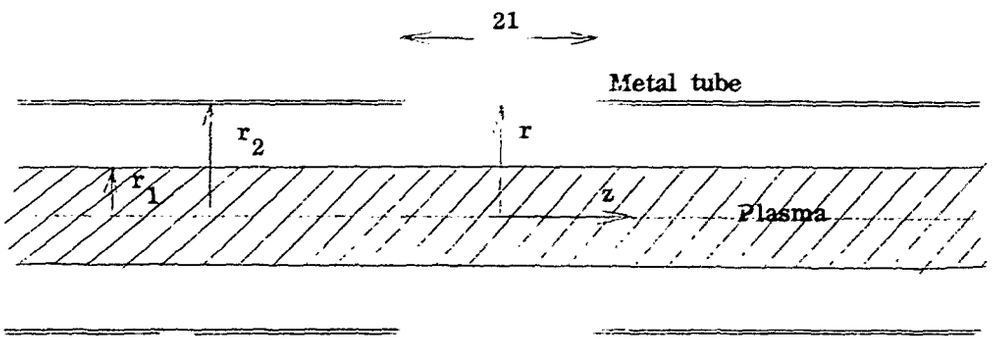

Fig. 1 Circularly cylindrical waveguide with central plasma column and a gap in the waveguide wall.

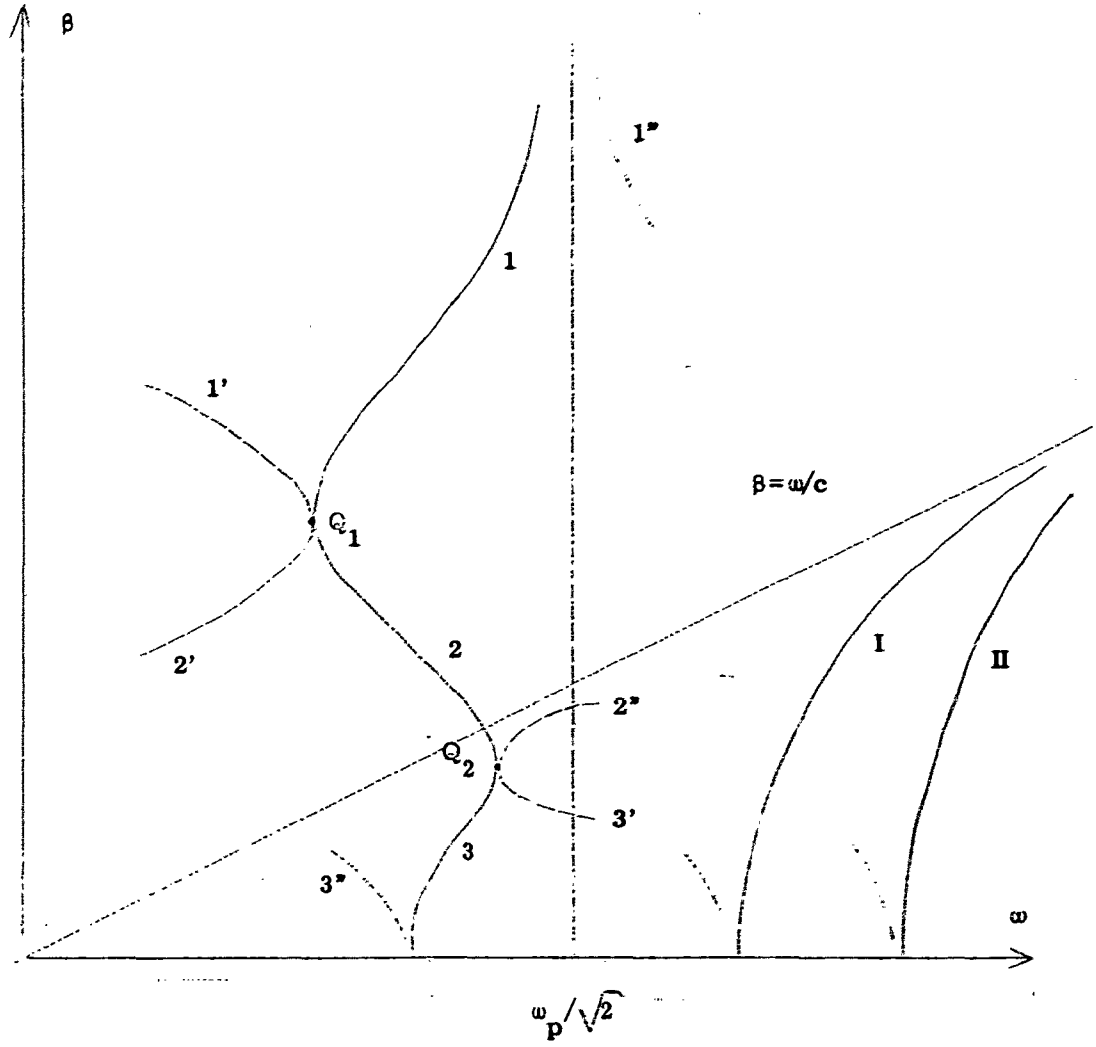

Fig. 2. Dispersion curves for different modes in the plasma waveguide in Fig. 1.

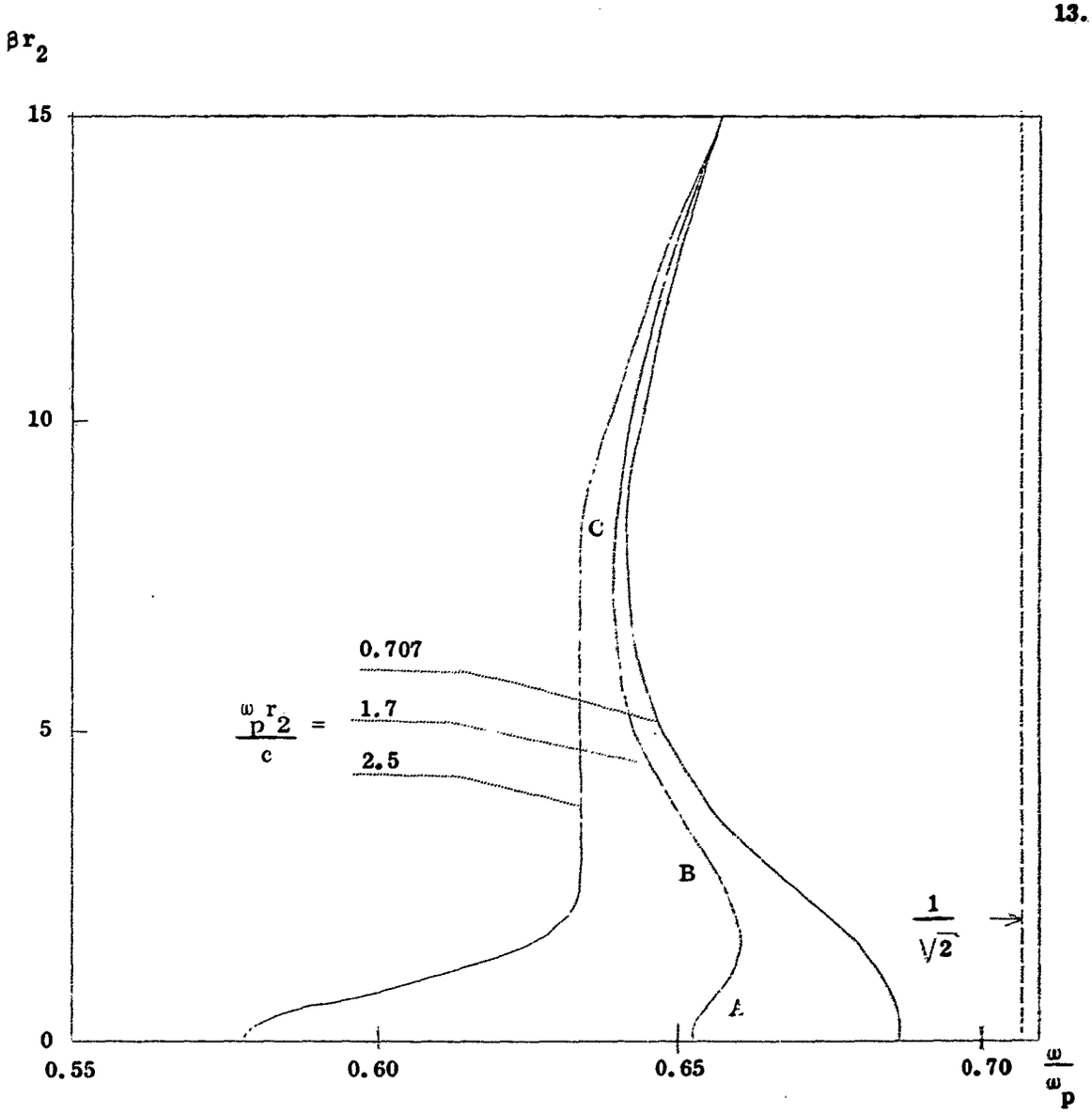

Fig. 3 Dispersion curves for three plasma waveguides with $\frac{r_2}{r_1} = 5$ and different values of $\frac{\omega_p r_2}{c}$. The vertical dashed line at $\frac{\omega}{\omega_p} = \frac{1}{\sqrt{2}}$ is the asymptote of all three curves.

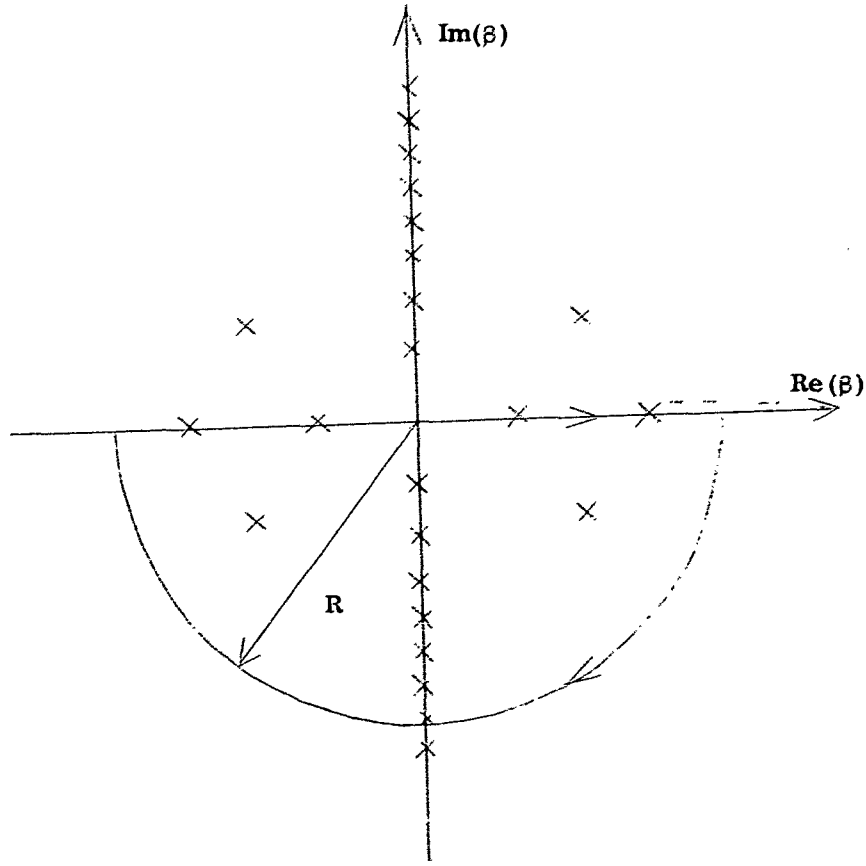

Fig. 4. Integration contour and poles in the complex β-plane.

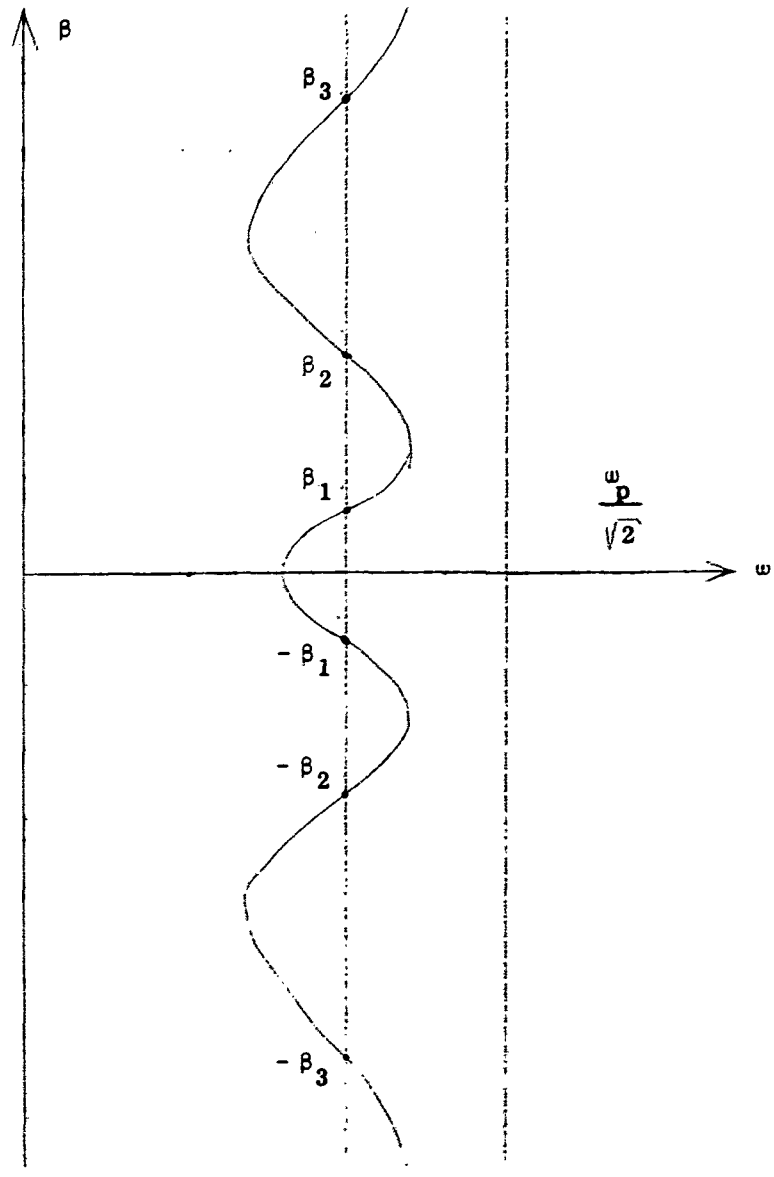

Fig. 5. Dispersion curve for the plasma modes.

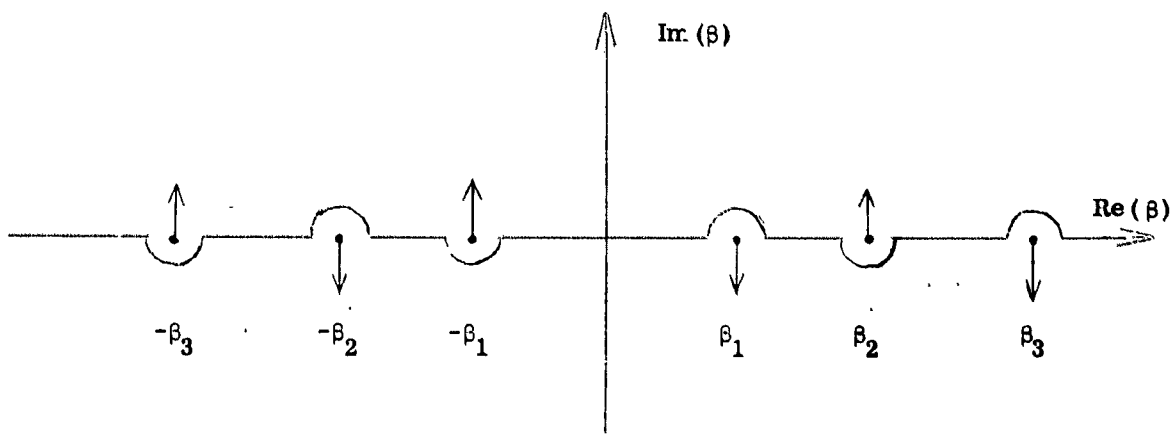

Fig. 6. Deformed integration contour.

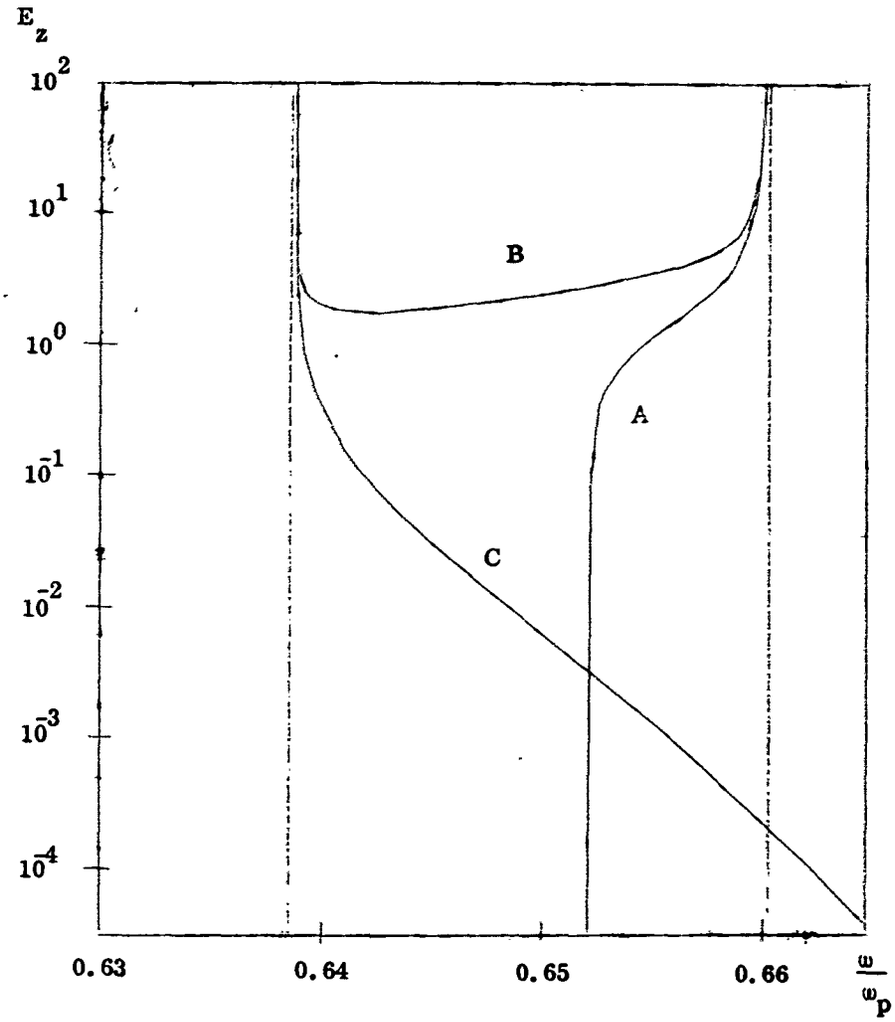

Fig. 7. The E_z-field at the plasma boundary obtained through gap excitation. The branches A, B and C correspond to the three branches of the dispersion curves for $\frac{\omega_p r_2}{c} = 1.7$ in Fig. 3.

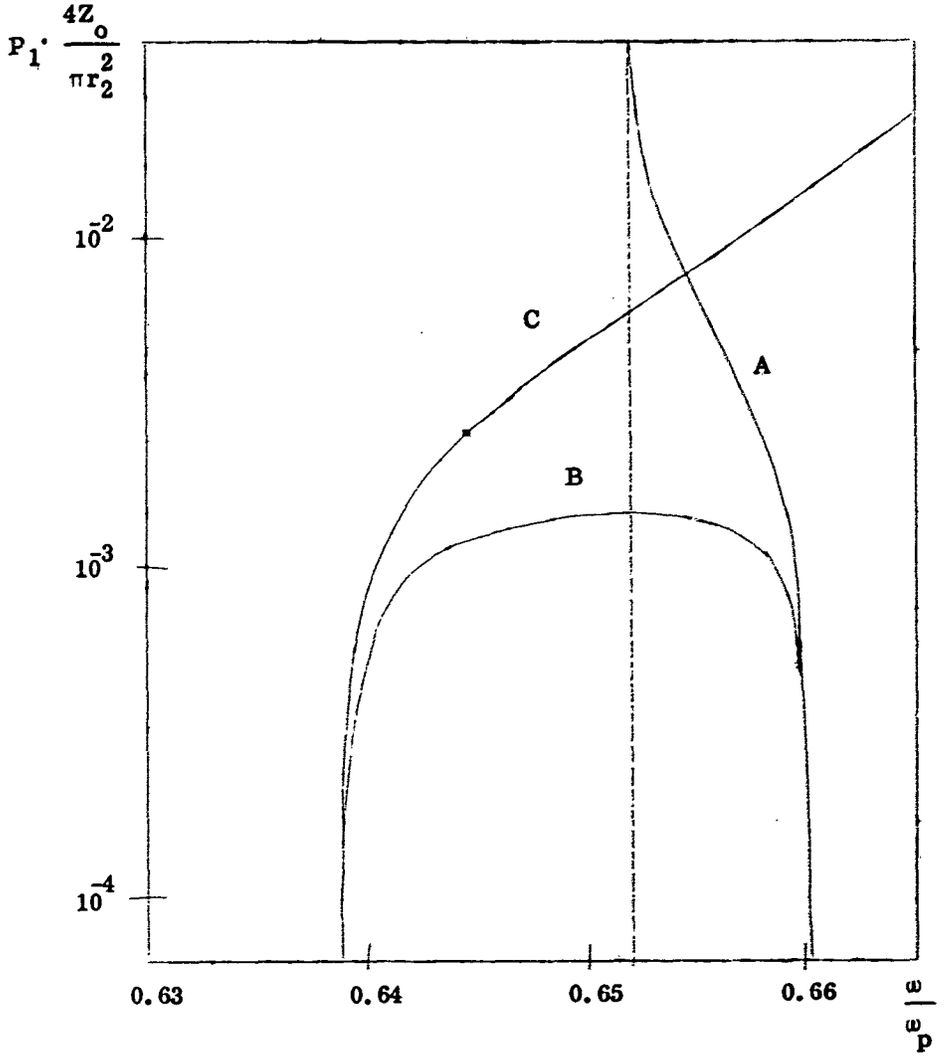

Fig. 8. Power flow in plasma modes.

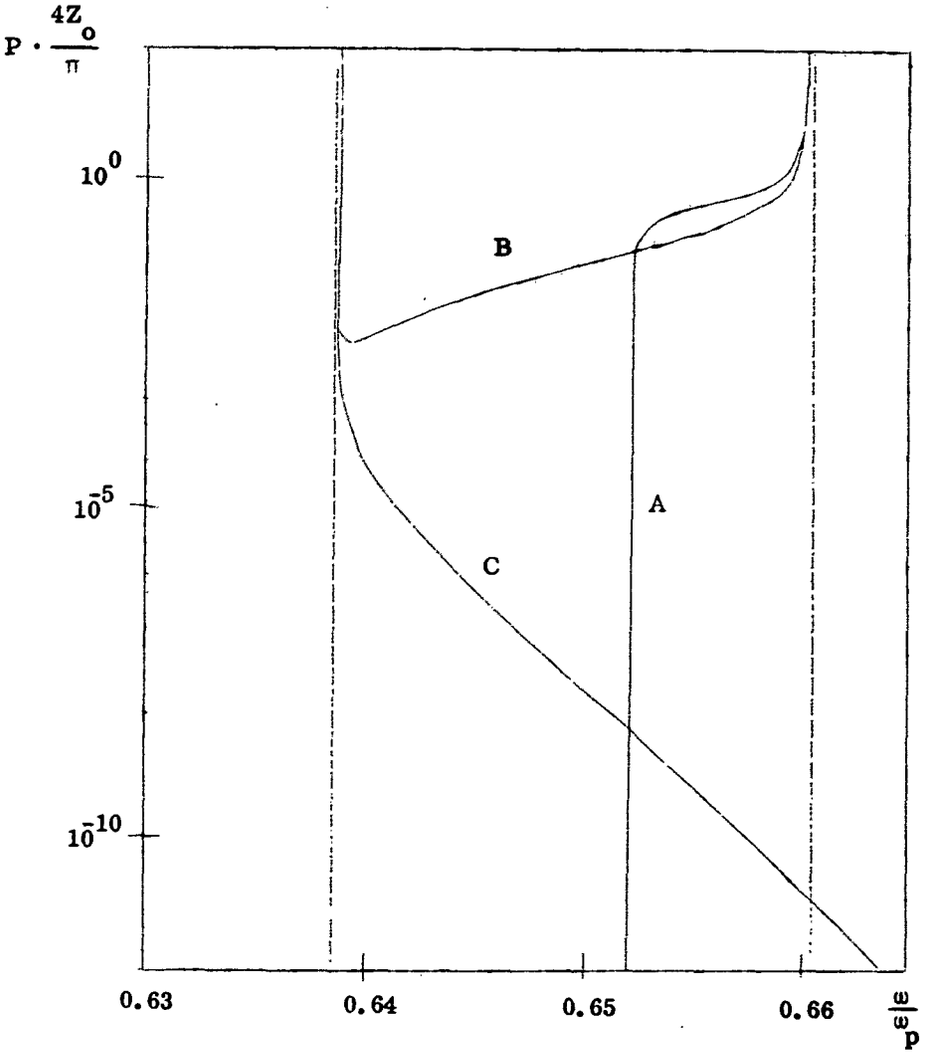

Fig. 9. Power flow in plasma modes obtained through gap excitation.

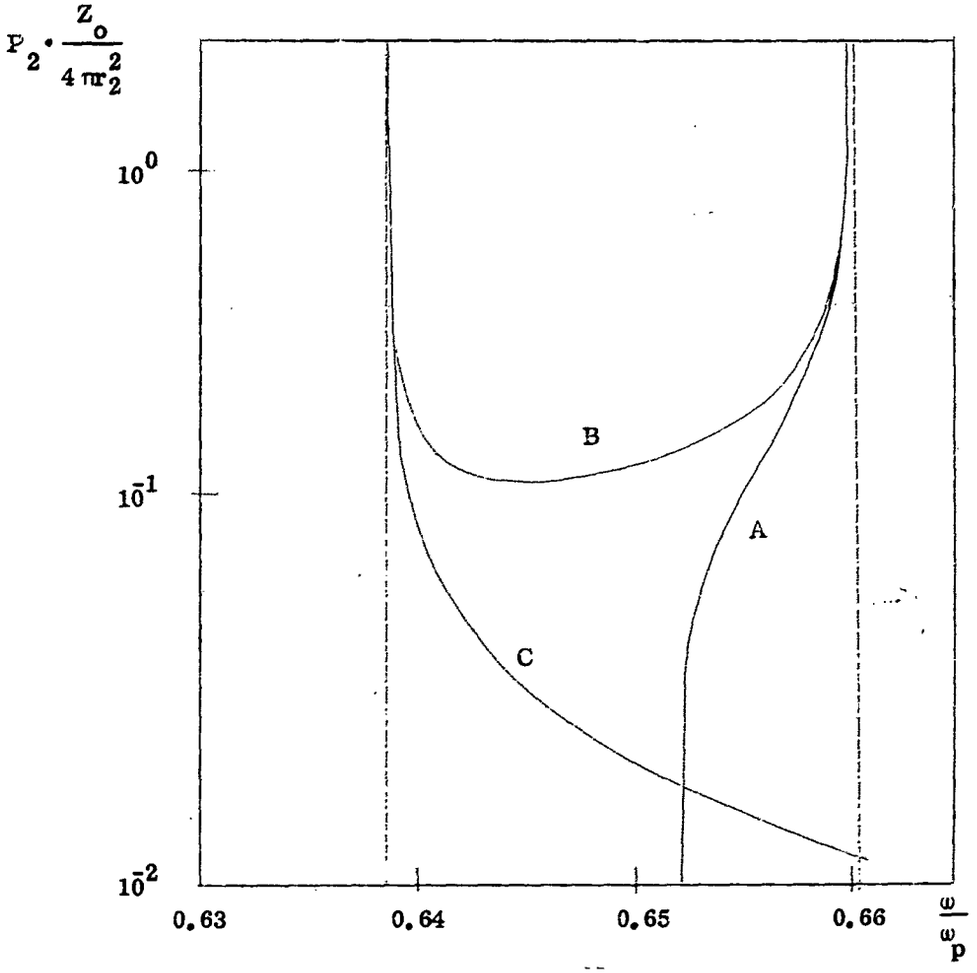

Fig. 10. Power flow in plasma modes obtained through excitation by a given transvers field.

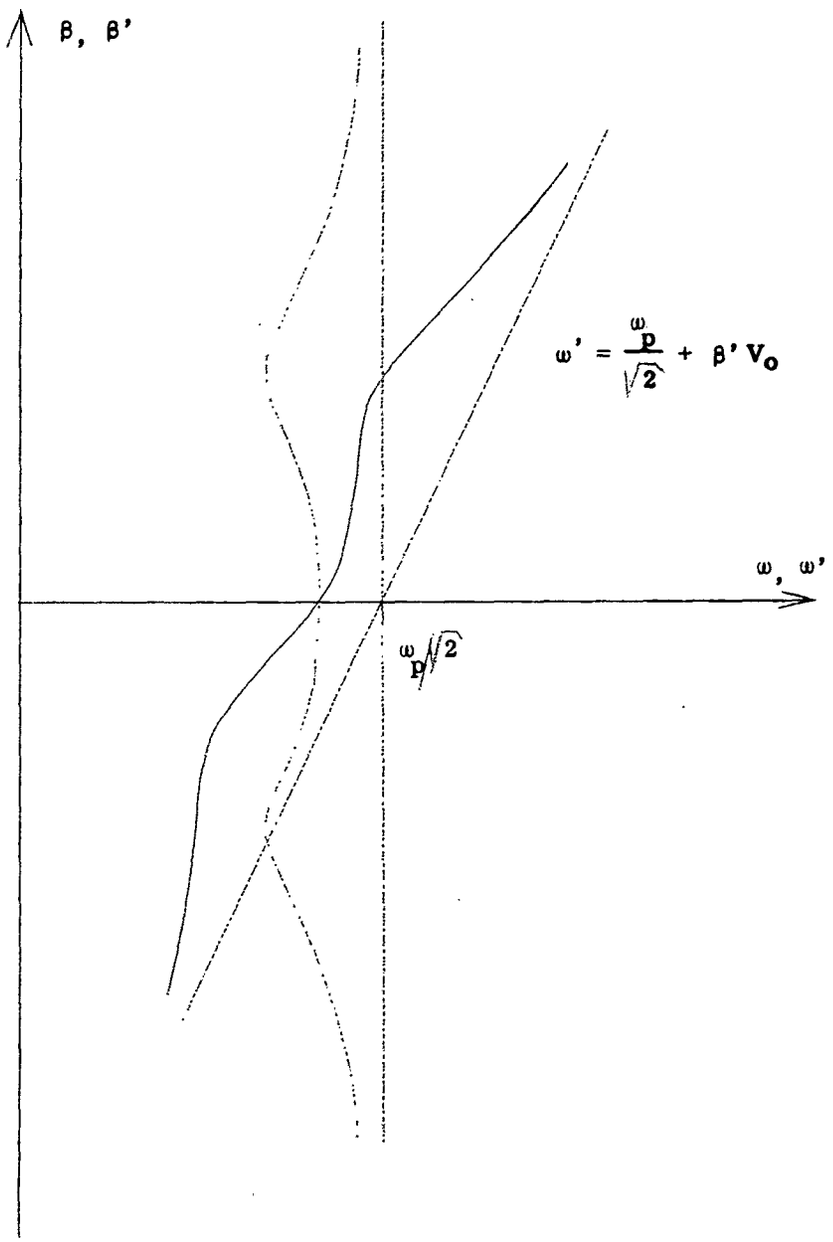

Fig. 11. Dispersion curve for waveguide with drifting plasma. The dashed curve is the dispersion curve for zero drift velocity.

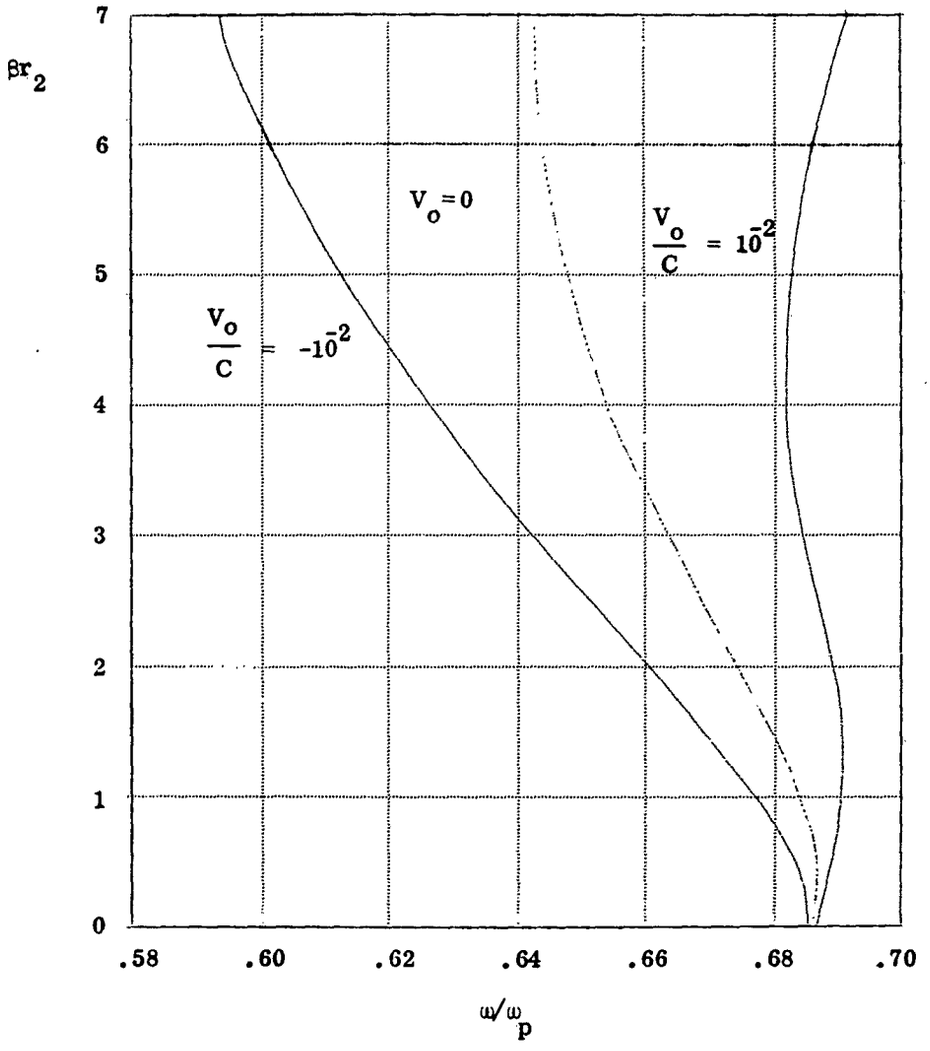

Fig. 12. Dispersion curves for waveguides with drifting plasma. $\frac{\omega_p r_2}{c} = 0.707$, $\frac{r_2}{r_1} = 5$.

II. A DISCONTINUITY PROBLEM IN A CIRCULAR WAVEGUIDE CONTAINING TWO DIELECTRICS

Introduction

In the study and application of plasma waveguides it is important to know how energy is transferred between conventional waveguides and plasma waveguides. An attempt to obtain approximate solutions of this problem by a variational method has been made (KALMYKOVA 1961).

In this paper we shall investigate a waveguide structure for which exact solutions can be obtained. The problem is formulated and solved for a waveguide that, for values of the dielectric constant less than one, represents a waveguide containing a cool, homogeneous plasma.

Chapter 1. Formulation of the problem

The waveguide system which we shall investigate in this paper is shown in Fig. 1. The part from $z = 0$ to $z = -\infty$ consists of a circularly cylindrical metal tube containing two concentric, lossless dielectrics. The dielectric constant is ϵ_1 in the region $r < a$ and ϵ_2 in $a < r < b$. In the following this waveguide will be called waveguide 1. The waveguide system from $z = 0$ to $z = +\infty$ is identical with the first part except for an infinitely thin metal tube between the two dielectrics. This part thus consists of two waveguides: a coaxial line (waveguide 2) filled with dielectric (ϵ_2), and a circularly cylindrical waveguide (waveguide 3) with radius a and filled with dielectric (ϵ_1).

We shall consider the effect of the discontinuity at $z = 0$ when the dominant, circularly symmetric TM-mode in waveguide 1 is incident from $z = -\infty$. Because of the discontinuity the incident wave will generally excite all circularly symmetric TM-modes in the three waveguides, including the TEM-mode in waveguide 2. For each mode,

only the wave with the group velocity directed away from the discontinuity will be excited.

By means of a method based on the WIENER-HOPF technique (see e.g. JONES 1952, HALLÉN 1953) we obtain the solution to MAXWELL's equations that gives the scattered field due to the discontinuity. The general solution has such a complex mathematical form that it is of little practical value. Simpler solutions can, however, be found for certain conditions. Thus we shall restrict the values of the parameters ε_1, ε_2, a, b, and the frequency of the incident wave, ω, so that a) in waveguide 1 only one mode can propagate while the other modes are cut off, b) in waveguide 2 all modes except the TEM-mode are cut off, c) in waveguide 3 all modes are cut off. The fields of the cut-off modes decrease exponentially away from the discontinuity. For large z-values they become negligible compared with the fields of the propagating modes. As the system is lossless, we now need only three parameters to completely characterize the fields far from the discontinuity, e.g. the amplitude and phase of the reflected dominant mode in waveguide 1 and the phase of the transmitted TEM-mode in waveguide 2.

Chapter 2. Some characteristics of the relevant modes

In this chapter we mainly consider how the conditions a, b, and c of Ch. 1 can be fulfilled.

For TM_{0m}-modes in waveguide 3 with a time- and z-dependence $e^{-j(\omega t-\beta_{3m}z)}$ we have the following dispersion relation:

$$J_0(a\sqrt{\varepsilon_1 k_0^2 - \beta_{3m}^2}) = 0 \tag{1}$$

or

$$\beta_{3m}^2 = \varepsilon_1 k_0^2 - (\frac{p_m}{a})^2 \tag{2}$$

where β_{3m} is the wave number for the TM_{0m}-mode

J_0 is the zero order BESSEL function

$k_0 = \frac{\omega}{c}$

c is the velocity of light

p_m is the m^{th} root of $J_0(p) = 0$

All modes are cut off in this waveguide if

$$\omega < \frac{p_1 c}{\sqrt{\varepsilon_1}\, a} \text{ or } \varepsilon_1 < 0 \tag{3}$$

In waveguide 2 the TEM-mode has the wave number

$$\beta_{21} = \frac{\omega\sqrt{\varepsilon_2}}{c} \tag{4}$$

and propagates if $\varepsilon_2 > 0$. If the wave number for the TM_{0m}-mode in this waveguide is denoted by $\beta_{2,m+1}$ we have:

$$\beta_{2,m+1}^2 = \varepsilon_2 k_0^2 - g_m^2 \tag{5}$$

where g_m is the m^{th} root of the equation:

$$J_0(ag)\, Y_0(bg) - Y_0(ag)\, J_0(bg) = 0 \tag{6}$$

where Y_0 is the zero order NEUMANN function.

All TM_{0m}-modes are cut-off if

$$\omega < \frac{g_1 c}{\sqrt{\varepsilon_2}} \tag{7}$$

The dispersion equation for TM_{0m}-modes in waveguide 1 is (see e.g. AGDUR & ENANDER 1961):

$$\varepsilon_2 J_0(ah_1)\,[J_0'(ah_2)Y_0(bh_2) - Y_0'(ah_2)J_0(bh_2)] - \\ - \frac{\varepsilon_1 h_2}{h_1} J_0'(ah_1)\,[J_0(ah_2)Y_0(bh_2) - Y_0(ah_2)J_0(bh_2)] = 0 \tag{8}$$

where $h_1 = (\varepsilon_1 k_0^2 - \beta_1^2)^{\frac{1}{2}}$

The wave numbers, β_{1m}, in this waveguide are those values of β_1 that satisfy Eq. (8). In order to fulfil condition a we must assume that only one of these, say β_{11}, is real.

The wave numbers for the cut-off modes in waveguide 1 may be complex[1] as distinguished from the wave numbers for the cut-off modes in waveguides 2 and 3 which are purely imaginary. If β_{1n} is a complex wave number that satisfies Eq. (8) then the complex conjugate value, β_{1n}^*, also satisfies this equation. This can be proved by means of the principle of reflection for analytic functions.

---

1) The proof by ADLER (ADLER 1952), that the wave numbers of a waveguide of this kind cannot be complex, is not correct.

Figure 2 shows dispersion curves for TM_{0m}-modes in waveguide 1 for a case where the inner dielectric is a plasma and the outer is vacuum. In this diagram complex branches of the dispersion curves (not shown in the figure) start out from points where the curves have a vertical slope, e.g. A_1 and A_2. The complex branches are in this case connected to branches where the wave number is purely imaginary as distinguished from the complex branches found for dipole modes in similar waveguides (AGDUR 1963, OLINER 1962, AGDUR & ENANDER 1963).

In the case shown in Fig. 2 the dominant mode has a zero-cut-off frequency and a phase velocity smaller than the velocity of light. This mode resembles the surface-wave mode on a plasma column and will always exist when $\varepsilon_1 < -\varepsilon_2$ and $\varepsilon_2 > 0$. When both ε_1 and ε_2 are positive, the dominant mode has a cut-off frequency different from zero and the dispersion diagram resembles that of an ordinary circular waveguide (BAÑOS 1951).

Chapter 3. Analysis

Assuming a time dependence $e^{-j\omega t}$, we find the following differential equation for the z-component of the total electric field in the coordinate system shown in Fig. 1.

$$\frac{\partial^2 E_{zt}}{\partial r^2} + \frac{1}{r}\frac{\partial E_{zt}}{\partial r} + \varepsilon k_0^2 E_{zt} + \frac{\partial^2 E_{zt}}{\partial z^2} = 0 \tag{9}$$

where $k_0^2 = \frac{\omega^2}{c^2}$

and $\varepsilon = \varepsilon_1$ when $r < a$

$\varepsilon = \varepsilon_2$ when $a < r < b$

The boundary conditions are:

$$E_{zt} = 0 \text{ when } r = b, \quad -\infty \leq z \leq +\infty \tag{10}$$

$$E_{zt} = 0 \text{ when } r = a, \quad 0 < z \leq +\infty \tag{11}$$

$$E_{zt} \text{ continuous when } r = a, \quad -\infty \leq z < 0 \tag{12}$$

The edge conditions at the discontinuity give (BOUWKAMP 1950)

$$E_{zt} \to C_1 z^{-\frac{1}{2}} \text{ when } r = a \text{ and } z \to -0 \tag{13}$$

We now divide the total electric and magnetic fields into two parts, one representing the incident field and one the scattered field, so that

$$E_{zt} = E_{zi} + E_z \tag{14}$$

In the whole region $-\infty \leq z \leq +\infty$, $r < a$, the field of the incident TM_{01}-mode is taken as

$$E_{zi} = J_0(rh_{11})\, e^{j\beta_{11} z} \tag{15}$$

where β_{11} is the propagation constant for the dominant mode in waveguide 1 and

$$h_{11} = (\varepsilon_1 k_0^2 - \beta_{11}^2)^{\frac{1}{2}}$$

The scattered field, E_z, shall satisfy the differential equation (9) and the conditions (10), (12) and (13) but not (11). Instead of (11), we require

$$E_z = -E_{zi} = -J_0(rh_{11})e^{j\beta_{11}z} \quad \text{when } r = a,\ 0 < z \leq +\infty \tag{16}$$

We shall now introduce small losses in the dielectric by letting ε_1 and ε_2 be complex. The two propagating modes are then slightly attenuated. The losses, which may be arbitrarily small, are introduced to facilitate the mathematical procedure; we shall eventually let them tend to zero.

The wave numbers for the two propagating modes, β_{11} and β_{21}, will now have small imaginary parts (smaller than the imaginary part of any wave number for the cut-off modes):

$$\begin{aligned} \beta_{11} &= \beta'_{11} + j\beta''_{11} \\ \beta_{21} &= \beta'_{21} + j\beta''_{21} \end{aligned} \tag{17}$$

where β'_{11}, β'_{21}, β''_{11}, and β''_{21} are real positive numbers (see Fig. 3). Choose δ equal to the smallest one of β''_{11} and β''_{21}. Then

$$|E_z| < C_1 \cdot e^{-\delta|z|} \quad \text{when } z \to -\infty \tag{18}$$

$$|E_z| < C_2 \cdot e^{-\delta|z|} \quad \text{when } z \to +\infty,\ r > a \tag{19}$$

$$|E_z| < C_3 \cdot e^{-\delta|z|} \quad \text{when } z \to +\infty,\ r < a \tag{20}$$

Introduce the FOURIER transform of E_z:

$$\psi = \frac{1}{(2\pi)^{\frac{1}{2}}} \int_{-\infty}^{+\infty} E_z\, e^{j\alpha z}\, dz \tag{21}$$

Transformation of Eqs. (9), (10), (12), and (15) yields

$$\frac{d^2\psi}{dr^2} + \frac{1}{r}\frac{d\psi}{dr} + (\varepsilon k_0^2 - \alpha^2)\psi = 0 \tag{22}$$

$$\psi = 0 \quad \text{at } r = b \tag{23}$$

$$\psi \text{ continuous at } r = a \tag{24}$$

The solution of Eq. (22) that satisfies the boundary condition (15) can be written

$$\psi = A(\alpha)\, I_0(\gamma_1 r) \qquad \text{for } 0 \leq r \leq a \tag{25a}$$

$$\psi = B(\alpha)\,[I_0(\gamma_2 r)\, K_0(\gamma_2 b) - K_0(\gamma_2 r)\, I_0(\gamma_2 b)] \qquad \text{for } a \leq r \leq b \tag{25b}$$

where I_0 and K_0 are the modified zero-order BESSEL functions and

$$\gamma_1 = (\alpha^2 - \varepsilon_1 k_0^2)^{\frac{1}{2}}$$
$$\gamma_2 = (\alpha^2 - \varepsilon_2 k_0^2)^{\frac{1}{2}} \tag{26}$$

γ_1 and γ_2 are made single-valued through suitable branch cuts in the complex α-plane.

For circularly symmetric TM-modes we have

$$-\frac{\partial E_z}{\partial r} = j\omega\mu_0 H_\varphi + \frac{j}{\omega \varepsilon \varepsilon_0} \frac{\partial^2 H_\varphi}{\partial z^2} \tag{27}$$

H_φ shall be continuous at $r = a$ for $-\infty \leq z \leq 0$

and satisfy the edge condition

$$H_\varphi \to C_2 z^{\frac{1}{2}} \text{ when } r = a \text{ and } z \to 0 \tag{28}$$

Denote the FOURIER transform of H_φ by Φ. Transformation of Eq. (27) gives:

$$\Phi = -\frac{j\omega\varepsilon\varepsilon_0}{\gamma^2} \frac{d\psi}{dr} \tag{29}$$

where $\gamma = \gamma_1$ for $r < a$ and $\gamma = \gamma_2$ for $r > a$

Using Eqs. (25a) and (25b) we get:

$$\Phi = -\frac{j\omega\varepsilon_1\varepsilon_0}{\gamma_1} A(\alpha)\, I_0'(\gamma_1 r) \qquad \text{for } 0 \leq r < a \tag{30}$$

$$\Phi = -\frac{j\omega\varepsilon_2\varepsilon_0}{\gamma_2} B(\alpha)\,[I_0'(\gamma_2 r)\, K_0(\gamma_2 b) - K_0'(\gamma_2 r)\, I_0(\gamma_2 b)] \qquad \text{for } a \leq r \leq b \tag{31}$$

Divide ψ and Φ into two parts

$$\psi = \psi_+ + \psi_- \qquad \Phi = \Phi_+ + \Phi_- \tag{32}$$

where

$$\psi_+ = \frac{1}{(2\pi)^{\frac{1}{2}}} \int_0^{\infty} E_z' \, e^{j\alpha z} \, dz; \qquad \psi_- = \frac{1}{(2\pi)^{\frac{1}{2}}} \int_{-\infty}^{0} E_z \, e^{j\alpha z} \, dz \tag{33}$$

and Φ_+ and Φ_- are similarly defined.

From the behaviour of the fields at $z = \pm\infty$, Eqs. (18), (19), and (20), we conclude that ψ_+ and Φ_+ are analytic functions in the half-plane $\mathrm{Im}(\alpha) > -\delta$, and that ψ_- and Φ_- are analytic for $\mathrm{Im}(\alpha) < \delta$.

At $r = a$, ψ_+, ψ_-, and Φ_- shall be continuous, whereas Φ_+ is discontinuous. Let the values at $r = a$ be $\psi_+(a)$, $\psi_-(a)$, $\Phi_-(a)$, $\Phi_+(a+0)$, and $\Phi_+(a-0)$. $\psi_+(a)$ is obtained from Eqs. (16) and 33):

$$\psi_+(a) = -\frac{j}{(2\pi)^{\frac{1}{2}}} \frac{J_0(h_{11}a)}{(\alpha + \beta_{11})} \tag{34}$$

From Eqs. (17), (18), (22), (23), (24), and (25), we now derive

$$\psi_-(a) - \frac{j}{(2\pi)^{\frac{1}{2}}} \frac{J_0(h_{11}a)}{(\alpha + \beta_{11})} = A\, I_0(\gamma_1 a) = \tag{35}$$

$$= B\,[I_0(\gamma_2 a)\, K_0(\gamma_2 b) - K_0(\gamma_2 a)\, I_0(\gamma_2 b)]$$

$$\Phi_+(a+0) + \Phi_-(a) = -B \frac{j\omega\varepsilon_2\varepsilon_0}{\gamma_2} [I_0'(\gamma_2 a)\, K_0(\gamma_2 b) - \tag{36}$$

$$- K_0'(\gamma_2 a)\, I_0(\gamma_2 b)]$$

$$\Phi_+(a-0) + \Phi_-(a) = -\frac{j\omega\varepsilon_1\varepsilon_0}{\gamma_1} A\, I_0'(\gamma_1 a) \tag{37}$$

By subtracting Eq. (37) from Eq. (36) and eliminating A and B from the resulting equation by means of Eq. (35) we get

$$\Lambda_+(a)\, L(\alpha) = \psi(a) - \frac{j}{(2\pi)^{\frac{1}{2}}} \frac{J_0(h_{11}a)}{(\alpha + \beta_{11})} \tag{38}$$

where we have put:

$$L = \{1/j\omega\varepsilon_0\} \cdot \{I_0(\gamma_1 a)\,\gamma_2^2\,[I_0(\gamma_2 a)\,K_0(\gamma_2 b) - K_0(\gamma_2 a)\,I_0(\gamma_2 b)]\}/\{\varepsilon_2\gamma_2 I_0(\gamma_1 a)\,[I_0'(\gamma_2 a)\,K_0(\gamma_2 b) - K_0'(\gamma_2 a)\,I_0(\gamma_2 b)] - (\varepsilon_1\gamma_2^2/\gamma_1)\,I_0'(\gamma_1 a)\,[I_0(\gamma_2 a)\,K_0(\gamma_2 b) - K_0(\gamma_2 a)\,I_0(\gamma_2 b)]\} \tag{39}$$

and $\Phi_+(a-0) - \Phi_+(a+0) = \Lambda_+(a)$ which, incidentally, is the FOURIER transform of the surface-current density in the inner conductor.

In Eq. (38), which is valid only in the strip $-\delta < \mathrm{Im}(\alpha) < \delta$ (see Fig. 3), both $\Lambda_+(a)$ and $\psi_-(a)$ are unknown functions of α. Nevertheless, they can be evaluated from this equation by means of LIOUVILLE'S theorem. To do this we shall rewrite Eq. (38) in such a form that one side of the equation is regular and bounded in the half-plane $\mathrm{Im}(\alpha) > -\delta$ and the other side is regular and bounded in the half-plane $\mathrm{Im}(\alpha) < \delta$.

We introduce

$$M(\alpha) = \frac{(\alpha - \beta_{11})}{(\alpha - \beta_{21})}\,\frac{(\alpha + \beta_{11})}{(\alpha + \beta_{21})}\,L(\alpha) \tag{40}$$

and assume that $M(\alpha)$ can be factored in the following way:

$$M(\alpha) = M_+(\alpha)\,M_-(\alpha) \tag{41}$$

where M_+ is regular and non-zero for $\mathrm{Im}(\alpha) > -\delta$ and M_- is regular and non-zero for $\mathrm{Im}(\alpha) < \delta$ and

$$\begin{aligned} M_+(\alpha) &\sim (\alpha^{-\frac{1}{2}}) \quad \text{when} \quad |\alpha| \to \infty,\ \mathrm{Im}(\alpha) > -\delta \\ M_-(\alpha) &\sim (\alpha^{-\frac{1}{2}}) \quad \text{when} \quad |\alpha| \to \infty,\ \mathrm{Im}(\alpha) < \delta \end{aligned} \tag{42}$$

Using Eq. (40) we write Eq. (38) in the following form

$$\Lambda_+(a)\,L_+(\alpha) + \frac{j}{(2\pi)^{\frac{1}{2}}}\,\frac{J_0(h_{11}a)}{L_-(-\beta_{11})(a+\beta_{11})} = \frac{\psi_-(a)}{L_-(\alpha)} - \frac{j}{(2\pi)^{\frac{1}{2}}}\,\frac{J_0(h_{11}a)}{(a+\beta_{11})}\,\left[\frac{1}{L_-(\alpha)} - \frac{1}{L_-(-\beta_{11})}\right] \tag{43}$$

where $L_+(\alpha) = \frac{\alpha + \beta_{11}}{\alpha + \beta_{21}} M_+(\alpha)$ and $L_-(\alpha) = \frac{\alpha - \beta_{11}}{\alpha - \beta_{21}} M_-(\alpha)$

The left-hand side of this equation is a regular function in the half-plane $\mathrm{Im}(\alpha) > \delta$ and the right-hand side is regular in the half-plane $\mathrm{Im}(\alpha) < \delta$. The two half-planes have a common strip and the two sides of Eq. (34) together define a function that is regular in the whole α-plane. Further, we find from the edge conditions (13) and (28) and the definitions of ψ_-, Eq. (33), and Λ_+ that

$$\begin{aligned} \Lambda_+ &\sim (\alpha)^{-3/2} \quad \text{when} \quad |\alpha| \to \infty, \quad \mathrm{Im}(\alpha) > 0 \\ \psi_- &\sim (\alpha)^{-1/2} \quad \text{when} \quad |\alpha| \to \infty, \quad \mathrm{Im}(\alpha) < 0 \end{aligned} \tag{44}$$

Combining this result with the assumed behaviour of M_+ and M_- at infinity we find that both sides of Eq. (43) tend to zero in their respective half-planes when $|\alpha| \to \infty$. According to LIOUVILLE'S theorem the integral function defined by the two sides of Eq. (43) must then be identically zero. Thus, putting the right-hand side equal to zero we have

$$\psi_-(a) = \frac{j}{(2\pi)^{\frac{1}{2}}} \frac{J_0(h_{11}a)}{(\alpha + \beta_{11})} \left[1 - \frac{L_-(\alpha)}{L_-(-\beta_{11})}\right] \tag{45}$$

and from Eq. (35)

$$\begin{aligned} A\, I_0(\gamma_1 a) = B \big[& I_0(\gamma_2 a)\, K_0(\gamma_2 b) - \\ & - K_0(\gamma_2 a)\, I_0(\gamma_2 b) \big] = - \frac{j}{(2\pi)^{\frac{1}{2}}} \frac{J_0(h_{11}a)}{(\alpha + \beta_{11})} \frac{L_-(\alpha)}{L_-(-\beta_{11})} \end{aligned} \tag{46}$$

The waveguide fields can then be obtained by using the FOURIER inversion theorem on Eqs. (25).

Before doing this, we shall construct functions M_+ and M_- having the required properties. Since

$$K_0(z) = - I_0(z) \ln(z) + f(z) \tag{47}$$

where f(z) is an even, integral function, the ln(z) terms in L, (Eq. (39)), cancel; thus L has no branch points. The numerator in the definition of L is an integral function of α which is zero if and only if

$$\alpha = \pm \beta_{2m} \quad \text{or} \quad \alpha = \pm \beta_{3m}$$

where β_{2m} and β_{3m} are the wave numbers for waveguides 2 and 3. The denominator is also an integral function of α and is zero if and only if $\alpha = \pm \beta_{1m}$, where β_{1m} are the wave numbers for waveguide 1. $M(\alpha)$ has the same properties as $L(\alpha)$ except that $M(\alpha)$ does neither have zeros at $\alpha = \pm \beta_{21}$ nor poles at $\alpha = \pm \beta_{11}$. We now define $M_+(\alpha)$ and $M_-(\alpha)$ by

$$\ln M_+(\alpha) = \frac{1}{2\pi j} P \int_{-\infty + jd}^{\infty + jd} \frac{\ln M(z)}{z - \alpha} \, dz \tag{48}$$

and

$$\ln M_-(\alpha) = \frac{1}{2\pi j} P \int_{-\infty + je}^{\infty + je} \frac{\ln M(z)}{z - \alpha} \, dz \tag{49}$$

where $-\delta < d < e < +\delta$

The use of CAUCHY principle values, indicated by P in front of the integral sign, is necessary because $M(\alpha) \sim |\alpha|$ when $\alpha \to \infty$ in the strip, so that the ordinary integrals are divergent.

Defined in this way, M_+ will be regular and non-zero in the half-plane $\text{Im}(\alpha) > d$. Similarly M_- will be regular and non-zero for $\text{Im}(\alpha) < e$. Further, from CAUCHY'S integral formula we find $M_+ M_- = M$, when $-\delta < \text{Im}(\alpha) < \delta$.

To investigate the behaviour of $M_+(\alpha)$ as $|\alpha| \to \infty$ in the upper half-plane, we write

$$P \int_{-\infty+jd}^{\infty+jd} \frac{\ln M(z)}{z-\alpha}\, dz = I_1 + I_2 + I_3$$

where

$$I_1 = \int_{-D+jd}^{D+jd} \frac{\ln M(z)}{z-\alpha}\, dz = O(\tfrac{1}{\alpha}) \quad \text{when } |\alpha| \to \infty$$

$$I_2 = \int_{D}^{\infty} \left(\frac{\ln x}{x+jd-\alpha} + \frac{\ln x}{-x+jd-\alpha}\right) dx$$

$$I_3 = \int_{D}^{\infty} \frac{\ln \frac{M(x+jd)}{x}}{x+jd-\alpha} + \frac{1}{-x+jd-\alpha} \frac{M(-x+jd)}{x}\, dx$$

It can be shown that

$$I_2 = -\frac{\pi}{j} \ln |\alpha| + O(1)$$

$$I_3 = O(1)$$

when $|\alpha| \to \infty$; $\operatorname{Im} \alpha \geq k$, where $d < k < 0$

Therefore

$$M_+(\alpha) = O(|\alpha|^{\frac{1}{2}}) \tag{50}$$

Similarly we find

$$\frac{1}{M_-(\alpha)} = O(|\alpha|^{-\frac{1}{2}}) \quad \text{when } |\alpha| \to \infty; \quad \operatorname{Im} \alpha \leq 1 \text{ where } e > 1 > 0$$

so that M_+ and M_-, defined by Eqs. (48) and (49), have the properties assumed earlier.

The fields in the waveguide system can be obtained from Eqs. (25) and (46) by means of the FOURIER inversion formula. As pointed out in the introduction, it is usually only the propagating modes that are of interest. The scattered E_z-field at any point in the region $r \leq a$ is given by

$$E_z = \frac{1}{(2\pi)^{\frac{1}{2}}} \int_{-\infty + jf}^{\infty + jf} A(\alpha)\, I_0(\gamma_1 r)\, e^{-j\alpha z}\, d\alpha \qquad (51)$$

where $-\delta < f < \delta$

For $z < 0$ we evaluate the integral in Eq. (51) by closing the integration path in the upper half-plane and using the calculus of residues.

From Eqs. (43), (36), and (32) we then obtain:

$$E_z = -\frac{j}{2\pi} \frac{J_0(h_{11}a)}{L_-(-\beta_{11})} \cdot \frac{2\beta_{11}}{\beta_{11} + \beta_{21}} \int_{C_0} \frac{L(\alpha)}{L_+(\alpha)} \frac{\alpha - \beta_{21}}{\alpha - \beta_{11}} \cdot \cdot \frac{I_0(\gamma_1 r)}{I_0(\gamma_1 a)} \frac{e^{-j\alpha z}}{\alpha + \beta_{11}}\, d\alpha \qquad (52)$$

The integrand in (52) has poles at and only at $\alpha = \beta_{1m}$ and the residues at these poles give the amplitudes of the reflected modes in waveguide 1. The reflected wave in the dominant mode is thus:

$$E_{zd} = \frac{\beta_{11} - \beta_{21}}{\beta_{11} + \beta_{21}} \frac{M(\beta_{11})}{M_-(-\beta_{11})\, M_+(\beta_{11})}\, J_0(h_{11}r)\, e^{-j\beta_{11}z} \qquad (53)$$

For the reflection coefficient R, defined as

$$R = \left(\frac{E_{zd}}{E_{zi}}\right)_{z=0},$$

we get from Eq. (53)

$$R = \frac{\beta_{11} - \beta_{21}}{\beta_{11} + \beta_{21}} \cdot \frac{M_-(\beta_{11})}{M_+(\beta_{11})} \qquad (54)$$

From Eqs. (48) and (49) we see that when the losses tend to zero

$$M_-(\beta_{11}) = M_+^*(\beta_{11})$$

so that

$$|R| = \left|\frac{\beta_{11} - \beta_{21}}{\beta_{11} + \beta_{21}}\right| = \left|\frac{\lambda_{11} - \lambda_{21}}{\lambda_{11} + \lambda_{21}}\right| \qquad (55)$$

where λ_{11} and λ_{21} are the wavelengths for the two propagating modes.

For $z > 0$ we can obtain the fields in an analogous way by closing the integration contour in the lower half-plane. The E_z-field will contain two propagating modes: one with the wave number β_{11}, which exactly cancels the incident wave; the other with the wave-number β_{21} is the transmitted TEM-mode. The phase of the TEM-mode together with the complex reflection coefficient (Eq. (54)) completely characterize the fields far away from the discontinuity.

The simple formula for the magnitude of the reflection coefficient Eq. (55) agrees with that obtained for the special case when $\varepsilon_1 = \varepsilon_2$ (MARCUWITZ 1951) with the preliminary results of an experimental investigation that is being performed at our laboratory.

Bibliography

1. ADLER, R.B.: Waves on Inhomogeneous Cylindrical Structures. Proc. I.R.E. 40, (1952), pp. 339-348.

2. AGDUR, B.: Notes on Waves in Plasmas. Symposium on Electromagnetic Theory and Antennas, Copenhagen, June 1962. Pergamon Press 1963, pp. 301-303.

3. AGDUR, B. & ENANDER, B.: Resonances of a Microwave Cavity Partially Filled with a Plasma. J. Appl. Phys. 33 (1962), pp. 575-581.

4. AGDUR, B. & ENANDER, B.: Excitation of Plasma Waveguides with Backward Wave Modes. Ericsson Tech. 19 (1963):2, pp. 251-268.

5. BAÑOS, A., SAXON, D.S. & GRUEN, H.: Propagation Characteristics in a Coaxial Structure with Two Dielectrics. J.Appl. Phys. 22 (1951), pp. 117-123.

6. BOUWKAMP, C.J.: Diffraction by Small Circular Disks and Holes. Philips Res. Rep. 5 (1950), p. 401.

7. HALLÉN, E.: Elektricitetslära. Stockholm 1953. English translation: Electromagnetic Theory. London 1962.

8. JONES, D.S.: A Simplifying Technique in the Solution of a Class of Diffraction Problems. Quart. J. Math. (2) 3 (1952), pp. 189-196.

9. KALMYKOVA, S.S.: On the Problem of Matching Plasma Waveguides. Zh. Tekh. Fiz. 31 (1961), pp. 1374-1378. English translation in Soviet Physics-Tech. Phys. 6 (1962), pp. 1001-1004.

10. MARCUVITZ, N.: Waveguide Handbook. Radiation Laboratory Series 10. New York 1951.

11. OLINER, A.A. & TAMIR, T.: Backward Waves on Isotropic Plasma Slabs. J. Appl. Phys. 33 (1962), p. 231.

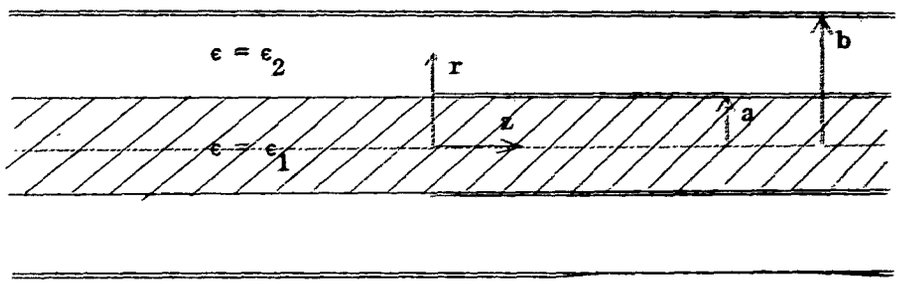

Fig. 1. Waveguide system.

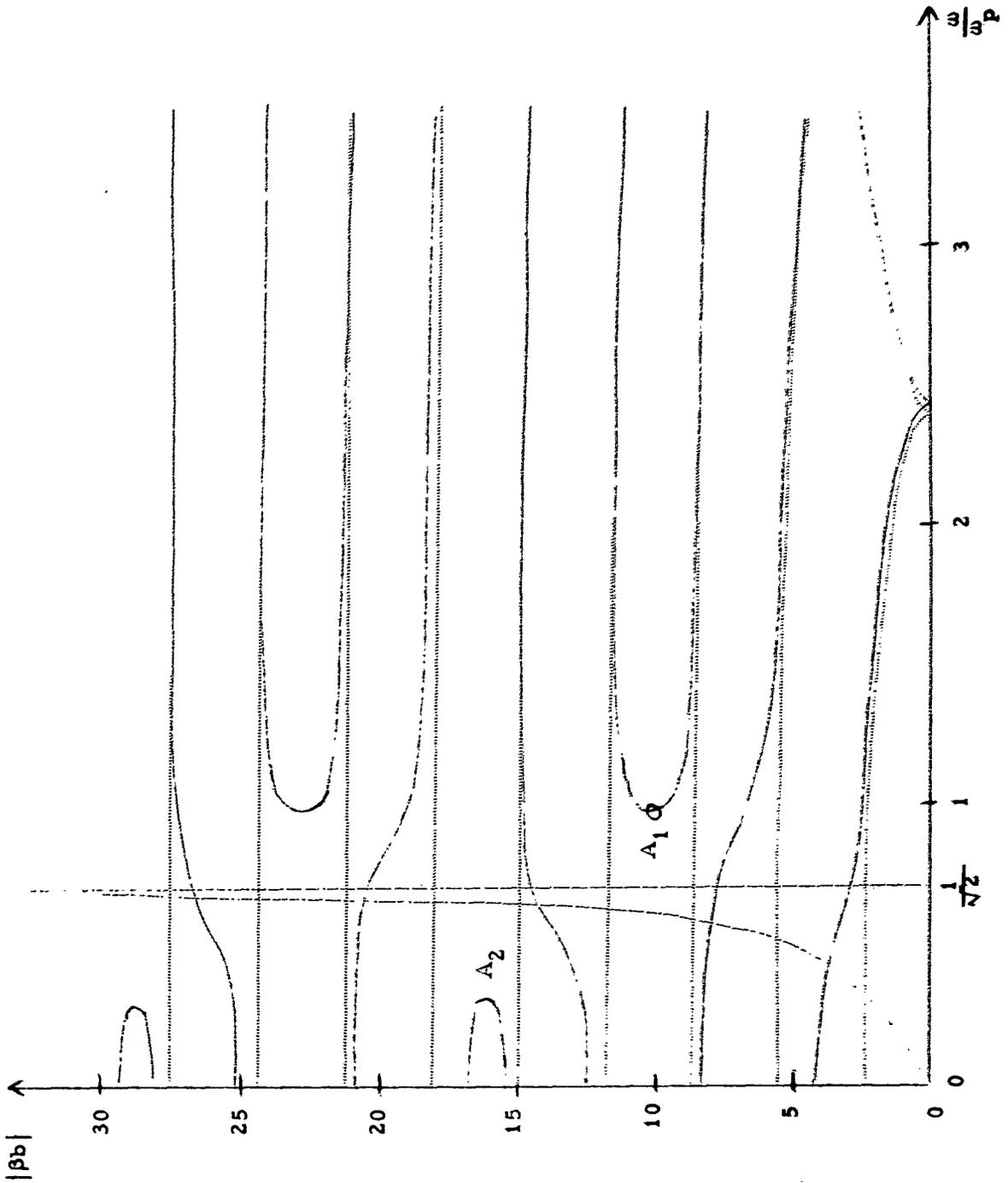

Fig. 2. ω - β diagram for a circularly cylindrical waveguide containing a central plasma column, b/a = 4; ω_p b/c = 1 (ω_p = plasma frequency). Dotted curves represent real values of β. Solid curves represent imaginary values of β. For comparison the ω - β diagram for an empty waveguide, radius = b, is shown by the dotted curves.

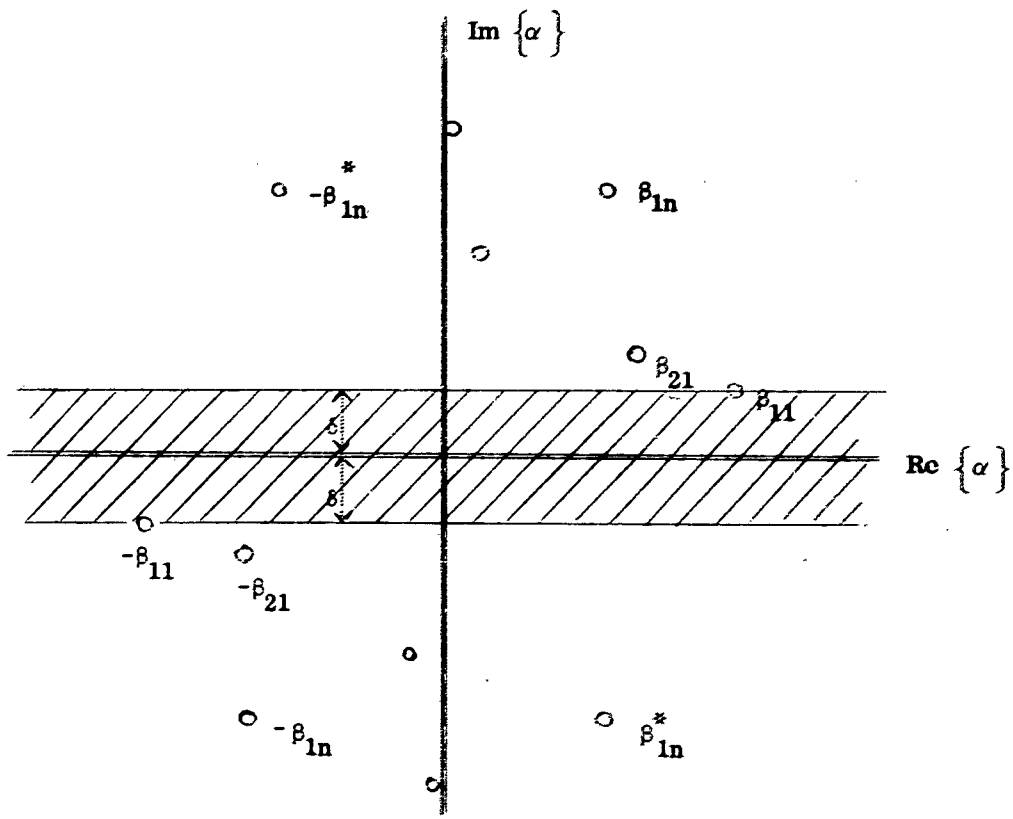

Fig. 3. Complex α-plane.

III. INVESTIGATION OF BACKWARD-WAVE MODES IN PLASMA WAVEGUIDES

Introduction

In recent years, some authors (TRIVELPIECE, 1959 and 1961, CLARRICOATS, 1960, NAPOLI and SWARTZ, 1963, OLINER, 1959, AGDUR and ENANDER, 1962) have studied wave propagation in inhomogeneous waveguides. Using ferrites, plasmas and ordinary dielectrics, it is possible to achieve propagating backward-wave modes in non-periodic waveguides. This paper describes the surface-wave dipole modes in the plasma waveguide systems shown in Figs. 1 a-c.

Some experiments have been performed which generally show good agreement with the theory.

Theory

I. General Remarks.

Wave propagation is studied in three different waveguide systems, infinite in the direction of propagation (z-direction), with the cross-sections shown in Figs. 1a-c.

The plasma, which is taken to be cool and lossless, is characterized by a dielectric constant $\varepsilon_p = 1 - \omega_p^2/\omega^2$ where ω_p is the plasma frequency. Further, the plasma is assumed to be homogeneous, i.e. no radial or axial density variations are taken into account. The signal frequency is assumed to be so high that the motion of the ions can be neglected.

The electromagnetic fields are assumed to be

$$\begin{bmatrix} E_i \\ B_i \end{bmatrix} = \left[a_i F_i(r) + b_i G_i(r) \right] \cdot e^{jn\varphi} \cdot e^{j(\omega t - \beta z)} \qquad (1)$$

where a_i and b_i are constants, $F_i(r)$ and $G_i(r)$ are Bessel functions, β is the propagation constant and n characterizes the azimuthal variation.

The dispersion equations are derived by matching the electromagnetic fields in the different regions using the ordinary boundary conditions. This leads to a linear, homogeneous system of equations in the undetermined amplitude coefficients. Non-trivial solutions exist when the system determinant equals zero. As soon as $n \neq 0$ there exist no pure TE- or TM-modes.

II. Plasma column surrounded by a homogeneous dielectric enclosed in a metal tube.

The system shown in Fig. 1 a consists of a central plasma column surrounded by a homogeneous dielectric (ε_r) and a metal tube ($\sigma = \infty$). The dispersion equation for this system has been derived by several authors. It is repeated here

as given by AGDUR and ENANDER, (1962)

$$\left[\varepsilon_p \frac{J'_{11}k_2}{J_{11}k_1}(J_{22}Y_{21} - Y_{22}J_{21}) - \varepsilon_r(J_{22}Y'_{21} - J'_{21}Y_{22})\right]\times$$

$$\times\left[\frac{J'_{11}k_2}{J_{11}k_1}(J'_{22}Y_{21} - Y'_{22}J_{21}) - (J'_{22}Y'_{21} - Y'_{22}J'_{21})\right] = \qquad (2)$$

$$n^2\beta^2\left[\frac{1}{k_1^2} - \frac{1}{k_2^2}\right]^2\left[\frac{k_2}{r_1k_o}\right]^2 (J_{22}Y_{21} - Y_{22}J_{21})(J'_{22}Y_{21} - J_{21}Y'_{22})$$

where J, Y, J' and Y' represent Bessel functions of the first and second kind and their derivatives. The following abbreviations have been used:

$$J_{11} = J_n(k_1r_1) \qquad J_{21} = J_n(k_2r_1) \qquad J_{22} = J_n(k_2r_2)$$

and similarly for Y, J' and Y'. Further

$$k_1 = k_o(\varepsilon_p - \tau^2)^{\frac{1}{2}}$$

$$k_2 = k_o(\varepsilon_r - \tau^2)^{\frac{1}{2}}$$

$$k_o = \omega/c$$

$$\tau = \beta/k_o$$

The field components, omitting the factor $e^{j(\omega t-\beta z)}$ are

$$E_Z = [AJ_n(k_2r) + BY_n(k_2r)] \cdot e^{jn\varphi} \qquad r_1 \le r \le r_2$$

$$E_Z = CJ_n(k_1r) \cdot e^{jn\varphi} \qquad r \le r_1$$

$$B_Z = [DJ_n(k_2r) + EY_n(k_2r)] \cdot e^{jn\varphi} \qquad r_1 \le r \le r_2 \qquad (3)$$

$$B_Z = FJ_n(k_1r) \cdot e^{jn\varphi} \qquad r \le r_1$$

$$E_\varphi = \frac{j\omega}{k_o^2(\varepsilon-\tau^2)}\left[\frac{\partial B_Z}{\partial r} - \frac{\tau}{rc}\cdot\frac{\partial E_Z}{\partial \varphi}\right]$$

$$E_r = \frac{-j\omega}{k_o^2(\varepsilon-\tau^2)}\left[\frac{1}{r}\cdot\frac{\partial B_Z}{\partial \varphi} + \frac{\tau}{c}\cdot\frac{\partial E_Z}{\partial r}\right]$$

$$B_\varphi = \frac{-j}{k_o^2(\varepsilon-\tau^2)}\left[\frac{\varepsilon}{\tau c}\cdot\frac{\partial E_Z}{\partial r} + \frac{1}{r}\frac{\partial B_Z}{\partial \varphi}\right]$$

$$B_r = \frac{j\beta}{k_o^2(\varepsilon-\tau^2)}\left[\frac{\varepsilon}{\tau cr}\frac{\partial E_Z}{\partial \varphi} - \frac{\partial B_Z}{\partial r}\right]$$

where the relations between the unknown amplitude coefficients are determined by the boundary conditions.

To find the expressions for the dipole modes we put $n = \pm 1$ in eqs. (2) and (3).

Fig. 2 shows the principal behaviour of the dispersion curves obtained from eq. (2). The velocity of light in the surrounding medium is $v = c\sqrt{\varepsilon_r}$. This gives the boundary between fast waves ($v_f > v$) and slow waves ($v_f < v$) which is indicated by a thin solid line. The figure shows two different types of curves E - F ... and A - B - C - D, indicating that there exist two different kinds of modes that can propagate along the waveguide. The first-mentioned curves - infinite in number - are fast modes related to those existing in the empty waveguide. In the following we shall mainly discuss the mode represented by A - B - C - D. This is a surface-wave mode (plasma mode), it is closely related to the modes on a free plasma column (discussed in section IV).

Points on the (ω,β)-curve where $\partial\omega/\partial\beta = 0$ are branch points which means that the dispersion curve, $F(\omega,\beta) = 0$, enters the complex β-plane along two complex conjugate branches.[x] The branches (A', B' ...) are drawn schematically in Fig. 2; the branches belonging to negative β-values are excluded. If the waveguide is lossless these complex conjugate modes do not contribute to the power transfer in the waveguide (CHORNEY, 1962).

If losses are introduced into the waveguide system the mode A - B - C - D will split up into three different modes and the branches A - B, B - C and C - D will not be connected to each other but to the complex modes so that the mode system will be for instance A' - A - B - B", B' - B - C - C" and C' - C - D - D'. This means that the plasma mode will split up into a number of different, separated plasma modes depending on how many branch points there are.

In the following the waveguide system is again taken to be lossless and the whole curve A - B - C - D is conveniently called the plasma mode. This mode shows many interesting properties. For large β-values the mode asymptotically approaches the line $\varepsilon_p + \varepsilon_r = 0$ (plasma resonance) and arbitrarily slow waves exist. The plasma mode is of TE-character when $\beta = 0$ and of TM-character when $\beta \to \infty$. The interval B - C exemplifies negative dispersion i.e. group and phase velocity of opposite sign.

---

x) The explicit form of the dispersion equation $\omega = f(\beta)$ is expanded in a Taylor series around the branch point. Using the relations $\omega_o = f(\beta)_o$ and $[\partial\omega/\partial\beta]_o = 0$ we find that $\Delta\omega = f''(\beta)_o(\Delta\beta)^2$, resulting in either real or purely imaginary values of $(\Delta\beta)$

The plasma mode also exhibits a continuous transition from slow waves to fast waves unless there is a branch point where the phase velocity equals the velocity of light.

In Figs. 3 and 4 dispersion curves are shown for the plasma mode with two different surrounding materials, viz. vacuum ($\varepsilon_r = 1$) and Pyrex ($\varepsilon_r = 4.5$). In these two figures the diameter ratio r_1/r_2 is kept constant and the dimensionless parameter ($\omega_p r_2/c$) is varied. To the right in each figure there is a dot-dash curve representing the quasistatic approximation, obtained by neglecting $\partial\bar{A}/\partial t$ in

$$\bar{E} = - \text{grad } V - \partial\bar{A}/\partial t$$

For a given β-value the exact solutions yield lower frequencies than the approximation. When $\beta \to \infty$ the exact and approximate solutions converge. The figures also show that the approximation is good only for relatively low plasma densities. Fig. 5 shows a set of dispersion curves where $\omega_p r_2/c$ is kept constant and the diameter ratio has been varied. Together Figs. 3-5 show that the curves, and especially the negative dispersion, are strongly dependent upon the geometry and the plasma density. The magnitude of the group and phase velocities in the region where negative dispersion exists is $|v_f| \approx v/10$ and $|v_g| \approx v/100$.

Using the notations in Fig. 2, we define the relative bandwidth for the range of negative dispersion

$$\frac{\Delta\omega}{\omega_o} = 2\,\frac{\omega'' - \omega'}{\omega'' + \omega'} \qquad (4)$$

We can see from Figs. 3 and 4 that for a given geometry the relative bandwidth of the exact solutions has an upper limit given by the relative bandwidth obtained by the quasi-static approximation. In Fig. 6 this maximum value is plotted vs. the diameter ratio; we find that the negative dispersion disappears when $r_1/r_2 > 0.45$ and has a maximum when $r_1/r_2 \to 0$. Fig. 6 also shows that a higher ε_r gives a larger relative bandwidth.

III. Plasma column surrounded by a two-layer dielectric enclosed in a metal tube.

The waveguide system of Fig. 1b consists of a central plasma column surrounded by two different, concentric, homogeneous dielectrics inside a metal tube. The characteristic equation can be written in determinant form

$$\begin{vmatrix} A_1 & A_2 & A_3 \\ A_4 & A_5 & A_6 \\ A_7 & A_8 & A_9 \end{vmatrix} = 0 \qquad (5)$$

where

$$A_1 = \left[Q + \frac{\varepsilon_p + \varepsilon_g}{\tau^2 Q} r_1^2 F_{21} F_{11} - \frac{\varepsilon_g}{\tau^2 Q} r_1^2 F_{21}^2 - \frac{\varepsilon_p}{\tau^2 Q} r_1^2 F_{11}^2 \right] \cdot J_{21}$$

$$A_2 = \left[Q + \frac{\varepsilon_g}{\tau^2 Q} r_1^2 F_{21} F_{11} - \frac{\varepsilon_g}{\tau^2 Q} r_1^2 F_{21} G_{21} - \frac{\varepsilon_p}{\tau^2 Q} r_1^2 F_{11}^2 + \frac{\varepsilon_p}{\tau^2 Q} r_1^2 F_{11} G_{21} Y_{21} \right.$$

$$A_3 = \frac{1}{\tau c J_{21}} \left[\frac{\varepsilon_g W_{21}}{k_2} \right]$$

$$A_4 = \left[F_{22} r_2 - \frac{P}{Q} F_{11} r_1 + \frac{P}{Q} F_{21} r_1 - T_1 r_3 \right] \cdot J_{22}$$

$$A_5 = \left[G_{22} r_2 Y_{22} - \frac{P}{Q} \frac{Y_{21}}{J_{21}} (F_{11} r_1 - G_{21} r_1) J_{22} - T_1 r_3 Y_{22} \right]$$

$$A_6 = \frac{1}{\tau c J_{21}} \left[\tau^2 P V_1 \right]$$

$$A_7 = \left[\frac{1}{\tau^2 Q} (\varepsilon_g F_{22} r_2 - T_2 r_3)(F_{11} r_1 - F_{21} r_1) - P \right] \cdot J_{22}$$

$$A_8 = \left[\frac{1}{\tau^2 Q} (\varepsilon_g F_{22} r_2 - T_2 r_3)(F_{11} r_1 - G_{21} r_1) \frac{Y_{21}}{J_{21}} J_{22} - P Y_{22} \right]$$

$$A_9 = \frac{1}{\tau c J_{21}} \left[\frac{\varepsilon_g V_2}{k_2} + T_2 V_1 r_3 \right]$$

The following abbreviations have been used:

$$F_{11} = \frac{1}{k_1 r_1} \frac{J'_{11}}{J_{11}} \qquad \text{and similarly for } F_{21} \text{ and } F_{22}$$

$$G_{21} = \frac{1}{k_2 r_1} \frac{Y'_{21}}{Y_{21}} \qquad \text{and similarly for } G_{22}$$

$$W_{21} = J_{21} Y'_{21} - Y_{21} J'_{21} \qquad \text{(Wronskian determinant)}$$

$$V_1 = J_{22}Y_{21} - J_{21}Y_{22}$$

$$V_2 = J_{21}Y'_{22} - J'_{22}Y_{21}$$

$$T_1 = \frac{1}{k_3 r_3} \frac{J'_{33}Y'_{32} - J'_{32}Y'_{33}}{J'_{33}Y_{32} - J_{32}Y'_{33}}$$

$$T_2 = \frac{1}{k_3 r_3} \frac{J_{33}Y'_{32} - J'_{32}Y_{33}}{J_{33}Y_{32} - J_{32}Y_{33}}$$

$$Q = \frac{n}{r_1}\left[\frac{1}{k_2^2} - \frac{1}{k_1^2}\right]$$

$$P = \frac{n}{r_2}\left[\frac{1}{k_3^2} - \frac{1}{k_2^2}\right]$$

$$k_1 = k_o(\varepsilon_p - \tau^2)^{\frac{1}{2}}$$

$$k_2 = k_o(\varepsilon_g - \tau^2)^{\frac{1}{2}}$$

$$k_3 = k_o(1 - \tau^2)^{\frac{1}{2}}$$

$$k_o = \omega/c$$

$$\tau = \beta/k_o$$

The short forms (J_{11}, J_{21} ...) are defined in the same way as in section II.

The principal behaviour of the dispersion curves given by eqs. (5) is the same as for eq. (2), see Fig. 2. What was said about the plasma mode in section II is valid also for this case except that the position of the asymptote is now given by $\varepsilon_p + \varepsilon_g = 0$. This means that only the inner dielectric affects the asymptote and, as the cut-off frequency is less dependent upon the inner dielectric, a proper choice of dielectric material may give rise to negative dispersion.

Solutions of eq. (5) are shown in Figs. 7 and 8 for $\varepsilon_g = 4.5$ and $\varepsilon_r = 1$. This corresponds to a plasma column inside a glass tube. In Fig. 7 the dot-dash curve again represents the quasi-static solution. Calculations show that as long as $\omega_p r_3/c < 1$, the approximation is in good agreement with the exact solutions, except for small β-values. In this case (Fig. 7) the maximum relative bandwidth (33 %) is considerably larger than for glass only (15 %) or vacuum only (10 %).

IV. Plasma column surrounded by an infinite homogeneous dielectric.

The waveguide system of Fig. 1c consists of a plasma column in an infinite homogeneous dielectric. The dispersion equation is

$$\left[\frac{\varepsilon_p}{h_1 r_1}\cdot\frac{I_n'(h_1 r_1)}{I_n(h_1 r_1)} - \frac{\varepsilon_r}{h_2 r_1}\cdot\frac{K_n'(h_2 r_1)}{K_n(h_2 r_1)}\right]\cdot\left[\frac{1}{h_1 r_1}\,\frac{I_n'(h_1 r_1)}{I_n(h_1 r_1)} - \right.$$

$$\left. - \frac{1}{h_2 r_1}\,\frac{K_n'(h_2 r_1)}{K_n(h_2 r_1)}\right] = n^2\tau^2\left[\frac{1}{(h_1 r_1)^2} - \frac{1}{(h_2 r_1)^2}\right]^2 \qquad (6)$$

where I_n, K_n and their derivatives are modified Bessel functions of the first and second kind and

$$h_1 = k_o(\tau^2 - \varepsilon_p)^{\frac{1}{2}}$$

$$h_2 = k_o(\tau^2 - \varepsilon_r)^{\frac{1}{2}}$$

$$k_o = \omega/c$$

$$\tau = \beta/k_o$$

Solutions to eq. (6) are shown in Fig. 9 where the two different families of curves correspond to different ε_r. The dot-dash curve represent the quasi-static approximation.

A comparison between Figs. 3, 4 and 7 and Fig. 9 shows that the surface-wave mode in the waveguide systems of Figs. 1 a-b is closely related to the surface-wave mode on a free plasma column - as was stated in section I.

Experiments

Measurements of the dispersion have been made, using the experimental set-up shown in Fig. 10. The waves could be excited at either or both ends of the tube. Different methods of coupling microwave energy to the plasma mode have been studied experimentally by KERZAR (1963). With reference to his results we chose a simple loop that could be turned around in the azimuthal direction.

The plasma was the positive column of a low-pressure hot-cathode mercury discharge. The, indirectly heated, oxide cathodes were shielded from direct ion bombardment by a metal screen and the transition from the cathode region to the useful plasma column was made long and smooth. This arrangement gave very small oscillations of a low frequency (10-100 kHz) and the discharge seemed to be stable in a relatively large temperature interval (10 °C - 50 °C). During the measurements the temperature of the coldest wall of the plasma tube was kept

constant at 20 °C ± 0.5 °C by means of forced cooling and a heat exchanger. Thus, the estimated neutral gas pressure was $1.2 \cdot 10^{-3}$ mm Hg. The current through the plasma tube was between 250 - 500 mA and stabilized by a regulated power supply. The dimensions of the plasma tube were L = 750 mm, r_1 = 6 mm, r_2 = 7.5 mm and of the surrounding metal tube r_3 = 30 mm or 16 mm. The measurements were made at frequencies in the range 900-1400 MHz.

To measure the propagation constant of waves propagating in a structure there are basically two different methods (i) analyzing a standing wave pattern or (ii) analyzing an interference pattern. The different patterns were in this experiment plotted on an xy-recorder.

The plasma density was measured by a microwave-cavity method developed by HEDVALL (1963), which takes the surrounding glass tube into account. Fig. 11 shows a typical example of the plasma density plotted against position along the plasma column; the density is not constant along the tube. The influence of this density gradient upon the interference patterns was a continuous change of wavelength (phase velocity) along the tube. This density inhomogeneity has been observed earlier by von ENGEL (1955), AGDUR, KERZAR and NYGREN (1963), and Mc GUCKIN (1963).

The experimental results are shown in Fig. 12 together with theoretical curves for (i) a plasma column surrounded by vacuum, (ii) a plasma column surrounded by Pyrex, (iii) a plasma column surrounded by a two-layer dielectric. The figure shows that the agreement between theory and experiments is good when the glass tube is taken into account. The measurements, which were made at different plasma densities ($0.5 < \omega_p r_3/c < 1.5$) and with different geometries (r_3 = = 30 mm and r_3 = 16 mm), were in all cases in good agreement with the theory. When the phase velocity was equal to or larger than the velocity of light in the surrounding glass tube the waves disappeared and no measurements were possible. At low frequencies another limitation prevented measurements, viz. the symmetrical mode that was more strongly excited and much less attenuated than the dipole mode.

If we consider the theoretical curves (Fig. 7) in connection with the axial inhomogeneity in the plasma density (Fig. 11) we find that there should exist a cut-off phenomenon when waves are propagated towards a lower plasma density (in this case from anode to cathode). This cut-off was clearly visible in the experiment.

REFERENCES

AGDUR, B and ENANDER, B, 1962: Resonances of a microwave cavity partially filled with a plasma. - J. Appl. Phys. 33(1962), 575-581.

AGDUR, B, KERZAR, B and NYGREN, T, 1963: Variation of the electron density along a plasma column. - Phys. Rev. Letters 11(1963), 467-468.

CHORNEY, P, 1962: Power and energy relations in bidirectional waveguides. - Electromagnetics and fluid dynamics of gaseus plasma, 195-210. Polytechnic Press 1962.

CLARRICOATS, P J B and WALDRON, R A, 1960: Non-periodic slow-wave and backward-wave structures. - Electronics and Control 8(1960), 455.

von ENGEL, A, 1955: Ionized gases, 227-228. Oxford Univ. Press 1955.

Mc GUCKIN, J P, 1963: The pressure gradient in positive columns. - Brit. J. Appl. Phys. 14(1963), 528.

HEDVALL, P, 1963: Cavity method for measuring plasma properties. - Ericsson Tech. 19(1963), 96-107.

KERZAR, B, 1963: Experiments on propagation of slow waves in a plasma waveguide. - Radiovetenskapliga konferensen i Stockholm 1963 (RVK 63 föredrag Nr 38).

NAPOLI, L S and SWARTZ, G A, 1963: Wave propagation in a tubular plasma. - Phys. Fluids. 6(1963), 918-924.

OLINER, A A and TAMIR, T, 1959: Backward waves on isotropic plasma slabs. - J. Appl. Phys. 33(1959), 231.

TRIVELPIECE, A W and GOULD, R W, 1959: Space charge waves in cylindrical plasma columns. - J. Appl. Phys. 30(1959), 1784-1793.

TRIVELPIECE, A W, IGNATIUS, A and HOLSCHER, P C, 1961: Backward waves in longitudinally magnetized ferrite rods. - J. Appl. Phys. 32(1961), 259-267.

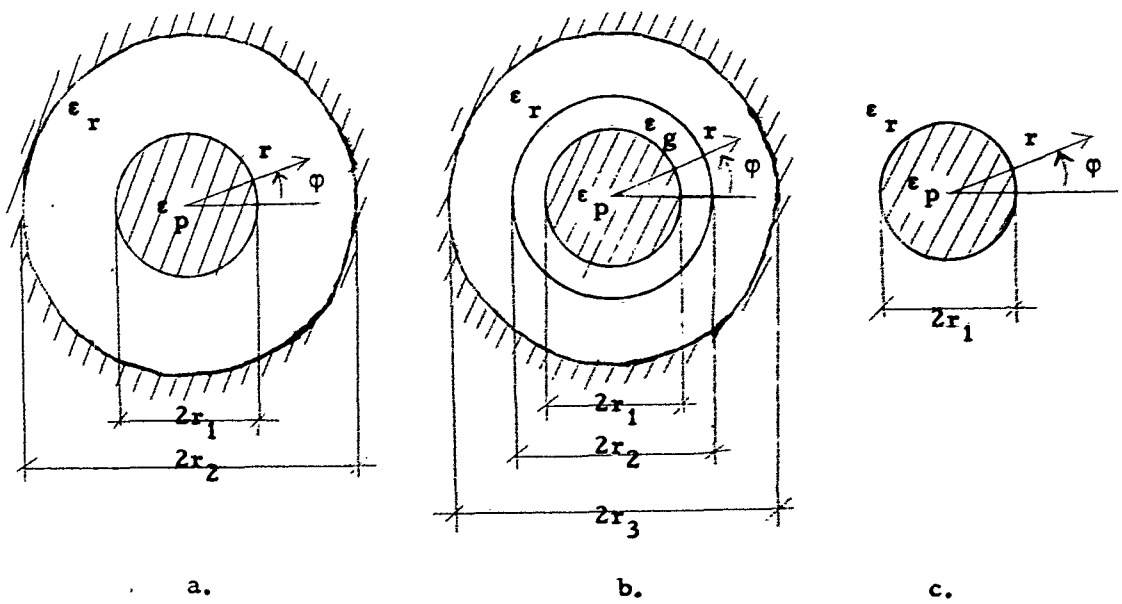

Fig. 1. Circularly cylindrical plasma waveguides.

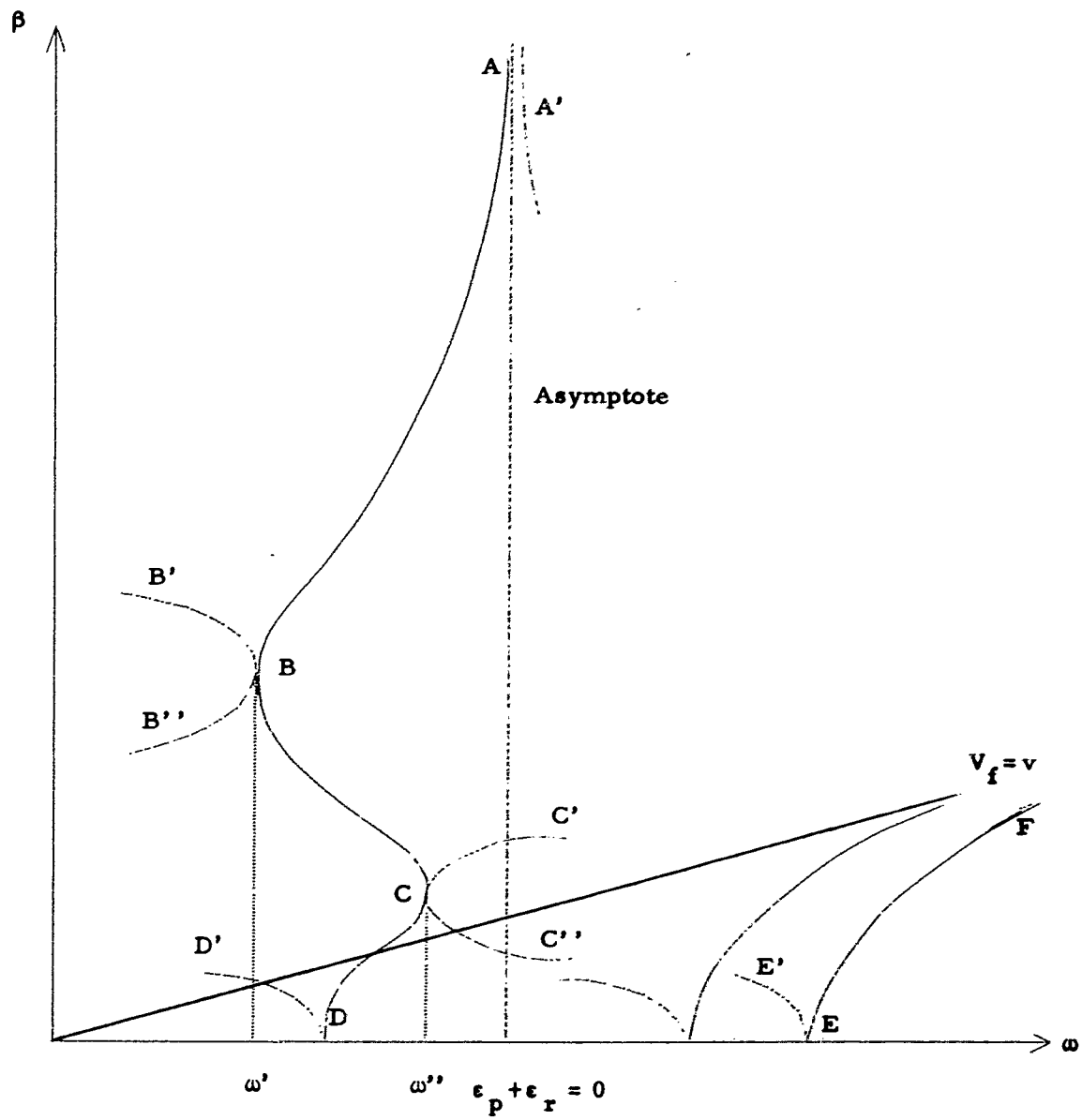

Fig. 2. The principal behaviour of the propagation constant as a function of the frequency. Solid lines indicate real solutions and dashed lines complex solutions.

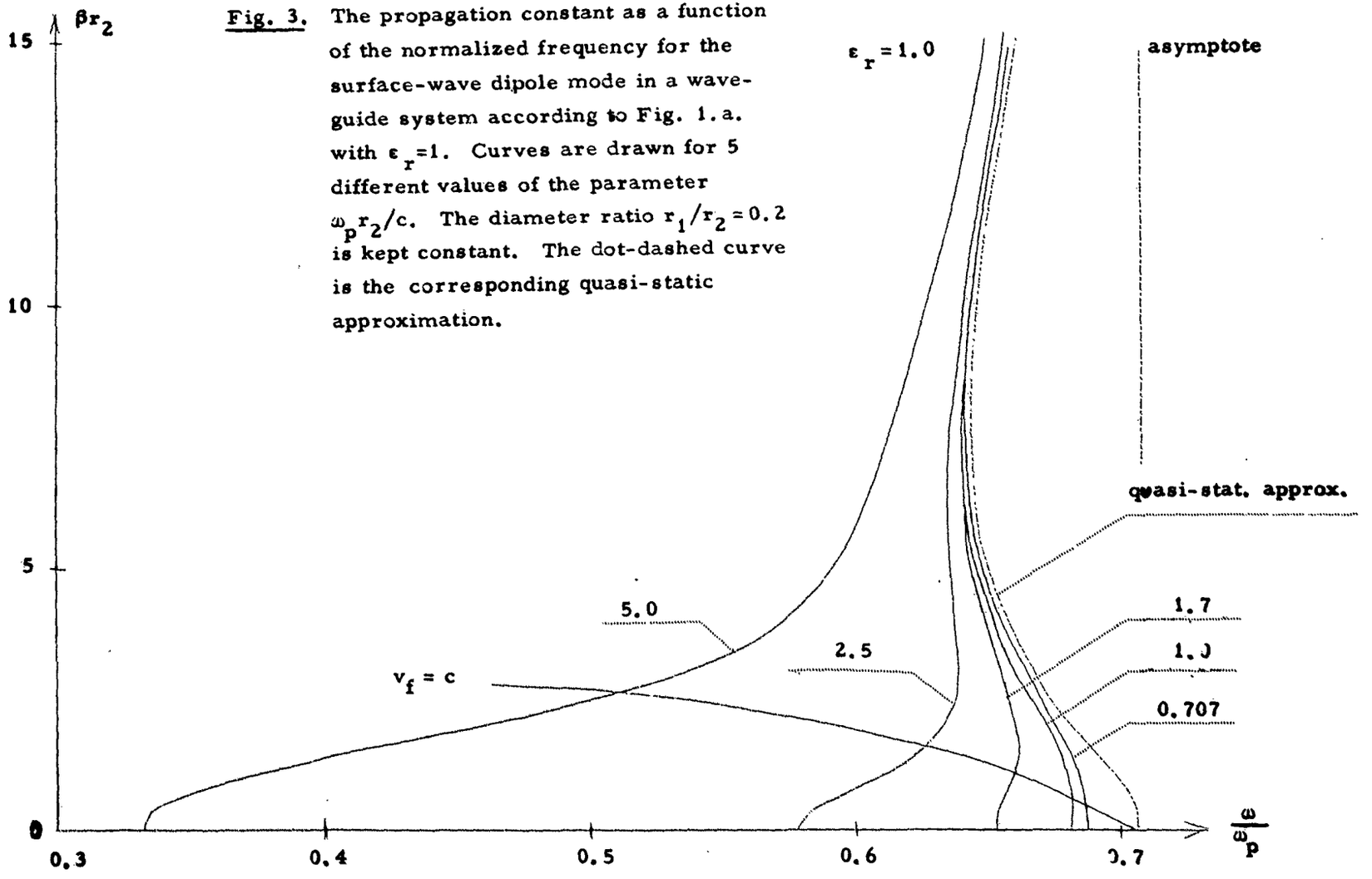

Fig. 3. The propagation constant as a function of the normalized frequency for the surface-wave dipole mode in a waveguide system according to Fig. 1.a. with $\varepsilon_r = 1$. Curves are drawn for 5 different values of the parameter $\omega_p r_2/c$. The diameter ratio $r_1/r_2 = 0.2$ is kept constant. The dot-dashed curve is the corresponding quasi-static approximation.

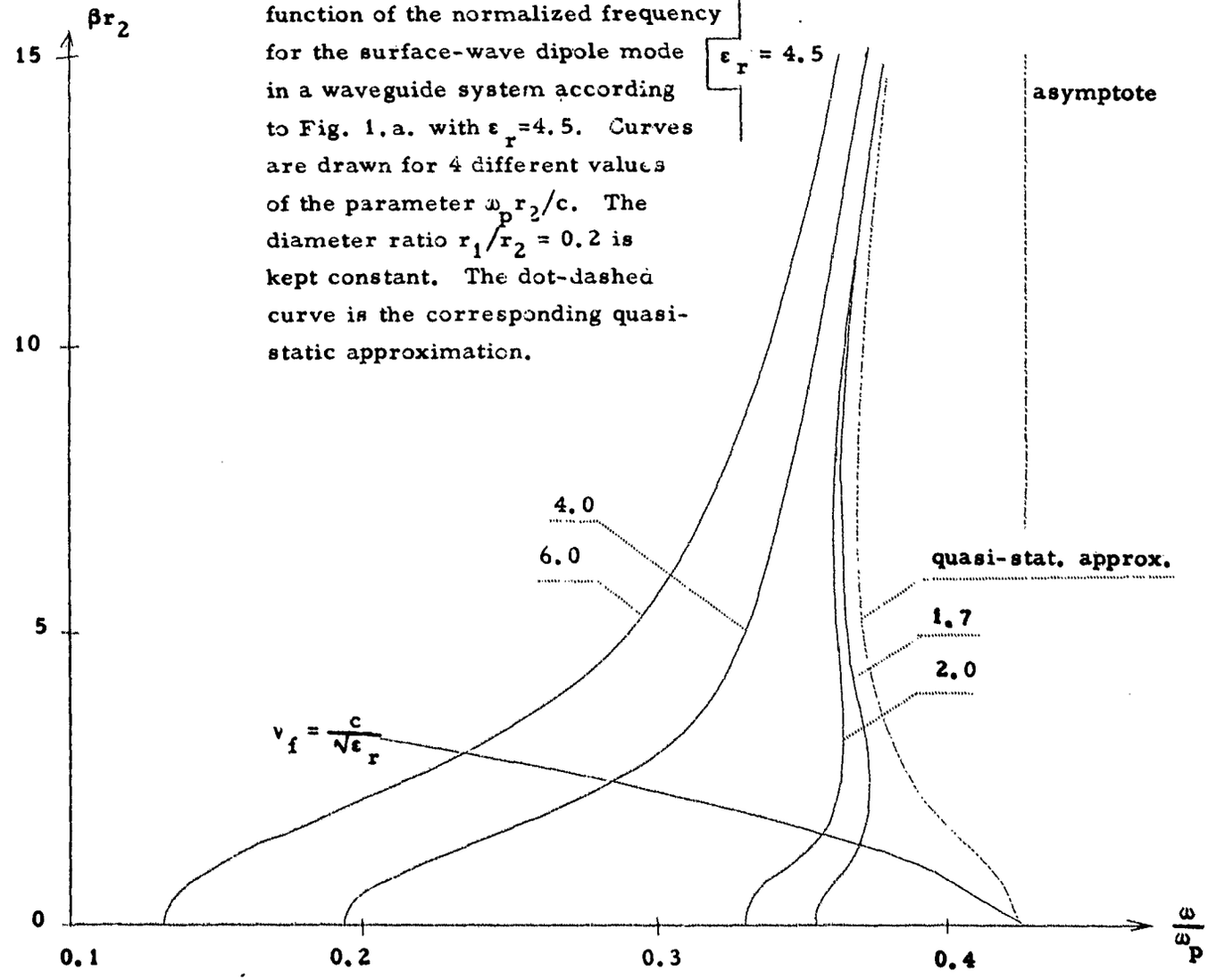

Fig. 4. The propagation constant as a function of the normalized frequency for the surface-wave dipole mode in a waveguide system according to Fig. 1, a. with $\varepsilon_r = 4.5$. Curves are drawn for 4 different values of the parameter $\omega_p r_2/c$. The diameter ratio $r_1/r_2 = 0.2$ is kept constant. The dot-dashed curve is the corresponding quasi-static approximation.

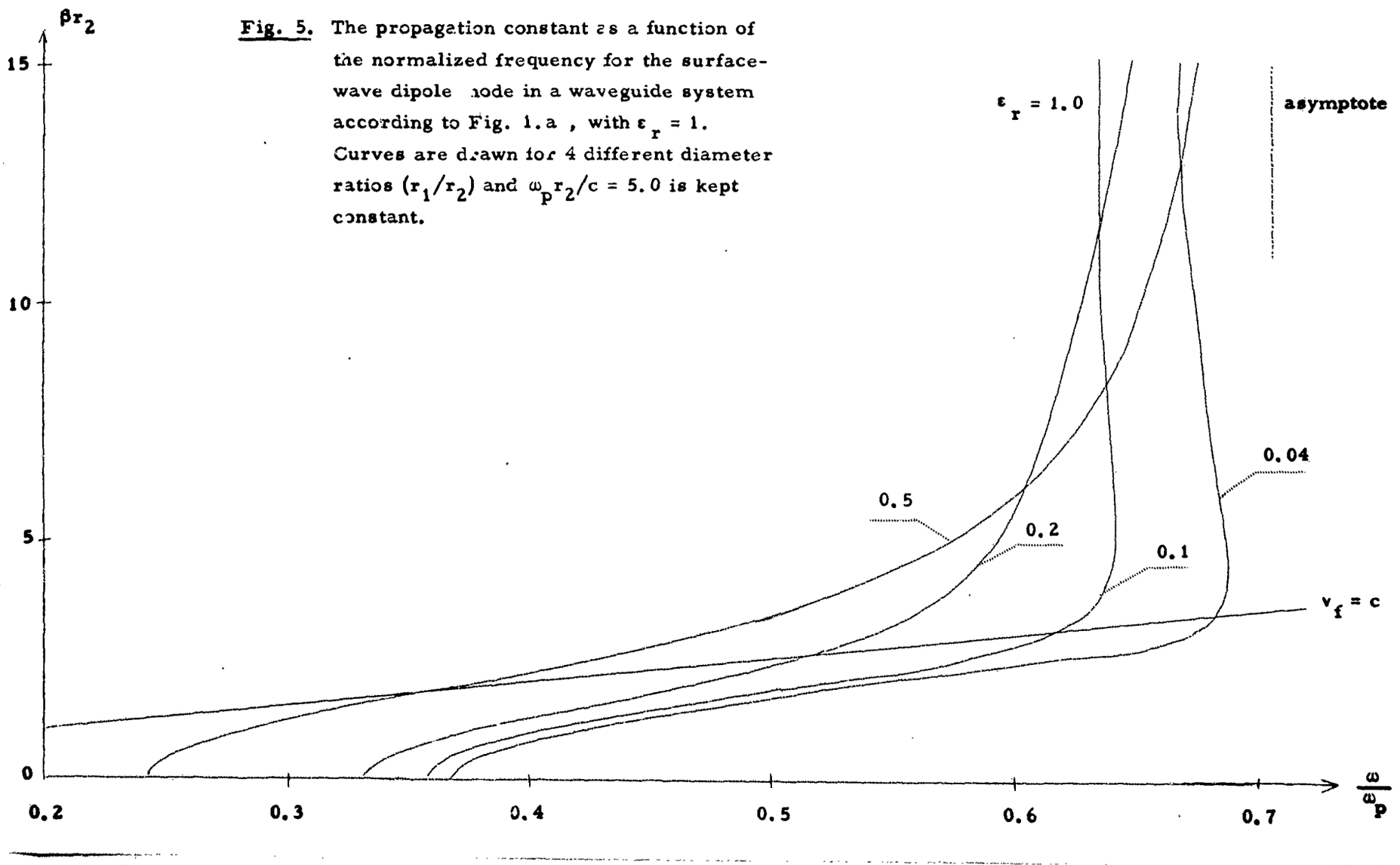

Fig. 5. The propagation constant as a function of the normalized frequency for the surface-wave dipole mode in a waveguide system according to Fig. 1.a , with $\varepsilon_r = 1$. Curves are drawn for 4 different diameter ratios (r_1/r_2) and $\omega_p r_2/c = 5.0$ is kept constant.

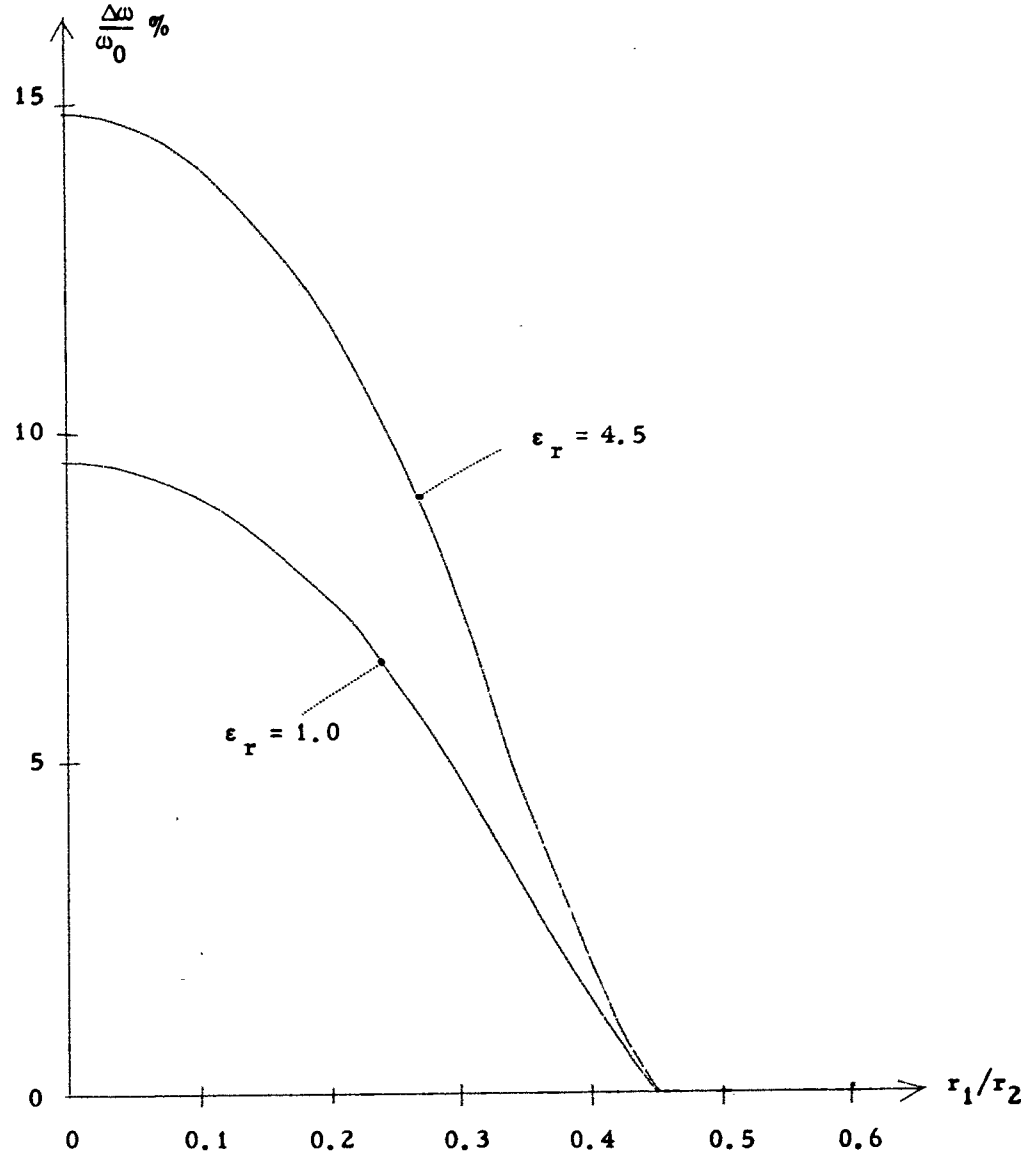

Fig. 6. The maximum relative bandwidth as a function of the diameter ratio. The relative bandwidth is defined in Eq. (4) and Fig. 2. Two curves are drawn for different values of ε_r.

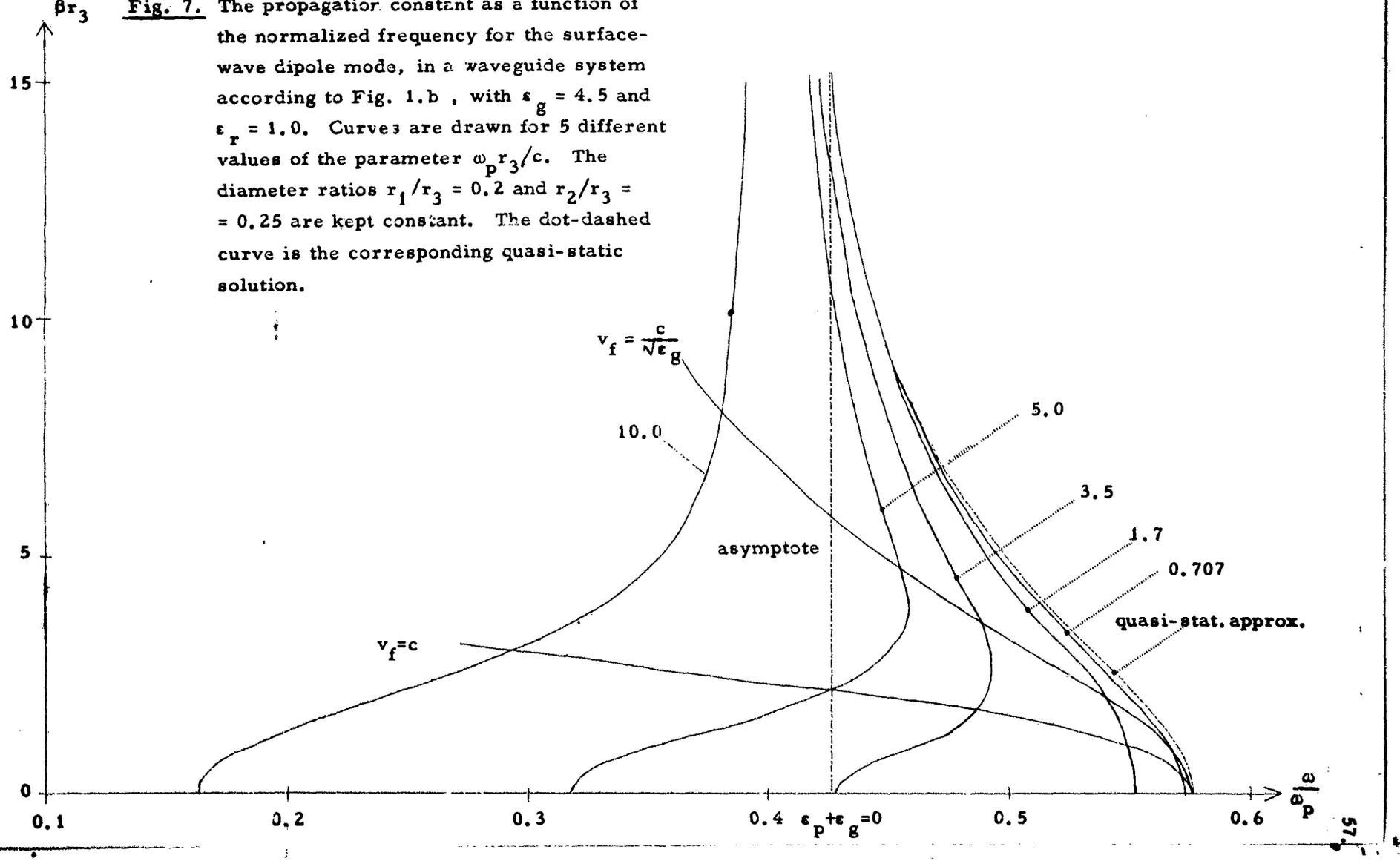

Fig. 7. The propagation constant as a function of the normalized frequency for the surface-wave dipole mode, in a waveguide system according to Fig. 1.b , with $\varepsilon_g = 4.5$ and $\varepsilon_r = 1.0$. Curves are drawn for 5 different values of the parameter $\omega_p r_3/c$. The diameter ratios $r_1/r_3 = 0.2$ and $r_2/r_3 = 0.25$ are kept constant. The dot-dashed curve is the corresponding quasi-static solution.

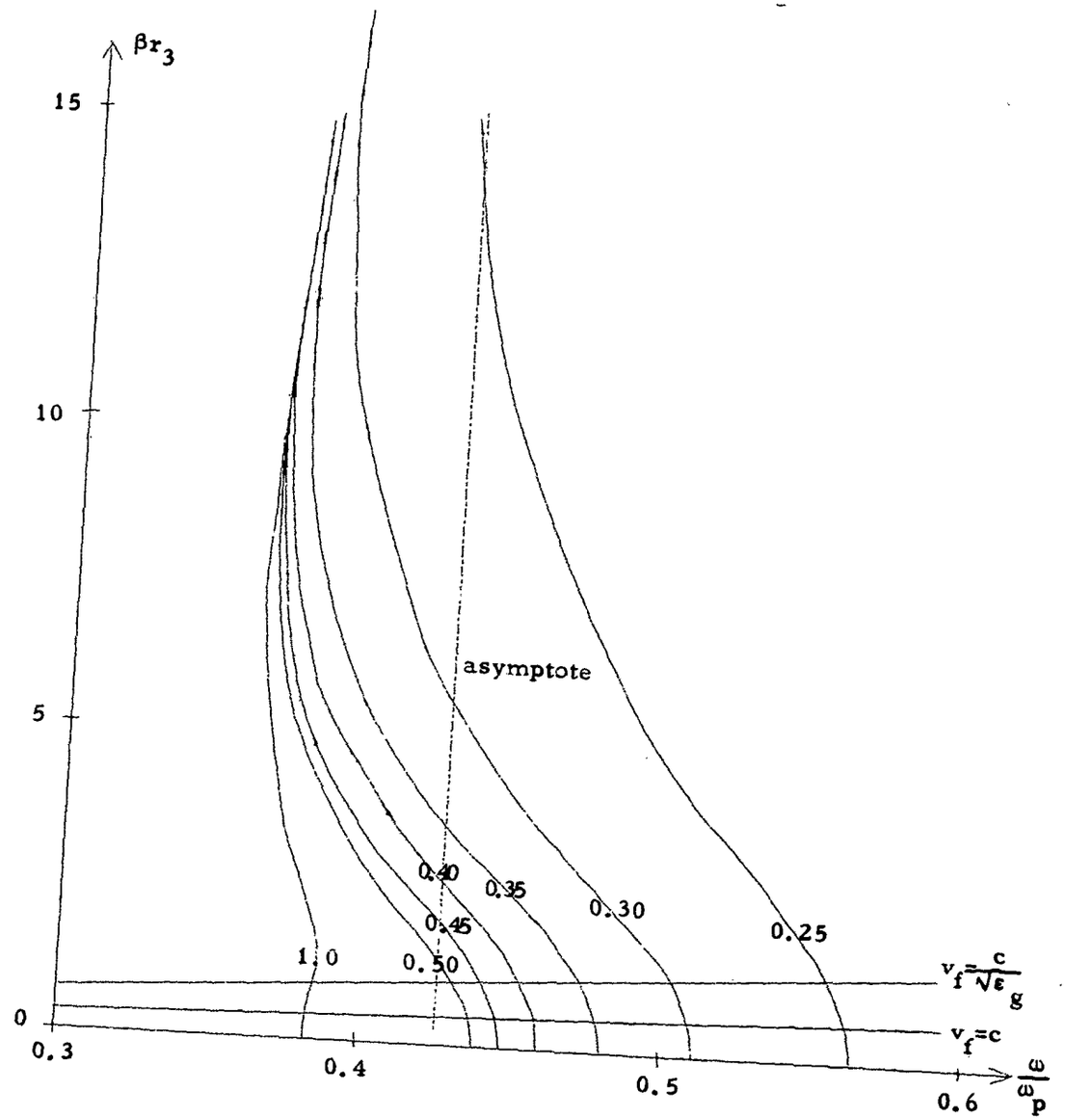

Fig. 8. The propagation constant as a function of the normalized frequency for the surface-wave dipole mode in a waveguide system according to Fig. 1.b., with $\varepsilon_g = 4.5$ and $\varepsilon_r = 1.0$. Curves are drawn for 7 different values of the glass thickness (r_2/r_3); $r_1/r_3 = 0.2$ and $\omega_p r_3/c = 1.2$ are kept constant.

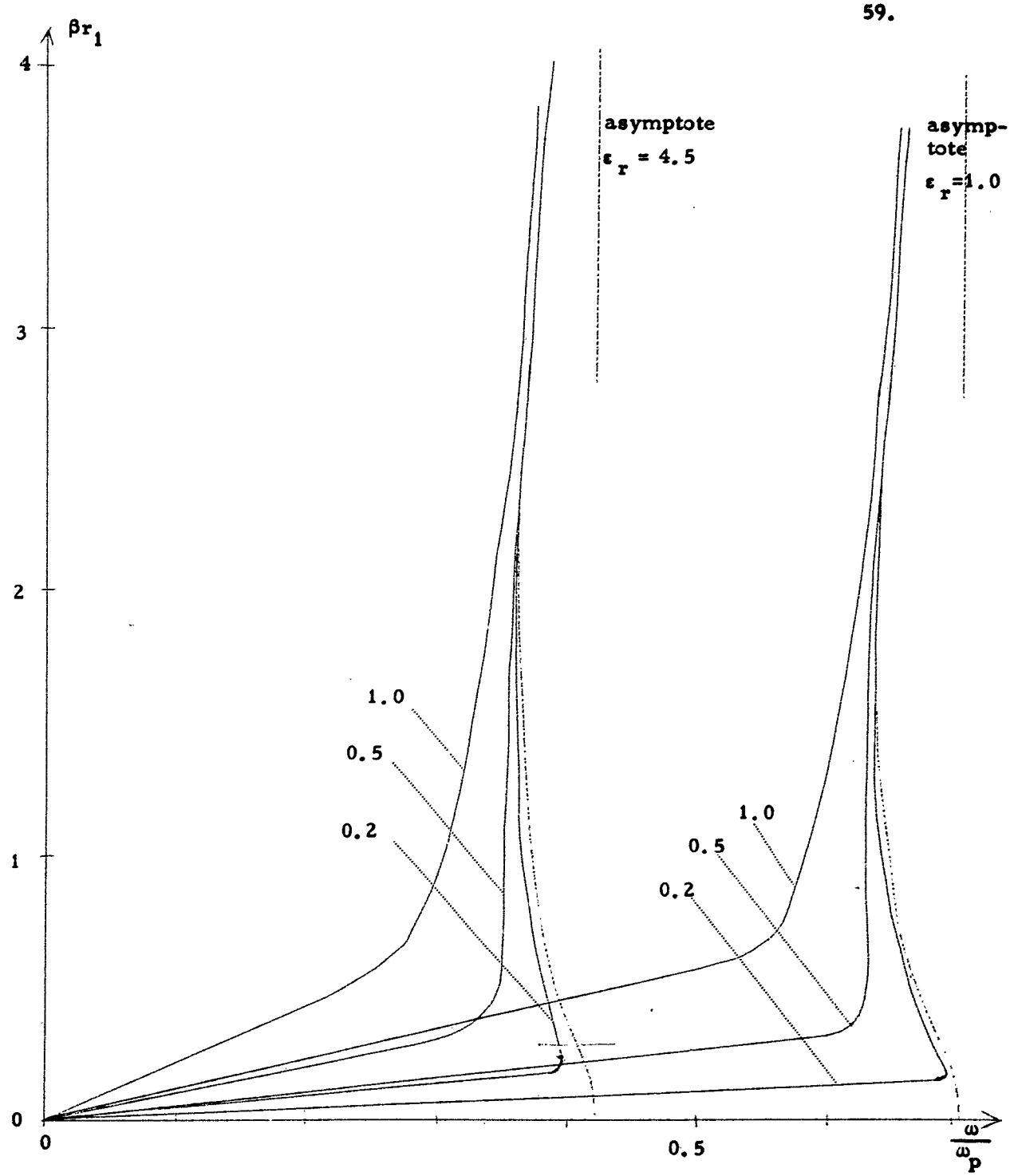

Fig. 9. The propagation constant as a function of the normalized frequency for the surface-wave dipole mode in a waveguide system according to Fig. 1.c. Curves are drawn for 2 different values of ε_r with $\omega_p r_1/c$ as a parameter. The dot-dashed curves are the corresponding quasi-static approximations.

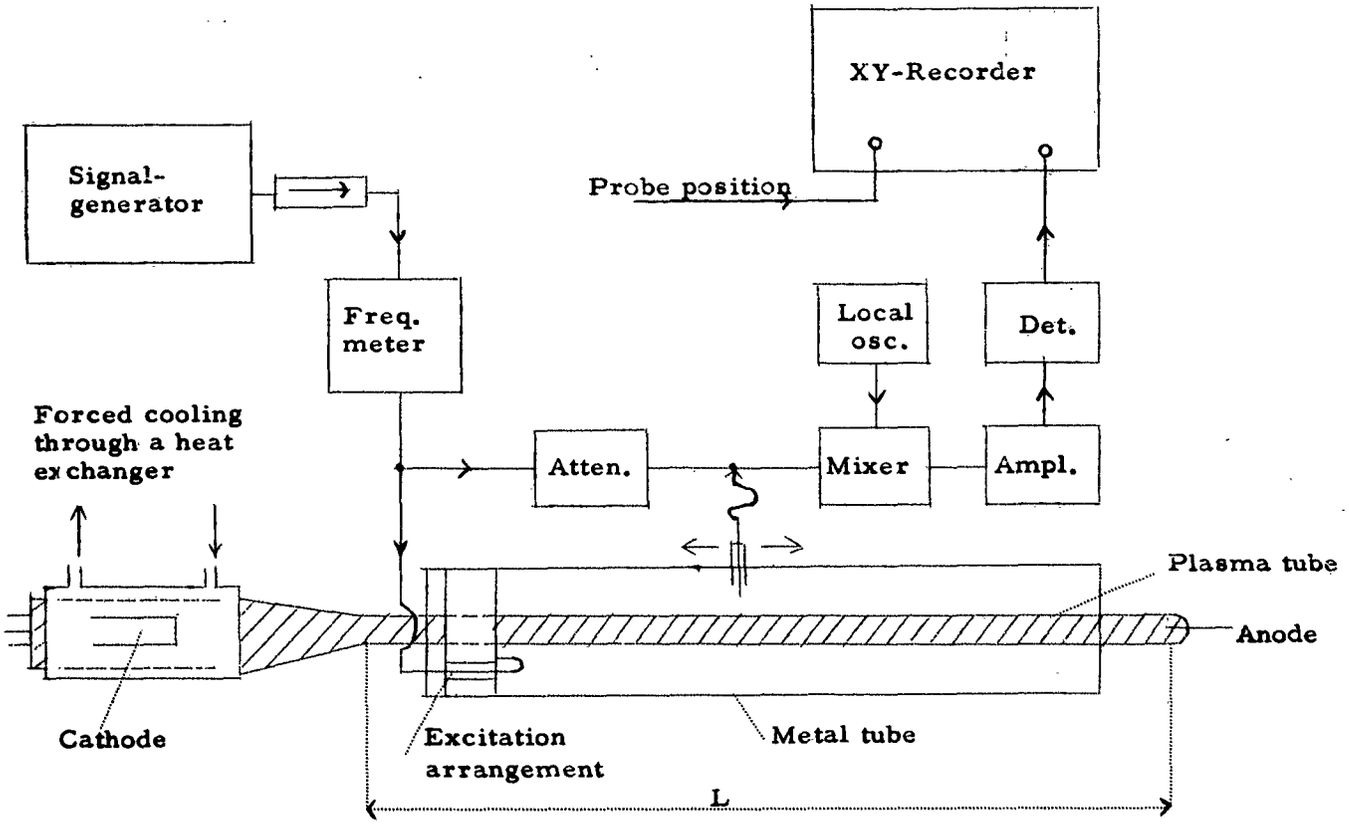

Fig. 10. The experimental set-up used in the dispersion measurements.

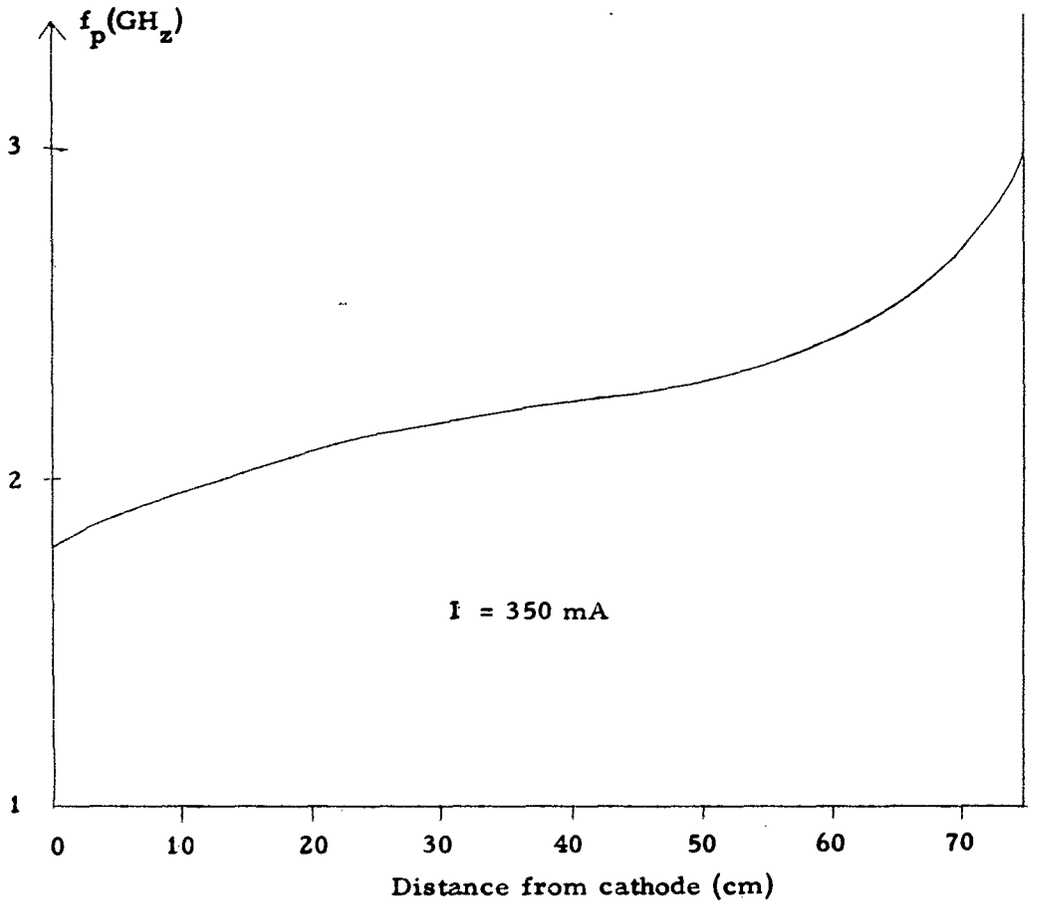

Fig. 11. The plasma frequency, $f_p = \omega_p/2\pi$, as a function of the distance from the cathode.

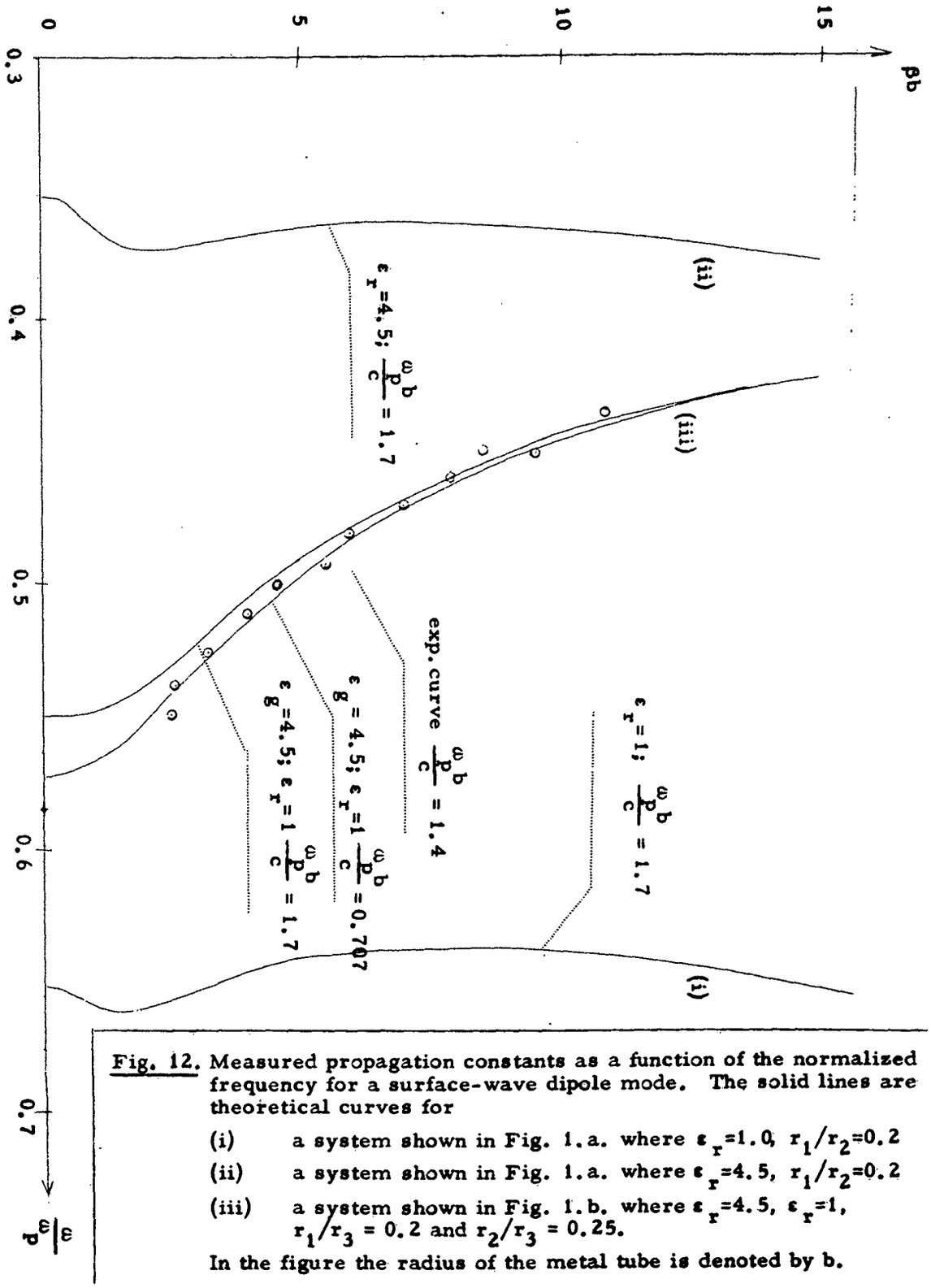

Fig. 12. Measured propagation constants as a function of the normalized frequency for a surface-wave dipole mode. The solid lines are theoretical curves for

(i) a system shown in Fig. 1.a. where ε_r=1.0, r_1/r_2=0.2

(ii) a system shown in Fig. 1.a. where ε_r=4.5, r_1/r_2=0.2

(iii) a system shown in Fig. 1.b. where ε_r=4.5, ε_r=1, r_1/r_3 = 0.2 and r_2/r_3 = 0.25.

In the figure the radius of the metal tube is denoted by b.

IV. PLASMA RESONANCE IN A GERMANIUM ROD

1. INTRODUCTION

The study of cyclotron resonance in semiconductors has yielded much valuable information on their energy-band structure[1,2,3]. In order to increase resonance detectability, a high carrier concentration is desirable, but this introduces magneto-plasma resonance effects as the carriers oscillate collectively[4,5]. Earlier, pure plasma resonance has been observed in flat samples of semiconducting material, where it is exhibited in a transition from a highly reflecting to a transmitted state, as the frequency of the incident wave is varied through resonance[6]. After the investigation described in the present paper was finished (Dec. 1961), it became known to the author that magnetoplasma resonance absorption in small Ge specimens in a constant field had been measured and successfully interpreted theoretically by Michel and Rosenblum[7]. They obtained good agreement between electron density determinations with Hall effect and with magneto-plasma resonance absorption. In the present paper the author investigates plasma resonance absorption with zero static magnetic field for a different geometry, i.e. a thin, semiconducting rod situated in an inhomogeneous field. This work is connected with similar studies on gas discharge plasma[8] and metal plasma[9] carried out at this laboratory. The agreement between density determinations with Hall effect and with plasma resonance absorption turns out to be good also in the present case of a rod.

2. THEORY

The theory presented here describes the effect on the wave propagation in a rectangular wave-guide that is exerted by a thin transverse plasma rod perpendicular to the electric field vector. The wave-guide propagates the TE_{10}-mode only and the plasma is rather lossy. The configuration is shown in Fig. 1.

2.1. Plasma permittivity

The plasma rod is treated as having an isotropic permittivity (relative dielectric constant) given by the formula[10]:

$$\varepsilon_3 = [\varepsilon - \frac{(\omega_p/\omega)^2}{(1 + \frac{1}{i\omega\tau})}] \qquad (1)$$

where ε = dielectric constant of the crystal lattice,

ω_p = plasma frequency,

τ = relaxation time of charge carriers in the plasma.

We consider an n-type semiconductor of cubic symmetry in equilibrium at low temperature. Thus, we may neglect contributions from positive-hole conduction and thermal motion of the electrons. The cubic symmetry is sufficient to make the permittivity a scalar in spite of the anisotropy of the crystal. Thus, the permittivity formula will hold for n-doped Ge and

$$\omega_p^2 = \frac{e^2 n_0}{\varepsilon_0 m^*}$$

where n_0 = density of conduction electrons

m^* = effective mass of conduction electrons.

There has been some confu ion in the past about the so-called Lorentz contribution to the local electric field acting on the electrons[10]. The inclusion of such a contribution in the formula for the permittivity is discussed in the Appendix.

2.2.

Plasma rod in a waveguide

The theory of microwave scattering by a plasma rod across a waveguide is given briefly in the Appendix. A thin rod of plasma, that is lossy, but not too dense, is seen to be adequately described by the equivalent lumped circuit in Fig. 2.

The lumped elements are given by the equations

$$C_1 = \frac{\varepsilon - 1}{\varepsilon + 1} \cdot \frac{\varepsilon_0 \pi a r_0^2}{b^2} \tag{2}$$

$$C = \frac{2}{\varepsilon + 1} \cdot \frac{\varepsilon_0 \pi a r_0^2}{b^2} \tag{3}$$

$$L = \frac{(\varepsilon + 1)^2}{2\omega_p^2} \cdot \frac{b^2}{\varepsilon_0 \pi a r_0^2} \tag{4}$$

$$r = \frac{(\varepsilon + 1)^2}{2\omega_p^2 \tau} \cdot \frac{b^2}{\varepsilon_0 \pi a r_0^2} \tag{5}$$

and the characteristic admittance of the waveguide is given by Eq. (57).

The displacement current due to vibrating lattice electrons flows through C_1. The series resonance circuit (C, L, r) carries the convection current of free electrons. Both these currents shunt the transmission line. There are thus two different resonances in the system: one series resonance, $\omega_1 = \sqrt{1/LC}$, giving a high shunt current and a reflection maximum, and one parallel resonance, giving a low shunt current and a reflection minimum, $\omega_2 = \sqrt{(C + C_1)/LCC_1}$, where $\omega_2 > \omega_1$.

Expressed in physical quantities one has from Eqs. (2) - (4):

$$(\omega_p/\omega_1)^2 = (\varepsilon + 1) \tag{6}$$

$$(\omega_p/\omega_2)^2 = (\varepsilon - 1) \tag{7}$$

The series resonance, ω_1, is called plasma resonance and is pronounced only when the rod is thin and the damping is not too high.

The validity range of the equivalent circuit of Fig. 2 is given by four conditions:

1. The rod diameter shall be small compared to the waveguide height:
$$(2r_0/b)^2 \ll 1 \qquad (8)$$

2. The rod diameter shall be small compared to the free space wave-length:
$$(2\pi r_0/\lambda)^2 \ll 1 \qquad (9)$$

3. The rod diameter shall be small compared to the wave-length in the rod (or the skin depth, if the waves are evanescent):
$$|\varepsilon_3|\ (2\pi r_0/\lambda)^2 \ll 1 \qquad (10)$$

4. The electron relaxation time must not be too long in order that the dipole field shall predominate as is assumed. This is expressed in the following condition:
$$(2\pi r_0/\lambda)^2 \lesssim \frac{2(\varepsilon + 1)}{\pi(\omega\tau)} \qquad (11)$$

3. EXPERIMENTAL SET-UP

In order to observe plasma resonance in a semiconductor it is imperative to reduce the damping by choosing the semiconducting material and the experimental conditions carefully with the aim to get an $(\omega_1\tau)$-value as high as possible. As ω_1 and ω_p are coupled by the resonance condition (6), a high ω_1 implies a low resistivity semiconductor, which, in turn, would have a small τ-value. A decrease in the temperature will increase τ, but at the same time the electron density and therefore ω_p and ω_1 will decrease. The best choice available appeared to be a Ge-rod, doped with Sb so as to have a room-temperature resistivity of 6.55 Ω cm, and to put it in an 8 mm waveguide at liquid hydrogen temperature. This should give an $(\omega_1\tau)$-value of about 3.

An analysis, based on the equivalent circuit of Fig. 2, shows that the reflection from such a rod is almost unaffected by the passage through plasma resonance. Therefore we chose to observe the absorption resonance, which remains pronounced down to $\omega_1 \tau \approx 2$. Instead of varying the frequency, ω, so as to pass through resonance, we varied the plasma frequency (electron density), by changing the rod temperature. The electron density covers about three octaves, when the temperature is increased from the triple point to the boiling point of hydrogen (13.8°K to 20.4°K). This manner of changing the density of free electrons has the advantage that thermal equilibrium is conserved. The density is approximately the same everywhere in the rod.

The experimental set-up is shown in Fig. 3 and described below:

The microwave power, 46 mW at λ = 8.65 mm, is fed from a klystron through a calibrated attenuator to the section containing the Ge-rod (cross-section 0.45 x 0.60 mm). By means of a shaft, the rod can be rotated manually through 180° around its axis from outside the cryostat. The line is terminated by a matched load and the waveguide section inside the cryostat is filled with helium and it is pressure isolated from the outside by means of individually matched mica windows.

The cryostat has an outer container with liquid nitrogen and an inner container with liquid hydrogen. The inner container can be evacuated above the hydrogen surface to lower the temperature and can be filled with helium gas to avoid air being sucked into the cryostat.

The resistance of the Ge-rod has a large negative temperature coefficient. Thus, the microwave power absorbed by the rod can be measured by connecting the rod to a self-balancing thermistor bridge (Hewlett-Packard power meter). The rod is shunted with a variable resistance so that the bridge can be balanced for different rod resistances without changing the built-in bridge resistance of the meter. When the shunt resistance is known, the power absorbed in the rod may easily be calculated from the reading of the power meter.

The self-balancing bridge thus keeps the rod resistance constant and consequently also the density of free electrons. The surrounding hydrogen bath is kept at a temperature just below that of the rod. The calibrated attenuator is used to regulate the microwave power, so that the power meter shows a relatively constant deflection, in spite of the variations in the absorption coefficient with temperature.

4. EXPERIMENTAL RESULTS

4.1. Measurements

As described above, the ratio of the microwave power absorbed in the rod to the power incident on the rod - the absorption coefficient - was measured as a function of the rod resistance. The experimental results are plotted in Fig. 4.

The absorption coefficient shows the expected resonance behaviour. The points in Fig. 4 are measured with the rod oriented as shown in Fig. 5, which gives maximum absorption when the rod is rotated. Technological difficulties made it necessary to use a rod with a rectangular cross-section instead of the circular one, on which the theory is based. Thus, the isotropy of the permittivity could not be checked but the measured ratio, 0.8, of the variation of absorption with orientation of the rod is not inconsistent with the assumption of isotropy.

4.2. Comparison with Theory

The dimensions of the rod (length, l = 11.2 mm, cross-section, $S = 0.45 \times 0.60$ mm^2) determine the product $(n_0 R \mu)$, where R is the dc resistance and μ the carrier drift mobility in the rod

$$(n_0 R \mu) = \frac{l}{eS} \qquad (12)$$

As $\omega_p^2 = \frac{e^2 n_0}{\varepsilon_0 m^*}$ and $\mu = \frac{\varepsilon \tau}{m^*}$ one has

$$(\frac{\omega_p}{\omega})^2 = \frac{1}{S \varepsilon_0 \omega} \cdot \frac{1}{(\omega\tau)R} = \frac{21500}{(\omega\tau)R} \quad (R \text{ in } \Omega) \qquad (13)$$

An analysis of the equivalent circuit in Fig. 2 shows that, when ω_p is varied, the absorption maximum occurs at

$$(\frac{\omega_p}{\omega})^2 = (\varepsilon + 1)\sqrt{1 + \frac{1}{(\omega\tau)^2}} \qquad (14)$$

which should be compared with the plasma resonance condition of Eq. (6). In the derivation of Eq. (14) the variation of τ with temperature can be neglected as long as $(\omega\tau)$ is large enough to give an observable absorption resonance.

Finally, for $\epsilon = 16$, Eqs. (13) and (14) give

$$\omega\tau = \sqrt{\left(\frac{1265}{R_{res}}\right)^2 - 1} \qquad (15)$$

From Fig. 4 we find the rod resistance at the absorption maximum to be

$$R_{res} = 465\ \Omega$$

Eq. (15) now gives

$$(\omega\tau)_{res} = 2.53$$

$$\tau_{res} = 1.16 \cdot 10^{-11}\ \text{sec}$$

There is a slight inconsistency in this derivation, as the relaxation time in Eq. (13) has its dc value, while the relaxation time in Eq. (14) should be taken at the microwave frequency. These two values are not necessarily identical. As $(\omega\tau)^2 \gg 1$, Eq. (14) is almost independent of τ, which means that Eq. (15) gives the dc value of the relaxation time.

Germanium has ellipsoidal energy valleys in the conduction band, so that[12]

$$\frac{1}{m^*} = \frac{1}{3}\left(\frac{1}{m_{//}} + \frac{2}{m_{\perp}}\right), \qquad (16)$$

where $m_{//} = 1.58 \cdot m$ and $m_{\perp} = 0.082 \cdot m$ have been determined from cyclotron resonance measurements[2]. Eq. (16) is valid if the relaxation times along the valley axis and perpendicular to it are identical, which has been shown[13] to be a good approximation for Ge. Thus, $m^* = 0.12\ m$ from Eq. (16) giving

$$\mu = 17.0\ m^2/V \cdot \text{sec}$$

$$n_0 = 3.3 \cdot 10^{19}\ m^{-3}$$

at the absorption resonance, which occurs at about 16°K. These values are in good agreement with Hall-effect determinations of the mobility in similar Ge samples[14].

To establish the agreement between experiment and theory further, the resonance line width will now be investigated. A Q-value of the resonance is defined:

$$Q = \frac{2(\omega\tau)_{res}\,(\omega_p/\omega)^2_{res}}{[(\omega\tau)_2\,(\omega_p/\omega)^2_2 - (\omega\tau)_1\,(\omega_p/\omega)^2_1]} \tag{17}$$

where index 1 and 2 refer to the points where the absorption has half its maximum value.

From the equivalent circuit in Fig. 2 one gets

$$\frac{1}{Q} = \frac{\sqrt{4(\omega\tau)^2_{res} + 3 - 4(\omega\tau)_{res}\sqrt{1 + (\omega\tau)^2_{res}}} - (\omega\tau)_{res}\cdot\delta}{\sqrt{1 + (\omega\tau)^2_{res}}} \tag{18}$$

This expression is valid only when the absorption coefficient at resonance is much smaller than unity. It is assumed that

$$(\omega\tau)_1 = (\omega\tau)_{res}\,(1 + \delta) \text{ and } (\omega\tau)_2 = (\omega\tau)_{res}\,(1 - \delta),$$

where $\delta \ll 1$ and positive.

If $(\omega\tau)^2 \gg 1$, Eq. (18) is simplified:

$$\omega\tau \approx \frac{Q}{1 + Q\delta} \tag{19}$$

For our case, Eqs (13) and (17) yield

$$Q = \frac{2/R_{res}}{1/R_2 - 1/R_1} \tag{20}$$

Fig. 4 gives $R_1 = 595\,\Omega$ and $R_2 = 320\,\Omega$ so that

$Q = 2.98$

If it is assumed that $\delta = 0.1$, meaning a $\pm$ 10% variation of τ with temperature within the resonance width (cf. similar Ge specimens in Ref. 14), Eq. (18) gives $(\omega\tau)_{res} = 2.22$. This value, which should be valid at the microwave frequency, is about 10% lower than the dc value computed from Eq. 15. The accuracy is not good enough to warrant any conclusions, but one should expect the rf value to be lower than the dc value.

Finally the maximum value of the absorption coefficient, A, will be considered.

The equivalent circuit in Fig. 2 yields

$$A_{max} = \frac{A^{(0)}}{(1 + A^{(0)}/2)^2} \tag{21}$$

where

$$A^{(0)} = \frac{(\lambda/b)\,(2\pi r_0/\lambda)^2}{(\varepsilon + 1)\sqrt{1 - (\lambda/2a)^2}\left[\sqrt{1 + (\omega\tau)^2} - \omega\tau\right]} \tag{22}$$

λ = 8.65 mm and a = 7.1 mm and b = 3.55 mm are the dimensions of the waveguide.

From Fig. 4 we obtain the value

A_{max} = 0.067

and this together with the calculated value of ($\omega\tau$) enables us to assign an equivalent radius r_0 to the rod:

1) $\omega\tau$ = 2.53 $\quad$ $2r_0$ = 0.76 mm

2) $\omega\tau$ = 2.22 $\quad$ $2r_0$ = 0.81 mm

A comparison between the equivalent rod with diameter 0.81 mm and the actual rod with rectangular cross-section is made in Fig. 5.

It is now possible to determine the validity range of the equivalent circuit for the Ge-rod used. A plausible value of the equivalent rod diameter is chosen.

$2r_0 = 0.65$ mm, $\omega\tau = 2.22$ and $(\frac{\omega_p}{\omega})^2 = \frac{8500}{R}$

1. $(2r_0/b)^2 = 0.034$ and Condition (8) is thus fulfilled.

2. $(2\pi r_0/\lambda)^2 = 0.056$ and -"- (9) " " "

3. $|\varepsilon_3|\,(2\pi r_0/\lambda)^2 < 1$, if $R > 250\ \Omega$. The minimum value of $|\varepsilon_3|(2\pi r_0/\lambda)^2$ is 0.37, which occurs at $R = 530\ \Omega$. Cond. (10) is thus not fulfilled for $R < 250\Omega$ and only poorly fulfilled for $R > 250\Omega$ (cf. Fig. 4).

4. $\frac{2(\varepsilon + 1)}{\pi(\omega\tau)} = 4.9$ and Condition (11) is thus fulfilled.

In view of the fact that Condition (10) is poorly fulfilled for our rod, the agreement with the simple theory is surprisingly good.

The determination of $(\omega\tau)_{res}$ from R_{res}, using Eq. (15), or from Ω, using Eq. (18), is not influenced by an inclusion of a Lorentz contribution to the local electric field acting on the free carriers (see the App., especially Eq. (24)). The drift mobility would be given by $\mu = \frac{(2+\varepsilon)}{3}\frac{e\tau}{m^*}$ and take a value 6 times larger than before, and the case is exactly the same for the drift mobility determined from a Hall effect measurement. Those two measurements together are thus not sufficient to settle the question, whether a Lorentz term should be included or not. As mentioned in the App, a pulse drift measurement is needed combined with either a plasma resonance or a Hall effect measurement. Such a comparison with the directly determined drift mobility[15] shows that the Lorentz contribution is negligible.

There is no indication of discrepancy between the simple theory and the observed width and shape of the absorption resonance, as in the case of polarized resonant emission from a mercury discharge[8]. This may be due to the fact that the theoretical idealization of uniform plasma density and negligible temperature velocity is much closer to the truth for our Ge rod than for a gas discharge in a glass tubing.

Substitution of $(\omega\tau)$ from Eq. (15) into Eq. (13) shows that ω_p^2 and therefore also the electron density is directly determined by the rod resistance at resonance. As already observed by Michel and Rosenblum[7], the plasma resonance absorption thus could be used to determine the charge carrier density in semiconductors directly without recurrence to Hall effect measurements with their uncertainty as to the theoretical value of the ratio drift mobility to Hall mobility. The application and accuracy of the method are limited by the low Q-values attainable.

APPENDIX

The local electric field

There is a theoretical possibility that the local electric field, E_{loc}, acting on the conducting electrons, is different from the macroscopic field, E, in the crystal. In this general case the permittivity for the crystal with plasma is

$$\varepsilon_3 = [\varepsilon - (\frac{E_{loc}}{E}) \cdot \frac{(\omega_p/\omega)^2}{(1 + \frac{1}{i\omega\tau})}] \qquad (23)$$

At the lattice points in a crystal of cubic symmetry there is a local field[16]

$$E_{loc} = \frac{2 + \varepsilon}{3} \cdot E \qquad (24)$$

This field could possibly be the effective field for the conduction electrons also. There are, however, strong reasons to discard this assumption. It would mean that the theoretical value of the ratio drift mobility to Hall mobility should be multiplied by the factor $(\frac{2 + \varepsilon}{3})$ in contradiction to the general agreement between measured ratio values for Ge and Si and the theoretical values based on $E_{loc} = E$. The drift mobility can be measured directly by the pulse drift method[15] and the Hall mobility by a Hall effect measurement. It should be observed that $\frac{2 + \varepsilon}{3} = 6$ for Ge.

It is also possible that the local field is influenced by the dipole moment of the vibrating conduction electrons themselves, as has been proposed[17]. In considering this possibility we do not include the effect of a contribution from that source to the local field at the crystal lattice points. We get

$$E_{loc} = [\, 1 + \frac{1/3(\omega_p/\omega)^2}{1 + \frac{1}{i\omega\tau}} \,]^{-1} \cdot E \qquad (25)$$

$$\varepsilon_3 = \{\varepsilon - \frac{(\omega_p/\omega)^2}{[1 + \frac{1}{3}(\omega_p/\omega)^2 + \frac{1}{i\omega\tau}]}\} \qquad (26)$$

Thus $\mathrm{Re}(\varepsilon_3) < 0$ could never be reached for an ε larger than 3. This is contradicted by the observed rapid change from transmission to total reflection in heavily doped germanium in the far infrared[6], which is believed to be a consequence of passage through $\mathrm{Re}(\varepsilon_3) = 0$.

Theory of a circular plasma rod across a waveguide

The exact treatment of a circular plasma rod across a waveguide is indicated below (see Fig. 1), but only a limiting case valid for a thin rod with comparatively short electron relaxation time is worked out completely. The fields have the time dependence $\exp(i\omega\tau)$ and the temperature is so low, that the temperature-induced electrostatic field solution in the rod may be neglected.

Only the field vectors in the axial direction (z-direction) are given, as the transverse components are easily deduced from the formulas:

$$\beta^2 \mathbf{E}_t = \nabla_t\left(\frac{\partial E_z}{\partial z}\right) + i\omega\mu_0 (\hat{z} \times \nabla_t H_z) \tag{27}$$

$$\beta^2 \mathbf{H}_t = -\frac{i}{\omega\mu_0}\left[\beta^2 + \left(\frac{\pi}{a}\right)^2\right](\hat{z} \times \nabla_t E_z) + \nabla_t\left(\frac{\partial H_z}{\partial z}\right) \tag{28}$$

where $\beta = \sqrt{\left(\frac{\omega}{c}\right)^2 - \left(\frac{\pi}{a}\right)^2}$

$\hat{z}$ is the unit vector in the z-direction. Index t stands for "transverse" to the z-direction. Formulas (27) and (28) are applicable outside the rod; inside the rod β is replaced by k, defined as

$$k = \sqrt{\varepsilon_3\left(\frac{\omega}{c}\right)^2 - \left(\frac{\pi}{a}\right)^2}$$

The TE_{10}-mode, incident in the y-direction and arbitrarily normalized, has the form:

$$E_z^{(i)} = 0 \tag{29}$$

$$H_z^{(i)} = \cos\left(\frac{\pi z}{a}\right) \exp(-i\beta y) \tag{30}$$

Using the expansion $\exp(-i\beta y) = \sum_n J_n(\beta r) \exp(-in\varphi)$, where $y = r \cdot \sin\varphi$ and the summation is from $-\infty$ to $+\infty$, changes this into

$$E_z^{(i)} = 0 \tag{31}$$

$$H_z^{(i)} = \sum_n \cos\left(\frac{\pi z}{a}\right) J_n(\beta r) \exp(-in\varphi) \tag{32}$$

Although $E_z^{(i)} = 0$, the electric field inside the rod and the scattered electric field will have $E_z \neq 0$. This field component is excited by the longitudinal current in the plasma rod induced by the H_y-component. Inside the rod we get

$$E_z^{(1)} = \sum_n \sin\left(\frac{\pi z}{a}\right) A_n J_n(kr) \exp(-in\varphi) \tag{33}$$

$$H_z^{(1)} = \sum_n \cos\left(\frac{\pi z}{a}\right) C_n J_n(kr) \exp(-in\varphi) \tag{34}$$

If the walls at $x = \pm b/2$ were moved out to infinity, the scattering fields outside the rod would be represented by simple cylindrical waves

$$E_z^{(2)} = \sum_n \sin\left(\frac{\pi z}{a}\right) B_n H_n^{(2)}(\beta r) \exp(-in\varphi) \tag{35}$$

$$H_z^{(2)} = \sum_n \cos\left(\frac{\pi z}{a}\right) D_n H_n^{(2)}(\beta r) \exp(-in\varphi) \tag{36}$$

The walls will introduce mirror images of the rod and images of images in an infinite array. Thus, the boundary conditions at the walls are fulfilled by the complete scattering fields:

$$E_z^{(2)} = \sum_n \sum_m \sin\left(\frac{\pi z}{a}\right) B_n H_n^{(2)}(\beta r_m) \exp(-in\varphi_m) \tag{37}$$

$$H_z^{(2)} = \sum_n \sum_m \cos\left(\frac{\pi z}{a}\right) D_n H_n^{(2)}(\beta r_m) \exp(-in\varphi_m) \tag{38}$$

where r_m and φ_m are defined in Fig. 6. It should be observed that

$$A_{-n} = -A_n \qquad B_{-n} = -B_n$$

$$C_{-n} = C_n \qquad D_{-n} = D_n$$

For a point in the waveguide far away from the rod, $|y| \gg b$, it is possible to deduce the following asymptotic expressions:

$$E_z^{(2)} \to 0 \tag{39}$$

$$H_z^{(2)} \to \sum_n \frac{2}{\beta b} \cos\left(\frac{\pi z}{a}\right) \left(\frac{y}{|y|}\right)^n D_n \exp(-i\beta |y|) \tag{40}$$

which are valid as long as the waveguide can propagate only the TE_{10}-mode. The scattered wave may thus be described as one back-scattered wave giving a voltage reflection coefficient

$$\Gamma = -\frac{2}{\beta b} \sum_n (-1)^n D_n \tag{41}$$

and one forward-scattered wave, which added to the incident wave gives a voltage transmission coefficient

$$T = \left(1 + \frac{2}{\beta b} \sum_n D_n\right) \tag{42}$$

Γ and T are referred to y = 0 (a plane through the centre of the rod), and give a complete description of the effect of the rod on the transmission line. The D_n can be determined from the conventional boundary conditions for the fields at the surface of the dielectric rod.

$(\beta r_0)^2 \ll 1$ and $|kr_0|^2 \ll 1$

The case $(\beta r_0)^2 \ll 1$ and $|kr_0|^2 \ll 1$ will now be considered in detail. As a zeroth order approximation, the contribution from the image fields to the fields at the rod boundary is neglected. We get to the lowest order in (βr_0):

$$D_0^{(0)} = - i \frac{\pi}{2} \left(\frac{\omega}{\beta c}\right)^2 \left(\frac{\beta r_0}{2}\right)^4 (\varepsilon_3 - 1) \tag{43}$$

$$D_n^{(0)} = - \frac{i\pi (\omega/\beta c)^2}{(n-1)!\, n!} \left(\frac{\beta r_0}{2}\right)^{2n} \left(\frac{\varepsilon_3 - 1}{\varepsilon_3 + 1}\right) \quad \text{for } n > 0;\ D_{-n} = D_n \tag{44}$$

The values of D_n are true at $\mathrm{Re}(\varepsilon_3) \approx -1$ only if

$$|\mathrm{Im}(\varepsilon_3)| \gg \frac{2\pi}{\beta b} \left(\frac{\omega r_0}{c}\right)^2 \tag{45}$$

For a semiconductor this is equivalent to the condition

$$(\omega\tau) \ll \frac{\beta b(\varepsilon + 1)}{2\pi \left(\frac{\omega r_0}{c}\right)^2} \tag{46}$$

Only D_1 and D_{-1} will contribute to Γ and T to the lowest order in (βr_0):

$$\Gamma^{(0)} = - \frac{i\pi}{\beta b} \left(\frac{\omega r_0}{c}\right)^2 \left(\frac{\varepsilon_3 - 1}{\varepsilon_3 + 1}\right) \tag{47}$$

$$T^{(0)} = 1 + \Gamma^{(0)} \tag{48}$$

The restriction on $\mathrm{Im}(\varepsilon_3)$ in Eq. (45) is equivalent to stating that $|\Gamma^{(0)}| \ll 1$ is a condition for $\Gamma \approx \Gamma^{(0)}$ to be valid. A further step in the approximation procedure will replace this condition by the less restrictive

$$|\mathrm{Im}(\varepsilon_3)| \gtrsim \frac{\pi}{2} \left(\frac{\omega r_0}{c}\right)^2 \tag{49}$$

which gives: $(\omega\tau) \lesssim \frac{2}{\pi} \frac{(\varepsilon + 1)}{(\omega r_0/c)^2}$ (50)

The new condition guarantees that still only the dipole mode, D_1 and D_{-1}, will contribute to the reflection coefficient at plasma resonance, $\mathrm{Re}(\varepsilon_3) = -1$. If $|\mathrm{Im}(\varepsilon_3)|$ is further decreased, at first the quadrupole mode, D_2 and D_{-2}, and later the sextupole mode, D_3 and D_{-3}, and higher modes contribute to the absorption and reflection at plasma resonance.

In this first order approximation, the image fields are added to the fields at the rod boundary and to this order of approximation:

$$D_1^{(1)} = \frac{D_1^{(0)}}{\left[1 - \frac{4}{\beta b} D_1^{(0)}\right]} \tag{51}$$

which gives

$$\Gamma^{(1)} = \frac{\Gamma^{(0)}}{\left[1 - \Gamma^{(0)}\right]} \tag{52}$$

$$T^{(1)} = \left[1 + \Gamma^{(1)}\right] = \frac{1}{\left[1 - \Gamma^{(0)}\right]} \tag{53}$$

The result is thus

$$\Gamma \approx \frac{\Gamma^{(0)}}{\left[1 - \Gamma^{(0)}\right]} \tag{54}$$

$$T \approx [1 + \Gamma] \approx \frac{1}{\left[1 - \Gamma^{(0)}\right]} \tag{55}$$

valid for $(\beta r_0)^2 \ll 1$

$|kr_0|^2 \ll 1$

with the addition of condition (50).

The form $T = (1 + \Gamma)$ tells us, that the rod constitutes a lumped shunt element in the waveguide. It is easily observed from Eq. (54), that the normalized shunt admittance is given by

$$\frac{Y}{Y_c} = -2\Gamma^{(0)} \tag{56}$$

where the characteristic admittance of the waveguide, Y_c, is given by

$$Y_c = \frac{a}{2b} \left(\frac{\beta c}{\omega}\right) (\varepsilon_0 c) \tag{57}$$

Using Eqs. (47), (1) and (57) the shunt admittance of Eq. (56) can be written

$$Y = \frac{\varepsilon_0 \pi a r_0^2}{b^2} \left[i\omega \left(\frac{\varepsilon - 1}{\varepsilon + 1}\right) + \frac{1}{\frac{(\varepsilon + 1)^2}{2\omega_p^2 \tau} + i\omega \frac{(\varepsilon + 1)^2}{2\omega_p^2} + \frac{1}{i\omega} \frac{(\varepsilon + 1)}{2}} \right] \tag{58}$$

A suitable equivalent circuit description of the rod in the waveguide is now obvious and given in Fig. 2 with the lumped elements as in Eq. (2) through (5).

REFERENCES

1. B. Lax, H.J. Zeiger and R.N. Dexter, Physica, 20, 818 (1954).
2. G. Dresselhaus, A.F. Kip and C. Kittel, Phys. Rev. 98, 368 (1955).
3. B. Lax, H.J. Zeiger and R.N. Dexter, Phys. Rev. 104, 637 (1956).
4. G. Dresselhaus, A.F. Kip and C. Kittel, Phys. Rev. 100, 618 (1955).
5. B. Lax, IRE Trans. on Microwave Theory and Techniques, 9, 83 (1961).
6. W.G. Spitzer, F.A. Trumbore and R.A. Logan, Journal of Appl. Phys. (USA), 32, 1822 (1961).
7. R.E. Michel and B. Rosenblum, Phys. Rev. 128, 1646 (1962).
8. B. Agdur, B. Kersar and F. Sellberg, Phys. Rev. 128, 1 (1962).
9. B. Agdur, G. Böling, F. Sellberg and Y. Öhman. Phys. Rev. 130, 996 (1963).
10. See e.g. R.A. Smith, "Semiconductors", Ch. 7.6, Camb. Un. Press (1959).
11. The history of the Lorentz term is given in J.A. Ratcliffe, "The Magneto-Ionic Theory", Ch. 15.2, Camb. Un. Press (1959).
12. C. Herring and E. Vogt, Phys. Rev. 101, 944 (1956).
13. H.P. Furth and R.W. Waniek, Phys. Rev. 104, 343 (1956).
14. P.P. Debye and E.M. Conwell, Phys. Rev. 93, 693 (1954).
15. J.R. Haynes and W. Shockley, Phys. Rev. 81, 835 (1951).
16. See e.g. C. Kittel, "Introduction to Solid State Physics", Ch. 7, (Wiley & Sons, New York 1959).
17. D.R. Hartree, Proc. Camb. Phil. Soc. 27, 143 (1931).

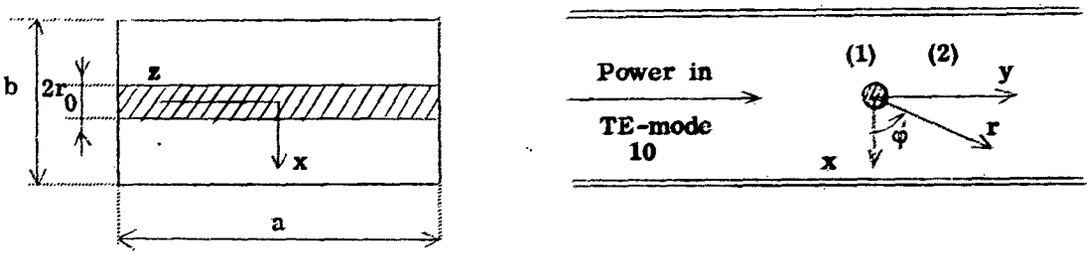

Fig. 1. Thin plasma rod mounted across a rectangular waveguide parallel to the broad walls.

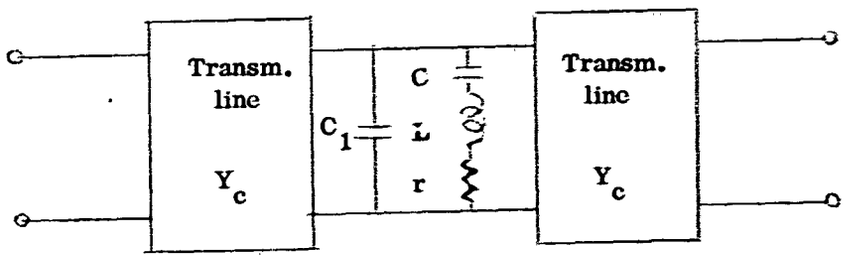

Fig. 2. Equivalent lumped circuit describing a thin plasma rod across a waveguide.

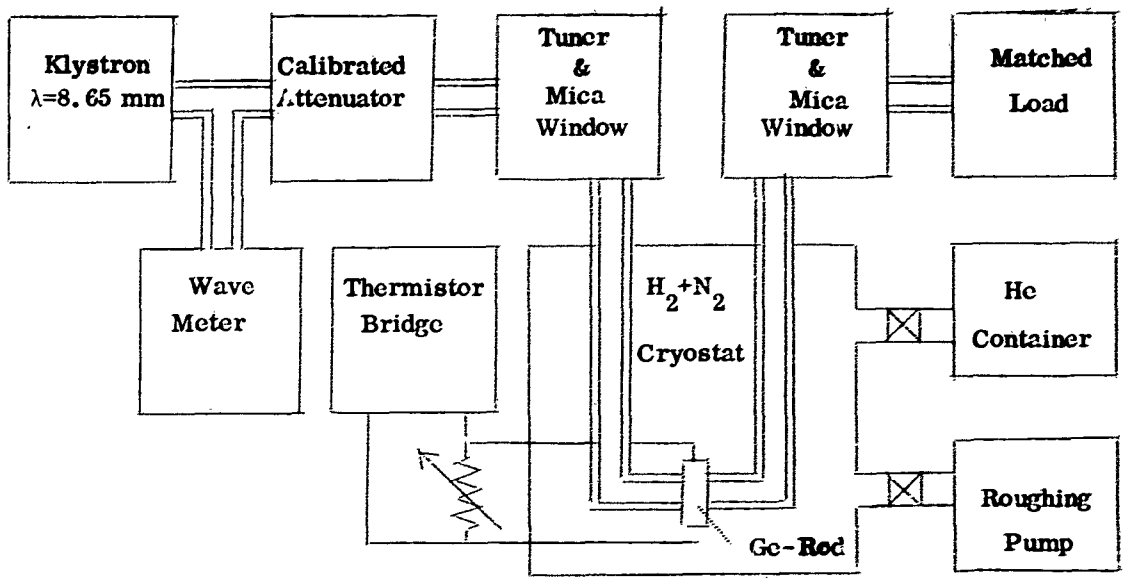

Fig. 3: Block diagram of experimental setup for plasma resonance measurement in Ge.

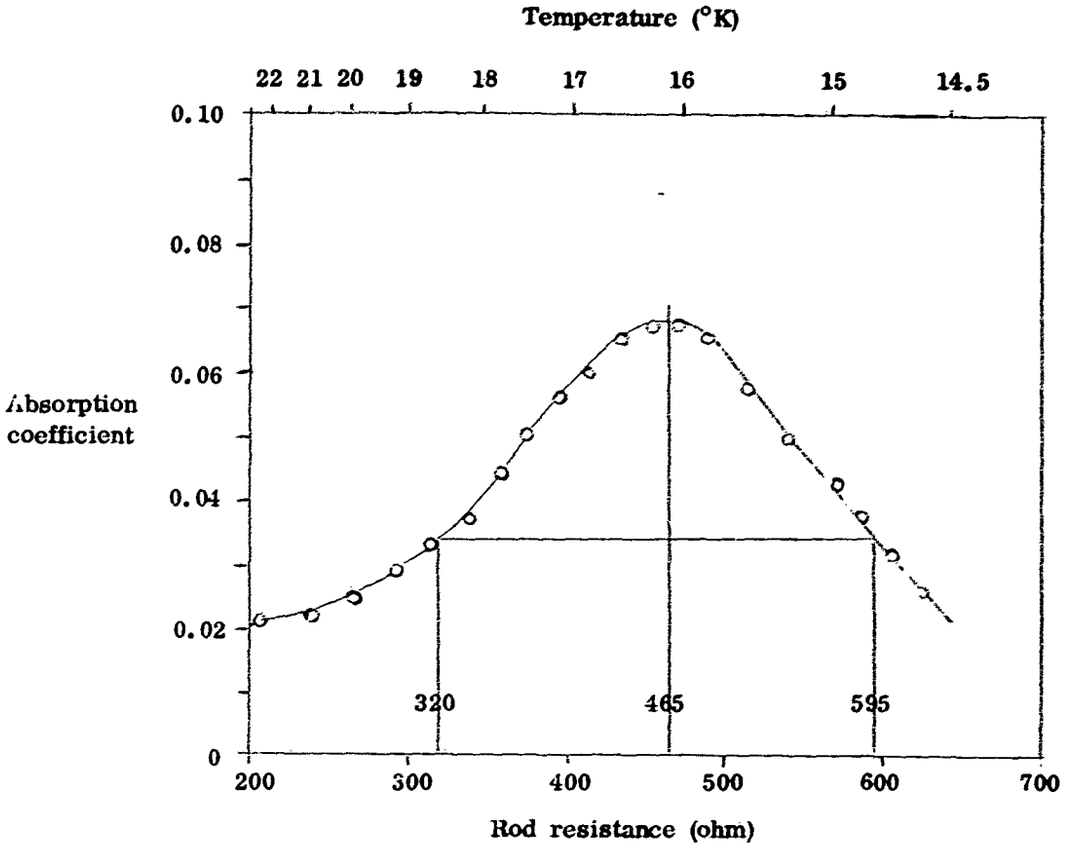

Fig. 4. Measured absorption coefficient (ratio absorbed power to incident power) of a Ge-rod at liquid H_2 temperature.

Fig. 5. Orientation in the microwave field of actual rectangular rod and for comparison an "equivalent" circular rod.

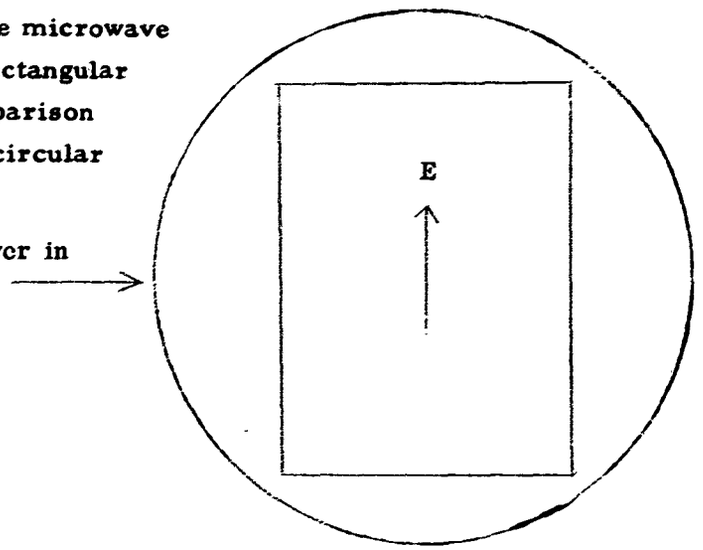

Fig. 6. Plasma rod in a waveguide and its reflected images in the waveguide walls.

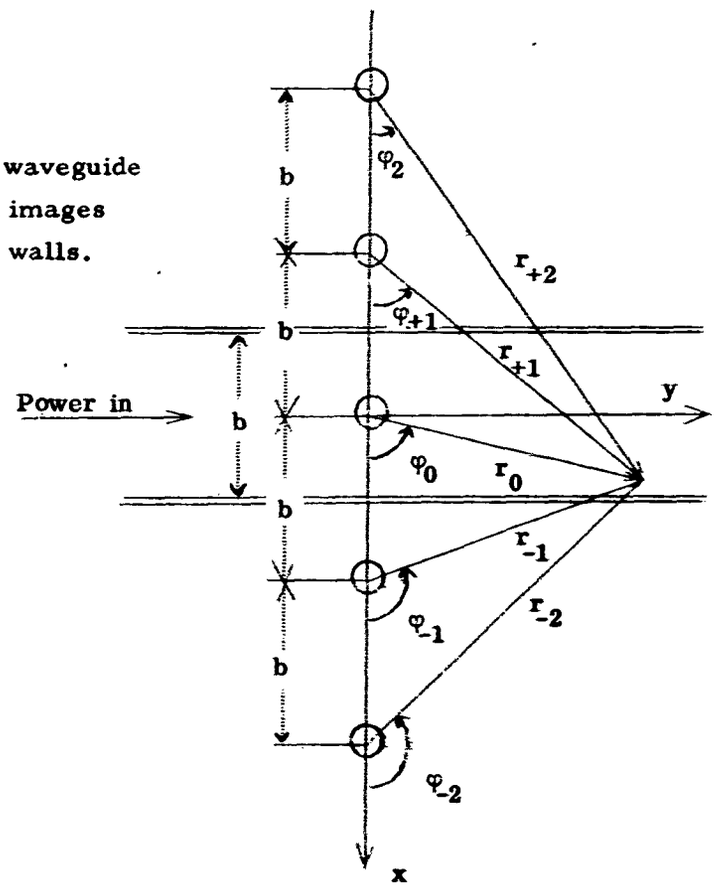

V. MAGNETO-PLASMA RESONANCE

Introduction

If a metal- or semiconductor-plasma sample is immersed in a d.c. magnetic field, and irradiated by an electromagnetic wave with a frequency much less than the plasma frequency and the gyrofrequency, then the plasma sample will be resonant for certain values of the frequency. These resonances, which are commonly called magneto-plasma resonances, have been observed experimentally in both metals[1,2] and semiconductors[3]. At our laboratory we have studied the associated propagating waves in a long semiconductor rod.

The resonances observed can generally be divided into two groups: 1) the main resonances with different mode number in the direction parallel to the magnetic field, and 2) the secondary (or satellite) resonances, corresponding to different transverse mode number.

The main resonances can be fairly well explained by assuming plane waves propagating along the magnetic field. (This simple approach is valid if the transverse dimensions are much larger than the wavelength along the magnetic field lines.)

The secondary resonances (which yet have been observed only in metal samples) can not be explained by the plane-wave approximation. To obtain a theory for these, one has to solve the proper boundary-value problem. This is done in an approximate manner for circularly cylindrical samples in the theory below.

Theory

The ordinary theory for a magnetized plasma, describes the plasma as an anisotropic dielectric medium, having the tensor dielectric constant:

$$[\varepsilon] = \begin{matrix} \varepsilon_1 & -j\varepsilon_2 & 0 \\ j\varepsilon_2 & \varepsilon_1 & 0 \\ 0 & 0 & \varepsilon_3 \end{matrix}$$

where

$$\varepsilon_1 = \varepsilon_r - \frac{\omega - j\nu}{\omega} \cdot \frac{\omega_p^2}{(\omega - j\nu)^2 - \omega_c^2} \qquad (1)$$

$$\varepsilon_2 = \frac{\omega_c}{\omega} \cdot \frac{\omega_p^2}{(\omega - j\nu)^2 - \omega_c^2}$$

$$\varepsilon_3 = \varepsilon_r - \frac{\omega_p^2}{\omega(\omega - j\nu)}$$

and ε_r = static dielectric constant

ω = signal frequency, ω_p = plasma frequency

ω_c = gyro frequency and ν = collision frequency

provided the d.c. magnetic field coincide with the z-direction.

The solutions of Maxwell's equations for plane waves give two possible normalized propagation constants

$$\tau^2 = (c/v_{ph})^2 = \varepsilon_1 \pm \varepsilon_2 \tag{2}$$

where v_{ph} = the phase velocity

and c = velocity of light

If now $\omega_c \gg |\omega - j\nu|$ and $\omega_p^2 > \varepsilon_r \omega\omega_c$ (as is generally the case in the magnetoplasma resonance experiments) only the left hand circularly polarized wave can propagate and the normalized propagation constant can in this case approximately be written:

$$\tau^2 = \varepsilon_r + \frac{\omega_p^2}{\omega \cdot \omega_c} \tag{3}$$

For a metal plasma $\omega_p^2/\omega\omega_c \gg \varepsilon_r$ and hence the main resonant frequencies are

$$\omega_{res} = \frac{\omega_c}{\omega_p^2} (\pi \frac{c}{z})^2 p^2; \qquad p = 1, 2, 3 \ldots \tag{4}$$

where z = length of the sample in the d.c. magnetic field direction.

and p = axial mode number.

We will now consider a circularly cylindrical plasma sample, with radius a and axial length z, and with the d.c. magnetic field parallel to the axis.

According to AGDUR[4] the z- and φ-components of the fields inside the plasma ($r < a$) can be written (omitting the factor $\exp[j(\omega t - \beta z + n\varphi)]$):

$$E_z = AJ_n(m_1 r) + BJ_n(m_2 r)$$

$$-jcB_z = AD_1 J_n(m_1 r) + BD_2 J_n(m_2 r)$$

$$E_\varphi = \frac{n}{\beta_o r Q}\left\{A\left[\alpha_1 J_n(m_1 r) + \frac{m_1 r}{n}\alpha_2 J_n'(m_1 r)\right] + \right.$$

$$\left. + B\left[\beta_1 J_n(m_2 r) + \frac{m_2 r}{n}\beta_2 J_n'(m_2 r)\right]\right\} \qquad (5)$$

$$-jcB_\varphi = \frac{n}{\beta_o r Q}\left\{A\left[\alpha_3 J_n(m_1 r) + \frac{m_1 r}{n}\alpha_4 J_n'(m_1 r)\right] + \right.$$

$$\left. + B\left[\beta_3 J_n(m_2 r) + \frac{m_2 r}{n}\beta_4 J_n'(m_2 r)\right]\right\}$$

where

$$m_{1,2}^2 = \frac{\beta_o^2}{2}\left\{(\varepsilon_1 - \tau^2)\left(1 + \frac{\varepsilon_3}{\varepsilon_1}\right) - \frac{\varepsilon_2^2}{\varepsilon_1} \pm \right.$$

$$\left. \pm \left(\left[(\varepsilon_1 - \tau^2)\left(1 - \frac{\varepsilon_3}{\varepsilon_1}\right) - \frac{\varepsilon_2^2}{\varepsilon_1}\right]^2 + 4\tau^2\varepsilon_3\frac{\varepsilon_2^2}{\varepsilon_1^2}\right)^{\frac{1}{2}}\right\}$$

$$\beta_o = \omega/c; \quad \tau = c/v_{ph}$$

and

$$D_{1,2} = \frac{\varepsilon_1}{\tau\varepsilon_2}\,\frac{\varepsilon_3}{\varepsilon_1}(\varepsilon_1 - \tau^2) - \frac{m_{1,2}^2}{\beta_o^2}$$

$$\alpha_1,\ \beta_1 = \tau(\varepsilon_1 - \tau^2) + \varepsilon_2 D_{1,2}$$

$$\alpha_2,\ \beta_2 = -\varepsilon_2\tau - (\varepsilon_1 - \tau^2)D_{1,2}$$

$$\alpha_3,\ \beta_3 = \varepsilon_2\tau^2 + \tau(\varepsilon_1 - \eta^2)D_{1,2}$$

$$\alpha_4,\ \beta_4 = \varepsilon_2^2 - \varepsilon_1(\varepsilon_1 - \tau^2) - \varepsilon_2\tau\, D_{1,2}$$

$$Q = (\varepsilon_1 - \tau^2)^2 - \varepsilon_2^2$$

J_n is the n:th order Bessel function and J_n' is its derivative. A and B are amplitude coefficients.

These fields must satisfy certain boundary conditions at the plasma boundary r = a, which gives the dispersion relation. We will here distinguish between two cases: A) the plasma surrounded by air, which applies to most experiments with metal plasmas, and B) the plasma surrounded by a metal tube ($\sigma \to \infty$), which applies to most experiments with semiconductor plasmas. These two cases, which will give different boundary conditions, are treated separately below.

Case A: Plasma surrounded by air

In this case the fields outside the plasma ($r > a$) are assumed to be the ordinary slow wave vacuum fields in cylindrical coordinates, i.e.:

$$\begin{aligned} E_z &= CK_n(\beta r) \\ -jcB_z &= EK_n(\beta r) \\ E_\varphi &= -\frac{n}{\beta r} CK_n(\beta r) + \frac{1}{\tau} EK_n'(\beta r) \\ -jcB_\varphi &= \frac{1}{\tau} CK_n'(\beta r) - \frac{n}{\beta r} EK_n(\beta r) \end{aligned} \tag{6}$$

where $\beta = \tau\beta_o$

K_n and K_n' are the modified second kind Bessel function of order n and its derivative. C and E are amplitude coefficients.

Matching the fields inside and outside the plasma at the boundary $r = a$ requires that the following determinant is zero:

$$\begin{vmatrix} 1 & 1 & 1 & 0 \\ D_1 & D_2 & 0 & 1 \\ \alpha_1 + \alpha_2 X_1 & \beta_1 + \beta_2 X_2 & -Q/\tau & QK/\tau \\ \alpha_3 + \alpha_4 X_1 & \beta_3 + \beta_4 X_2 & QK/\tau & -Q/\tau \end{vmatrix} = 0 \tag{7}$$

where $X_1 = \frac{m_1 a}{n} \frac{J_n'(m_1 a)}{J_n(m_1 a)}$; $X_2 = \frac{m_2 a}{n} \frac{J_n'(m_2 a)}{J_n(m_2 a)}$ and $K = \frac{\beta a}{n} \frac{K_n'(\beta a)}{K_n(\beta a)}$

If $\omega_c \gg |\omega - j\nu|$ and $\omega_p^2 \gg \omega \cdot \omega_c$, which means that $|\varepsilon_3| \gg |\varepsilon_2| \gg |\varepsilon_1|$, and if further τ^2 is assumed to be near the plane wave solution (i.e. τ^2 of the order of $|\varepsilon_2|$) then:

$$\begin{aligned} m_1^2 &\simeq -\beta^2 \frac{\varepsilon_3}{\varepsilon_1} F, \qquad |m_1 a| \gg 1 \\ m_2^2 &\simeq \beta^2 \frac{Q}{\tau^4} \cdot \frac{1}{F} \end{aligned} \tag{8}$$

where $F = 1 + \varepsilon_2^2/(\varepsilon_3 \tau^2)$

With these approximations one can show that an approximate solution to Eq. (7) is

$$J_n(m_2 a) \simeq 0$$

or

$$m_2 a \simeq x_{nm} \tag{9}$$

where x_{nm} is the m:th rooth of $J_n(x) = 0$ $(n \neq 0)$.

To obtain a simple expression for the resonant frequencies of a plasma rod with the length z, we approximate m_2^2 further:

$$m_2^2 \simeq 2\beta^2 \frac{|\varepsilon_2| - \tau^2}{\tau^2} = 2\beta_o^2 (|\varepsilon_2| - \tau^2)$$

This gives the resonant frequencies:

$$\omega_{res} = \frac{\omega_c}{\omega_p^2} \left(\frac{\pi c}{z}\right)^2 p^2 \left(1 + \frac{1}{2} \frac{x_{m,n}}{p\pi a} z^2\right) \tag{10}$$

This equation gives both the main resonances (n = m = 1, p = 1, 2 ....) and the secondary ones (p fixed and n, m = 1, 2 ...).

If $(x_{11} z)/(p\pi a) \lesssim 1$ then the plane wave approximation (Eq. (4)) gives the main resonances with good accuracy, and the secondary resonances will be very close to the main ones. The secondary resonances will only be detectable if the Q-values of the resonances are of the order of $f_o/2\Delta f$ or larger, where f_o is the main resonant frequency and Δf is the frequency spacing between the main and the first secondary resonance.

Case B: Plasma surrounded by a metal tube.

In this case the fields must satisfy the boundary conditions:

$$E_z = E_\varphi = 0 \quad \text{for} \quad r = a$$

With the expressions for E_z and E_φ in Eq. (5) these conditions lead to the following characteristic equation determining the propagation constant:

$$X_1 \alpha_2 - X_2 \beta_2 = \beta_1 - \alpha_1 \tag{11}$$

where X_1 and X_2 are given in Eq. (7).

If we introduce the same approximation as in case A, Eq. (11) can approximately be written:

$$m_2 a \frac{J_n'(m_2 a)}{J_n(m_2 a)} \simeq n \qquad \text{if} \quad n \ll |m_1 a| \tag{11a}$$

The solution to Eq. (11a) is:

$$J_{n+1}(m_2 a) = 0$$

or

$$m_2 a = x_{n+1,m}$$

where $x_{n+1,m}$ is the m:th rooth of $J_{n+1}(x) = 0$; $n \neq 0$. From this approximate equation one can derive the propagation constant τ:

$$\tau^2 = \varepsilon_1 - G + \left(|\varepsilon_2|^2 + G^2 + 2G(\varepsilon_1 - \varepsilon_r) \right)^{\frac{1}{2}} \tag{12}$$

where $$G = \frac{1}{2} \left(\frac{x_{n+1,m}}{\beta_o a} \right)^2$$

Experiments

We have at our laboratory made an experiment with a semiconductor plasma in a strong magnetic field. The semiconductor (at liquid nitrogen temperature) was immersed in a circularly cylindrical waveguide, the axis of which was along the magnetic field lines. The purpose of this experiment was to measure the propagation and the attenuation constants of a circularly polarized wave in the semiconductor, as a function of the magnetic field strength. The experimental conditions were such that the plane-wave approximation could be used. In this case the ordinary magneto-plasma theory gives the propagation constant (β) and the attenuation constant (α) of the extraordinary wave (see Eq. (2)):

$$\beta = \beta_o \left[\varepsilon_r + \frac{\omega_p^2}{\omega\omega_c} \right]^{\frac{1}{2}}$$

$$\alpha = \frac{\beta_o}{2} \cdot \frac{\omega_p^2}{\omega\omega_c} \cdot \frac{1}{\left[\varepsilon_r + \frac{\omega_p^2}{\omega\omega_c} \right]^{\frac{1}{2}}} \cdot \frac{\nu}{\omega_c} \tag{13}$$

These formulas are valid if $\omega_c \gg |\omega - j\nu|$. The ordinary wave is strongly attenuated and will not be considered here.

The semiconductor used was indium antimonide with $N \simeq 10^{21}$ electrons/m^3, $\mu \simeq 30$ m^2/Vs and $\varepsilon_r = 16$. With a signalfrequency of 35 GHz and a magnetic field strength of 1 Wb/m^2 (= 10^4 Gauss), the above formulas give $\beta = \beta_o \cdot 10$ which correnspond to a wavelength in the sample of 0.87 mm. The corresponding value of α is 104 m^{-1}, i.e. an attenuation length of about 1 cm.

The experimental setup is shown in Fig. (1). The incident, linearly polarized TE_{11}-mode in the empty waveguide can be divided into one ordinary and one extraordinary circularly polarized wave. Only the extraordinary wave can propagate through the semiconductor and reach the magic T. This signal interferes with a signal passing through the attenuator and the directional coupler.

The magnetic field is obtained by discharging a capacitor through the solenoid around the sample. The field reaches its maximum value ($\simeq 1.3 \cdot 10^4$ Gauss) in 0.005 sec.

An oscilloscope trace of the detector output as a function of the magnetic field strength, is shown in Fig. (2). The peaks of the curve are related to the wavelength in the sample, but it is not possible to get an absolute value of the wavelength; only the relative change of the wavelength can be measured. However, by taking one of the measured points as reference point, one can compare the measurements with the theory. In a similar way the measured attenuation can be compared with the theoretical value. (Fig. (3).)

In our experiment the length of the sample was several (10 - 15) wavelengths long. Consequently, owing to the relatively strong attenuation, the magneto plasma resonance observed by LIBSCHABER and VEILEX [3] could not be observed in our case.

We are presently preparing a new experiment in which we hope to see both the main and the satellite magneto plasma resonances in indium antimonide.

For dipole modes Eq. (12) gives

$$\tau^2 = \varepsilon_1 - G + \left\{ |\varepsilon_2|^2 + G^2 + 2G(\varepsilon_1 - \varepsilon_r) \right\}^{\frac{1}{2}} \qquad (14)$$

with $$G = \frac{1}{2} \left(\frac{x_{2,m}}{\beta_o a} \right)^2$$

m = 1, for the main resonance and

m = 2, 3 ... for the satellite resonances.

A numerical analysis of a reasonable case, shows that the spacing between the main and the proper secondary resonances is very small, but that the unloaded Q-values of the resonances are so large that the different resonances shall be separable. This means that the coupling to the semiconductor sample must be very small, in order not to lower the Q-values too much. We hope to achieve this low coupling, simply by applying metal irises to the end-faces of the sample.

References

1. TAYLOR, M.T., MERRILL, J.R. and BOWERS, R: Low Frequency Magneto-Plasma Resonance in Metals. Report No. 97, Cornell University (Nov. 1962).

2. MERRILL, J.R., TAYLOR, M.T., and GOODMAN, J.M.: Satellites in the Magneto-Plasma Resonance in Sodium. Report No. 114, Cornell University (April 1963).

3. LIBCHABER, A. and VEILEX, R.: Wave Propagation in Gyromagnetic Solid Conductor. Helicon, Phys. Rev. 127, No. 3, 774 (Aug. 1962).

4. AGDUR, B.: Notes on the Propagation of Guided Microwaves through an Electron Gas in the Presence of a Static Magnetic Field. Proc. Symp. Electr. Waveguides (Pol. Inst. Brooklyn, April 1958).

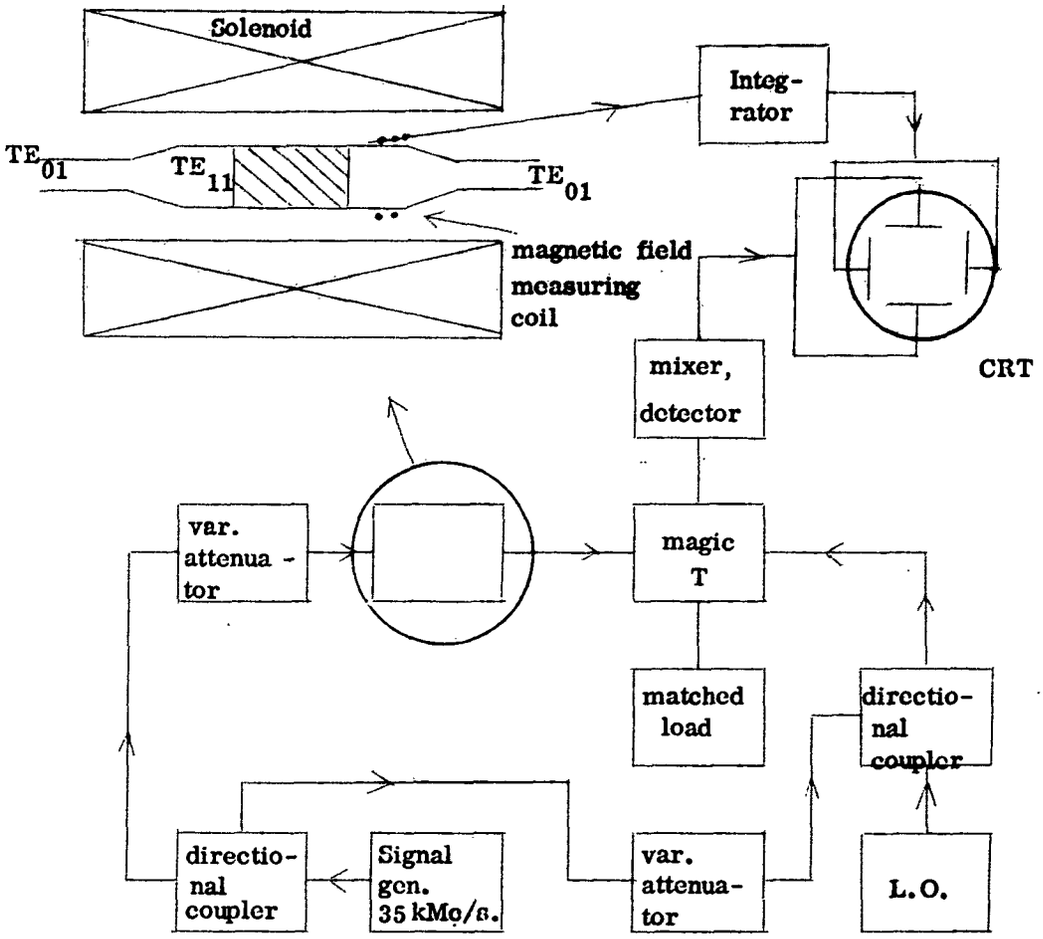

Fig. 1. Experimental set-up.

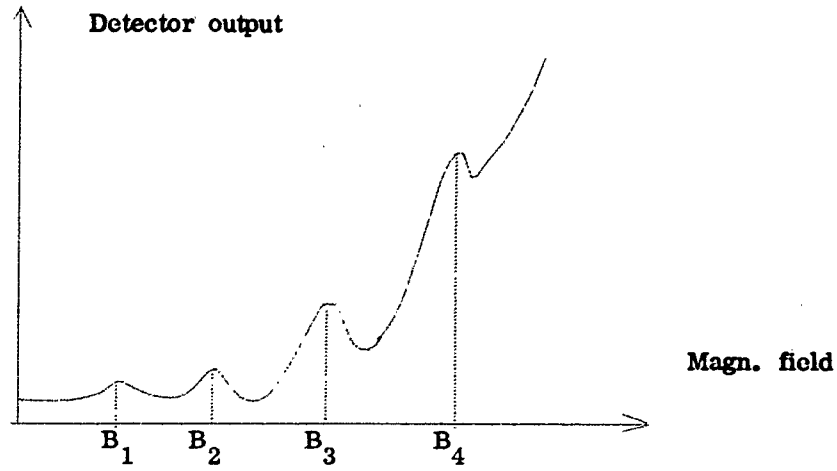

Fig. 2. Detector output as a function of the magnetic field.

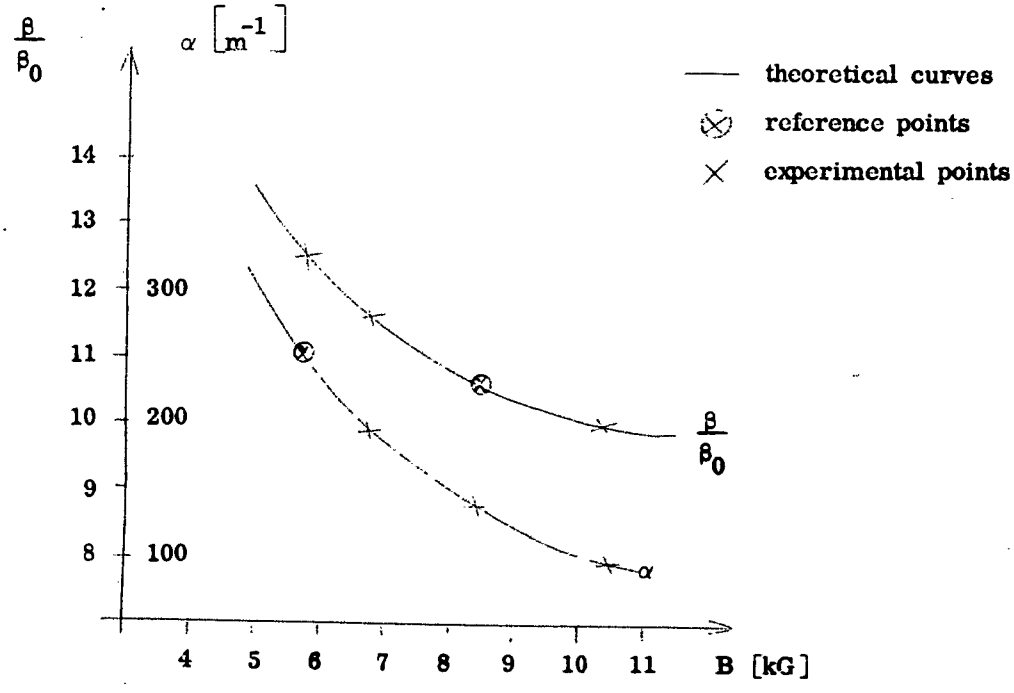

Fig. 3. Comparison between theory and experimental results.

VI. VARIATION OF PLASMA PARAMETERS ALONG THE POSITIVE COLUMN OF A MERCURY DISCHARGE

This investigation is a continuation of the work described in ref. 1, where experimental studies of the variation of the electron density along the positive column of a low-pressure mercury discharge are described. The electron density was measured by means of the microwave cavity method. It is the purpose of this experiment to obtain more information on the axial variation of the plasma parameters by introducing Langmuir probes, so that also the electron temperature and the axial d.c. electric field in the plasma can be measured.

The discharge tube (Fig. 1) has a length of 1 m, an inner diameter of 12 mm and an outer diameter of 15 mm. The neutral gas density is controlled by keeping the glass wall around the cathode at constant temperature T_g, which is below the temperature of the rest of the tube. Seven Langmuir probes are inserted along the tube with a distance of 14 cm between them. Only the circular end surfaces are exposed to the plasma and are situated on the axis of the tube. A sawtooth voltage with a sweep frequency of 50 c/s, is applied to the probes and a logarithmic current vs. linear voltage characteristic displayed on an oscilloscope (Fig. 2) after compensation for the ion-current. The circuitry is essentially the same as described by HARP[2]. The linear slope of the characteristic is a measure of the electron temperature and is determined by comparison with a reference line, the slope of which can be varied. The electron density can be determined from the saturation current when the area of the probe and the electron temperature are known.

Figs. 3 and 4 show the electron temperature and density at one place in the tube as a function of T_g for various tube currents. The density is measured with the cavity method. The results shown in the figures are in qualitative agreement with KLARFELD[3].

The variation of electron temperature along the tube is shown in Fig. 5. Apart from the maximum in the centre of the tube the variation indicates that there is a small positive pressure gradient towards the anode. Such pressure gradients have been discussed by KLARFELD and POLETAEV[4]. The maximum of electron temperature is however not understood.

The determination of electron density with probe measurements depends on the effective area of the probe which is difficult to determine accurately. The relative areas of the probes are found by measuring the density with the microwave cavity method at a small discharge current (100 mA). While the probe measurements give the density at the axis of the tube, the cavity method gives

approximately the mean density across the tube. If we assume that the radial density distribution is constant along the tube for I = 100 mA, the relative areas can be determined with good accuracy. Furthermore, we assume that the effective areas are independent of the tube current in the current region of our measurements.

Fig. 6 shows the axial variation of electron density measured by the probe method and the cavity method. The probe measurements are relative in the sense that N(probe) is put equal to N(cavity) for a tube current of 100 mA. The difference between the results of the probe measurements and the results of the cavity measurements indicates that the radial density distribution changes along the tube. This effect is more clearly demonstrated in Fig. 7 where α = = N(probe)/N(cavity) is plotted. This ratio which is normalized to unity at 100 mA is approximately proportional to N_{max}/N_{mean} under the above mentioned assumptions. It is seen that α is approximately constant over the greater part of the tube but decreases near the anode and near the cathode. In general it is increasing with the current.

If we assume that the pressure gradient causes the variation of electron density and temperature, and that these are determined by the local pressure, we can determine the pressure gradient from the measurements of the electron density distribution or the electron temperature distribution as plotted in Fig. 8. If we neglect the maximum of electron temperature, the variation of both the density and the temperature is in agreement with a positive pressure gradient, which can be determined to be about 1.3×10^{-5} mm Hg/cm. This figure is in good agreement with Klarfeld and Poletaev, who do not, however, take into account the gradient in electron density in their theoretical considerations.

The axial electric field has also been measured and was determined by using the probe characteristics to find the plasma potential at the different probe positions. The electric field was found to increase slightly towards the anode. Similarly, a higher gas pressure increased the field at a fixed position (Fig. 9). No dependence on the current could be observed (current range 100 - 600 mA).

As a conclusion we can say that the plasma parameters vary along the tube approximately in accordance with an increasing pressure towards the anode, with one major exception in the electron temperature. We intend to extend the measurements to higher gas pressures and possibly measure the pressure and its variation along the tube by spectroscopic means in order to get a unified picture of the phenomena.

References

1. AGDUR, B., KERZAR, B. and NYGREN, T. "Variation of the Electron Density along a Plasma Column". Phys. Rev. Letters, 10, 467 (June 1963).

2. HARP, R.S., "Circuit for the Display of Langmuir Probe Characteristics", Rev. Sci. Instr. 34, 416 (April 1963).

3. KLARFELD, B., "Characteristics of the Positive Column of Gaseous Discharge", Journ. of Physics, 5, 155 (1941).

4. KLARFELD, B. and POLETAEV, I., "Pressure Gradient in the Positive Column", Compt. Rend. 5, 460 (1939).

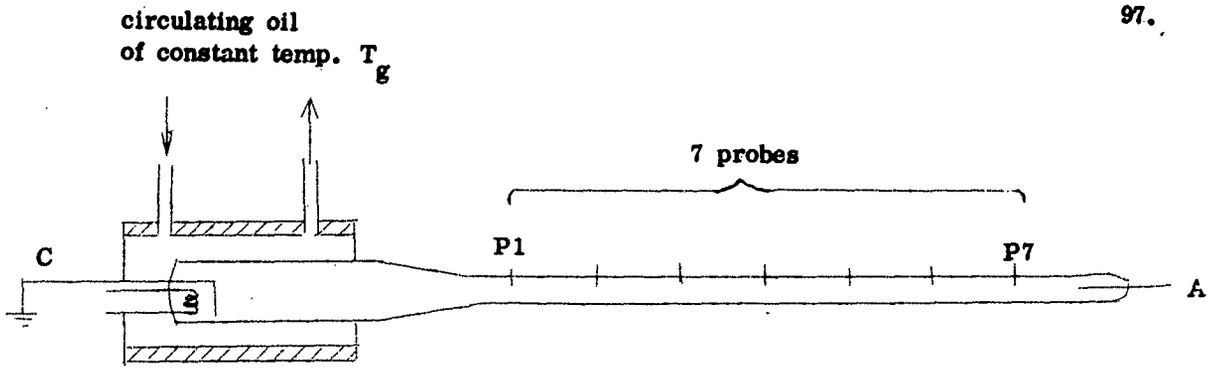

Fig. 1. Discharge tube.

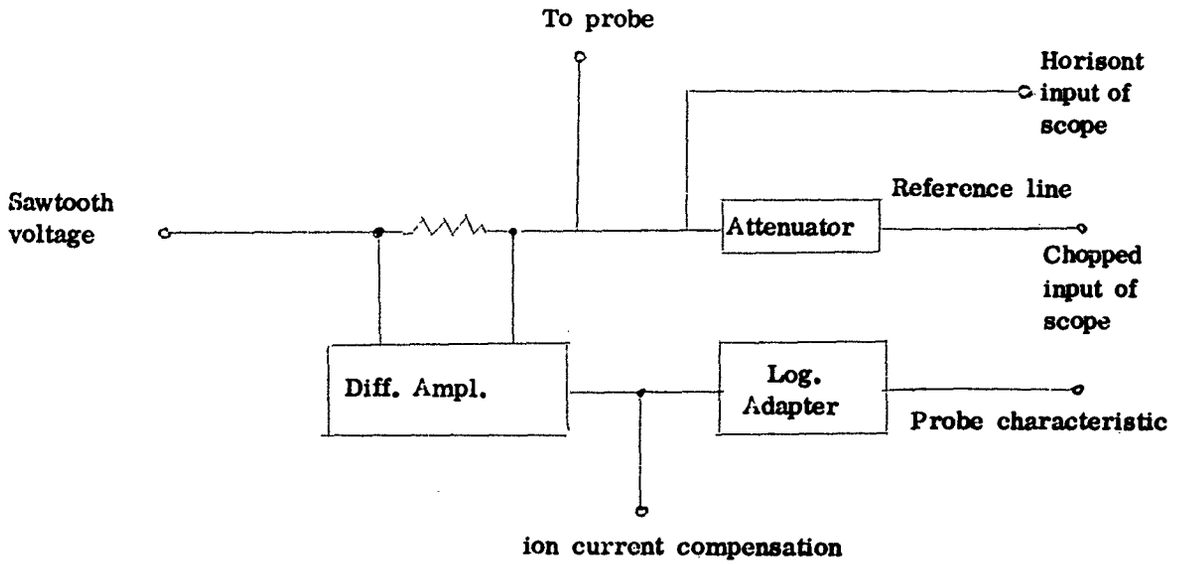

Fig. 2. Block diagram.

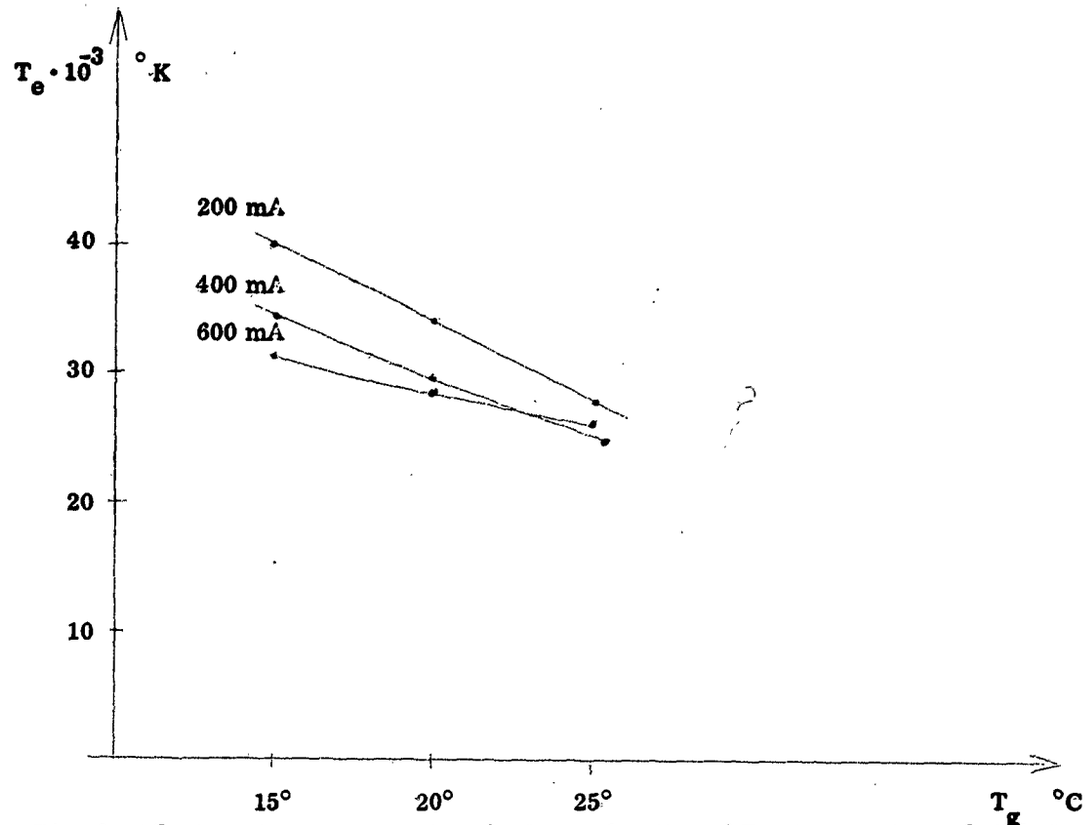

Fig. 3. Electron temperature at probe 3 as a function of T_g, temperature of oil bath.

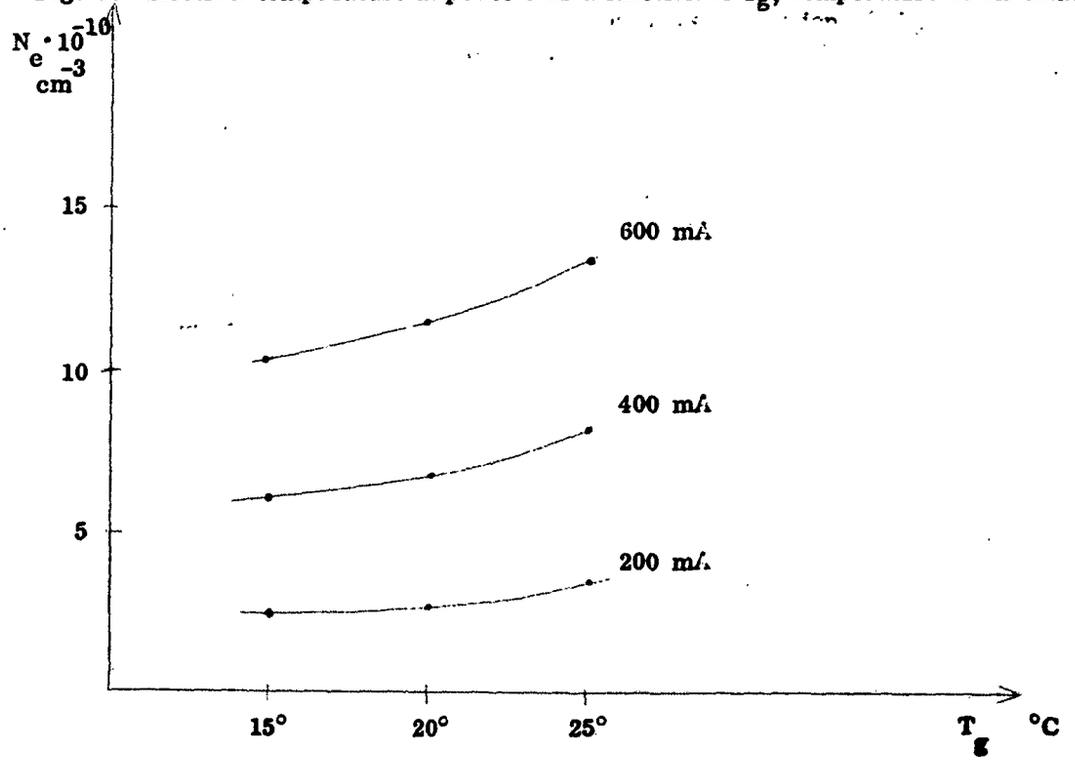

Fig. 4. Electron density (cavity method) as a function of T_g at probe 3.

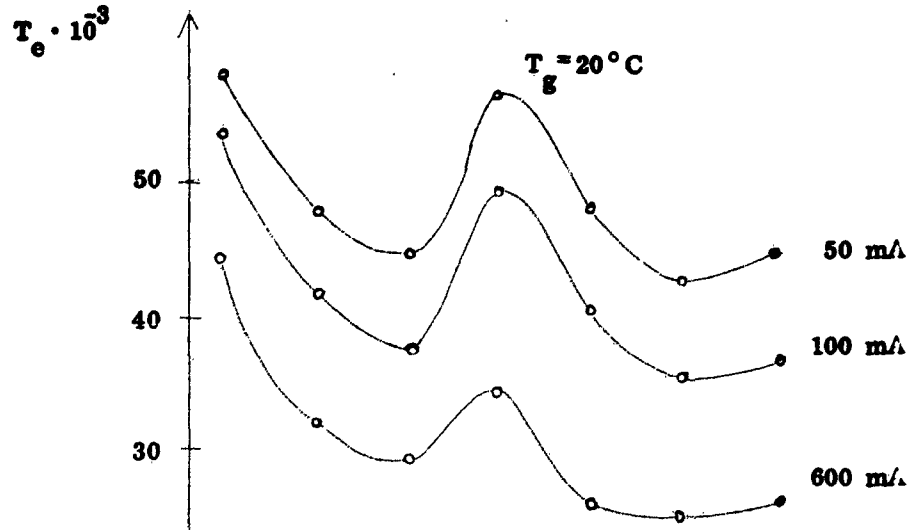

Fig. 5 Electron temperature along the tube for various tube currents.

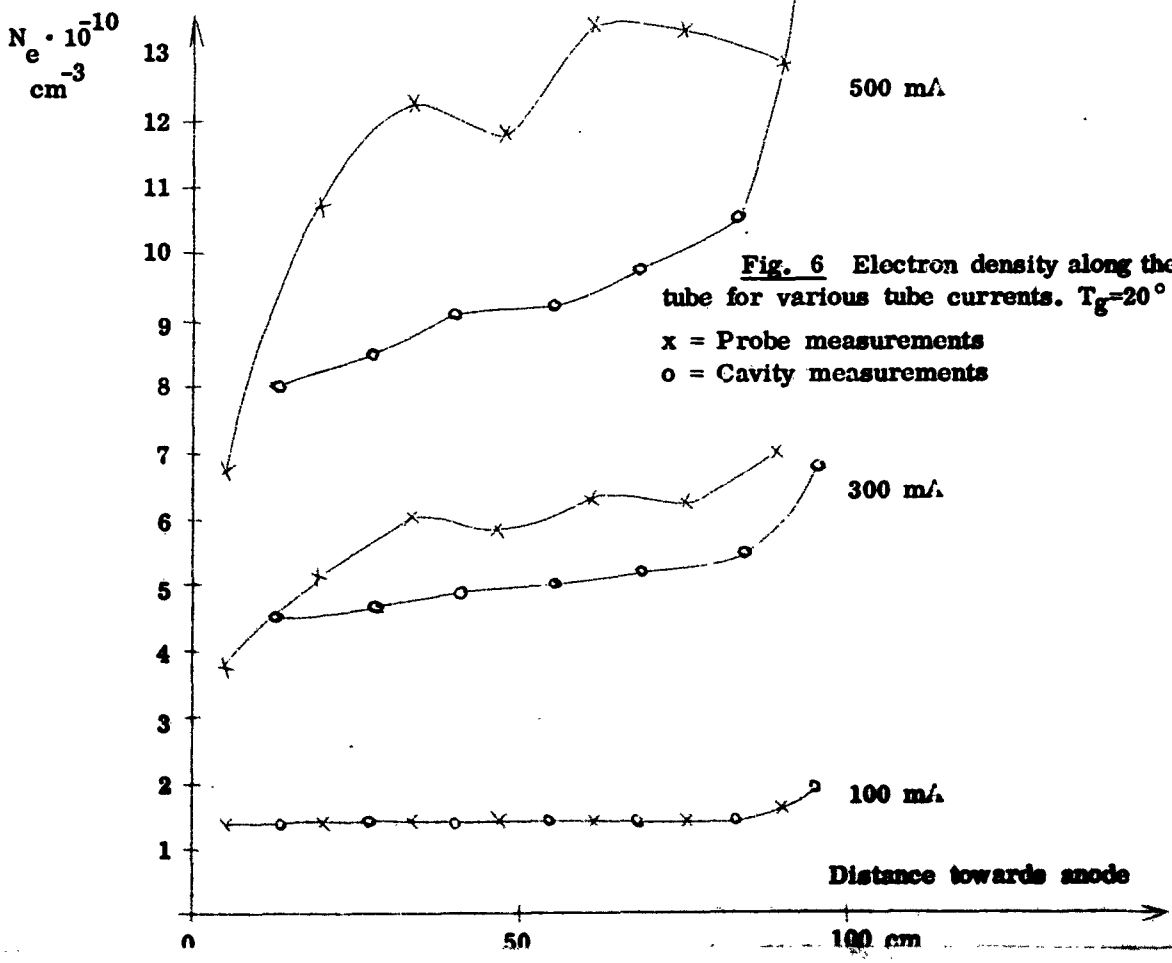

Fig. 6 Electron density along the tube for various tube currents. T_g=20°

x = Probe measurements

o = Cavity measurements

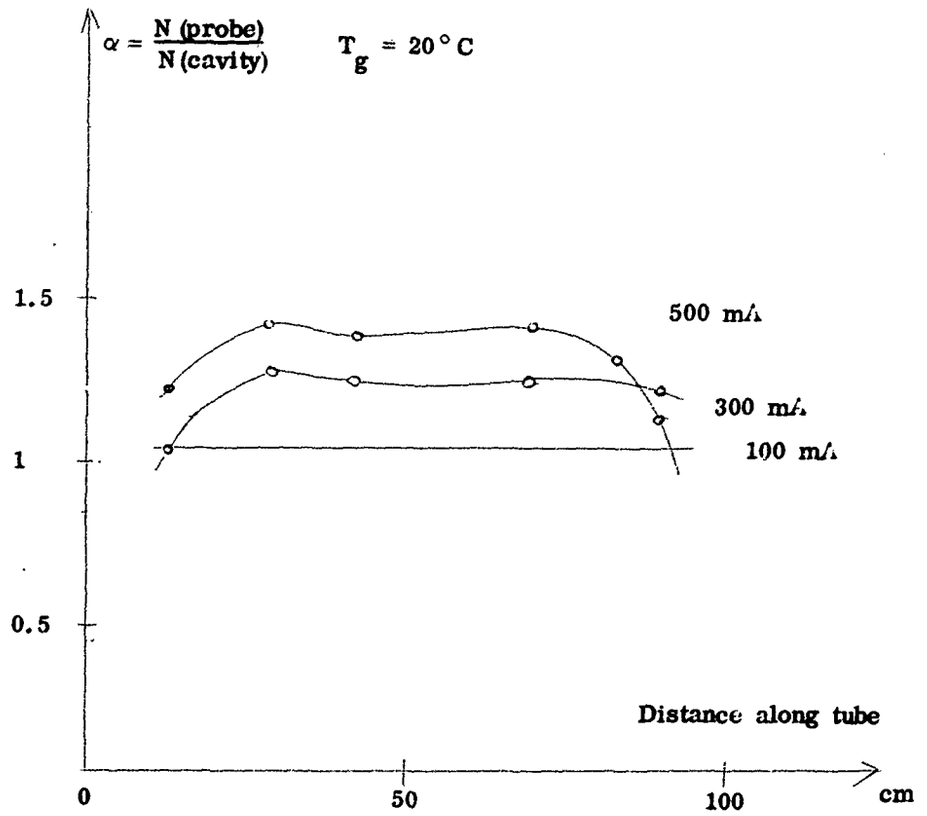

Fig. 7. Form factor N(probe)/(N(cavity) appr. equal to Nmax/Nmean normalized to unity at I = 100 mA.

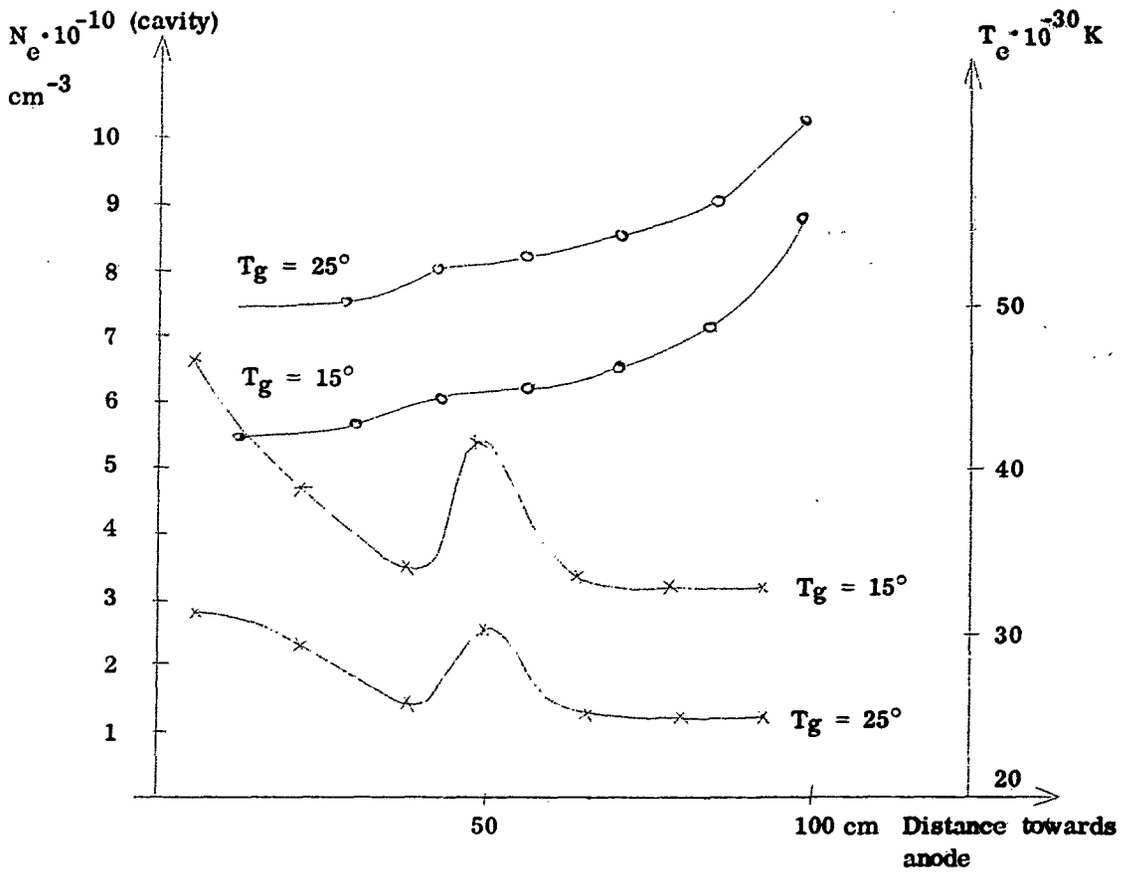

Fig. 8. Variation of electron temperature and density along the tube for various gas pressures. I = 400 mA.

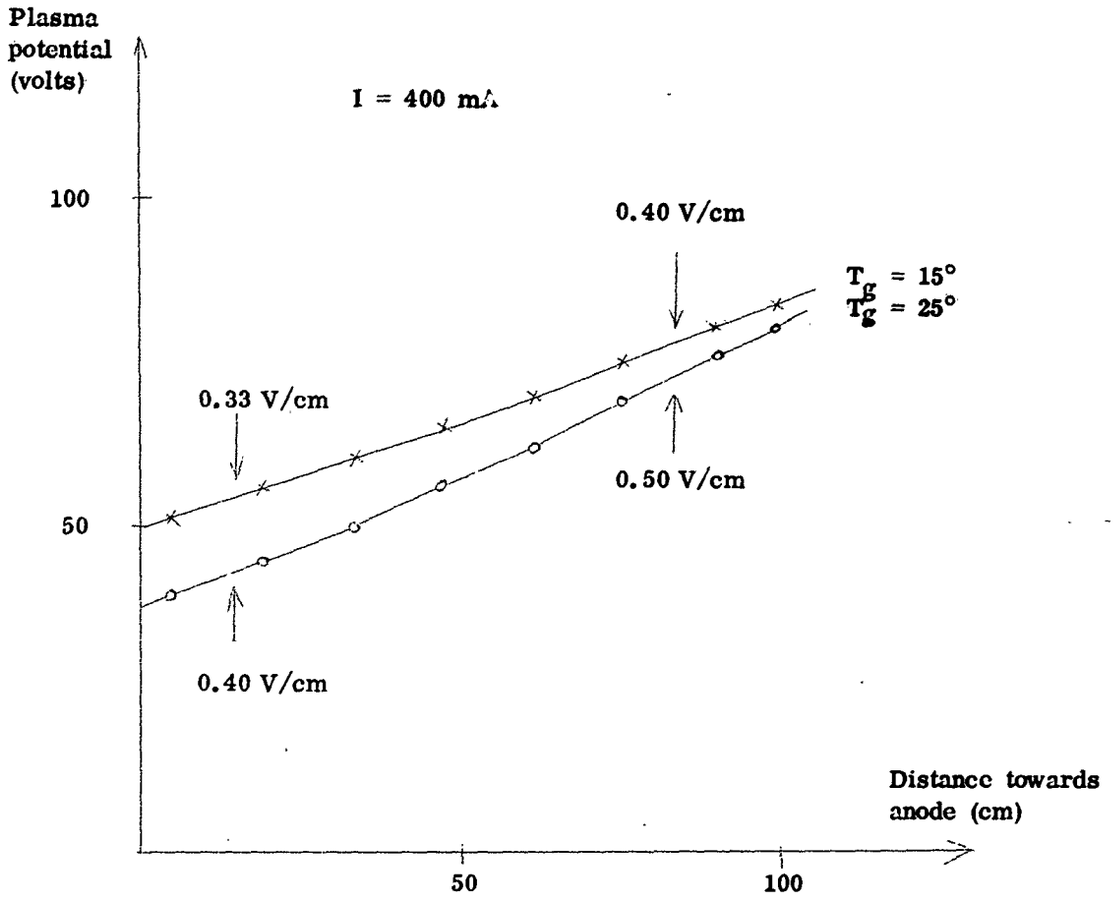

Fig. 9. Variation of the potential along the tube for two different gas pressures.

VII. EXPERIMENTS ON NOISE RADIATION FROM A PLASMA IN A WAVEGUIDE

Introduction

The work reported here is a continuation of our earlier experiments on noise radiation and coherent scattering from a low-pressure plasma column in free space and in a waveguide. The experiments are connected to the theoretical investigation, which is described elsewhere in this report. The experimental investigation is being continued and the results reported here are only preliminary. AGDUR et. al. have published experimental data on noise radiation and scattering from a plasma column in free space and in a waveguide. Strong polarization of noise was observed in the region of secondary peaks. The aim of this report is to present more experimental data on noise radiation from a cylindrical plasma column situated in a waveguide.

Experimental set-up

The noise power radiated from the plasma column was measured by means of a radiometer, operating at a frequency of 3100 Mc/s with a bandwidth of 10 Mc/s. A block diagram of the radiometer used is shown in Fig. 1. The noise radiation from the plasma column was compared with the noise radiation from a calibrated noise source. In this way, drift and nonlinear effects of the post r.f. amplifier were eliminated. The combined noise signal was then amplified in a low noise travelling wave tube and an I.F. amplifier operating at 30 Mc/s with a bandwidth of 10 Mc/s. The amplified signal was rectified by a "square law" detector and the resulting low frequency signal was fed into a selective amplifier ($f = 70$ c/s, $\Delta f = 5$ c/s) followed by a synchronous detector and integrator with an integration constant of 15 sec. The lowest detectible temperature change was about 20°K.

The noise power radiated from a plasma tube in a frequency interval Δf is spread over an infinite number of modes. Only the noise power carried by the dominant mode of the waveguide will reach the radiometer. It should be pointed out that no attempt was made to match the plasma tube to the waveguide system. Therefore one cannot relate the electron temperature and the noise power in a simple way. Simultaneous measurements of the frequency spectra for noise, scattering and absorption were made for two typical positions of the plasma tube: one with the E-vector of the dominant

waveguide mode (TE_{01}) parallel with the plasma tube and the other with the E-vector perpendicular to the plasma tube. We will here call them transverse and longitudinal polarization. See Fig. 3.

Two experimental mercury vapour discharge tubes with hot cathodes were used, having a diameter of 7 and 12.5 mm respectively. The neutral gas density could be varied from $5 \cdot 10^{19}$ to $3 \cdot 10^{20}$ molekules/m^3. The electron density was measured by means of the microwave cavity method.

Measurements

By means of the experimental arrangement the following data can be obtained as functions of the electron- and neutral gas density: (i) radiated noise power from the plasma tube, (ii) absorption, transmission and reflection of a coherent microwave signal (iii) exitation and propagation of slow wave plasma modes along the plasma column.

Transverse polarization

The measured emission and absorption spectra have substantially the same shape. This similarity indicates that the plasma investigated is in thermal equilibrium.

The spectra of noise and absorbed power possess sharp maxima at substantially the same frequencies as the maxima for the TONKS-DATTNER resonances. The noise radiation and the absorption at the dipole resonance depend strongly on collision frequency and the plasma tube diameter. At low neutral gas densities where the mean free path of the electrons is several times larger than the diameter of the plasma tube, wall collisions are more frequent than volume collisions. Under these conditions and if the diameter of the plasma tube is small compared with the wavelength ($d/\lambda \ll 1$), the shape of the noise and scattering spectra is nearly the same (see Fig. 4). When the tube diameter is increased the transmission at the dipole resonance tends to zero and the noice radiated decreases rapidly. The shape of the spectra for TONKS-DATTNER resonances, however, remains unchanged. (See Fig. 5.)

At higher neutral gas densities the mean free path of electrons becomes smaller than the diameter of the plasma tube and the volume collisions get more frequent. The noise spectrum for the case when the volume collisions are predominant is shown in Fig. 6. The noise radiation at the dipole resonance increases with collision frequency and becomes comparable to the radiated noise power at TONKS-DATTNER resonances.

The microwave fields in the waveguide can excite slow waves which will propagate along the plasma column, and couple energy out of the waveguide. In the frequency range where the dipole resonance occurs, a backward-wave with one variation of the electric field in azimuthal direction (dipole plasma mode) will propagate. Small peaks in the noise and scattering spectra are observed, which are related to the excitation of these modes. (See Figs. 5 and 6.)

Longitudinal polarization

The noise level for longitudinal polarization is about 10 dB below the noise level for transversal polarization. As shown in Figs. 4, 7 and 8 the noise power increases linearly with the plasma density ($P_n \sim \omega_p^2$). The noise spectrum possesses maxima at frequencies for TONKS-DATTNER resonances. However, no noise peak was measured at the dipole resonance. At the end of the bandpass of the backward-wave a sharp maximum in noise and absorption spectra occurs as shown in Figs. 7 and 8.

References

B. Agdur, B. Kerzar and F. Sellberg, Noise Radiation and scattering from a cylindrical plasma column. Phys. Rev. 128 (1962) pp 1-5.

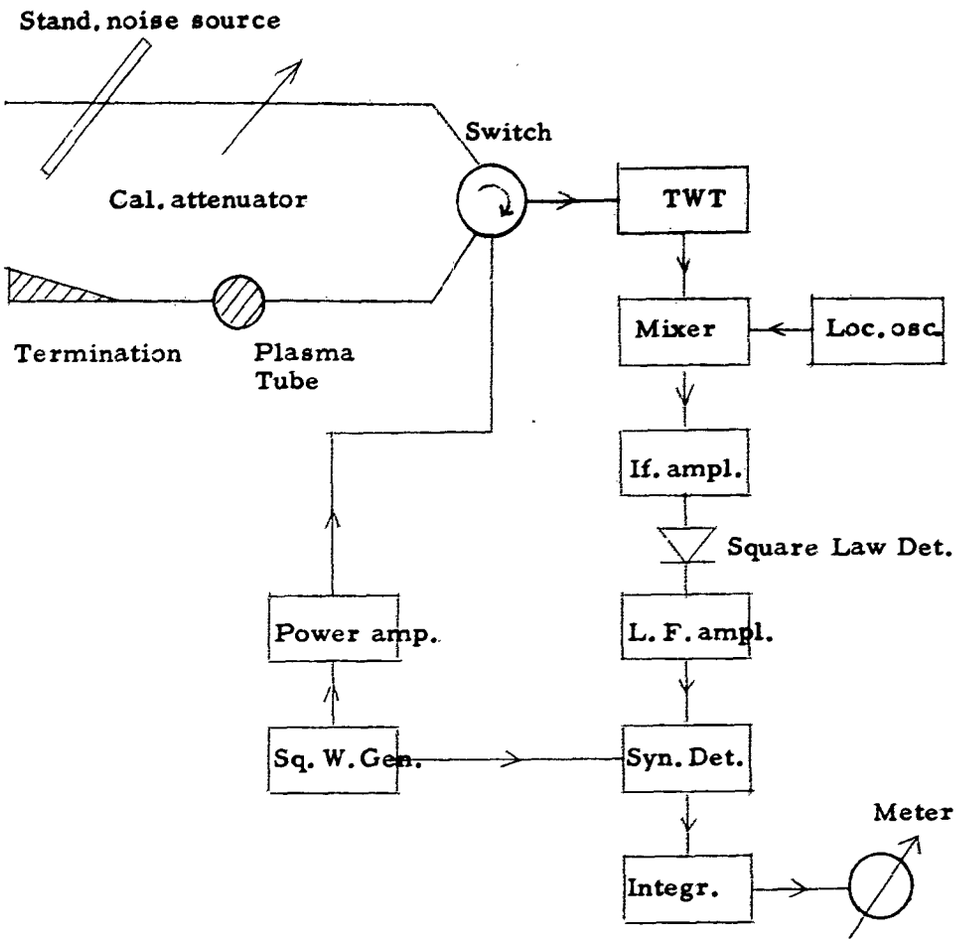
Stand. noise source
Switch
Cal. attenuator
TWT
Termination
Plasma Tube
Mixer
Loc. osc.
If. ampl.
Square Law Det.
Power amp.
L. F. ampl.
Sq. W. Gen.
Syn. Det.
Meter
Integr.

Fig. 1.

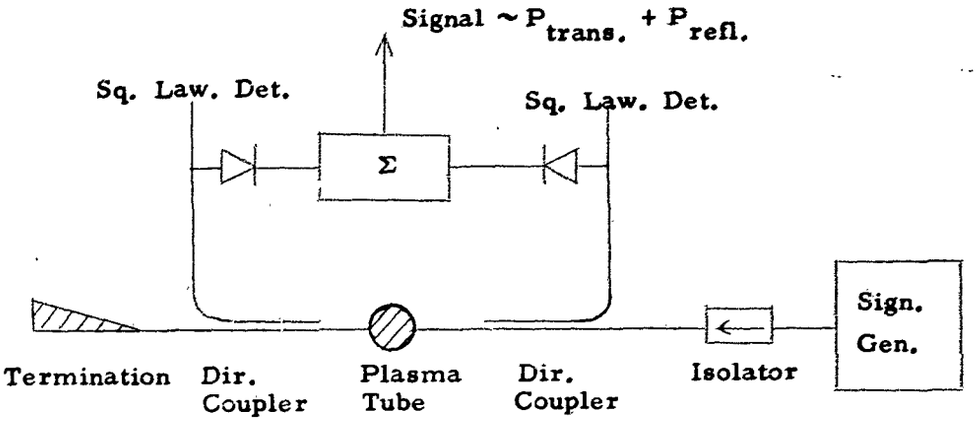
Signal ~ P trans. + P refl.
Sq. Law. Det.
Sq. Law. Det.
Σ
Sign. Gen.
Termination
Dir. Coupler
Plasma Tube
Dir. Coupler
Isolator

Fig. 2.

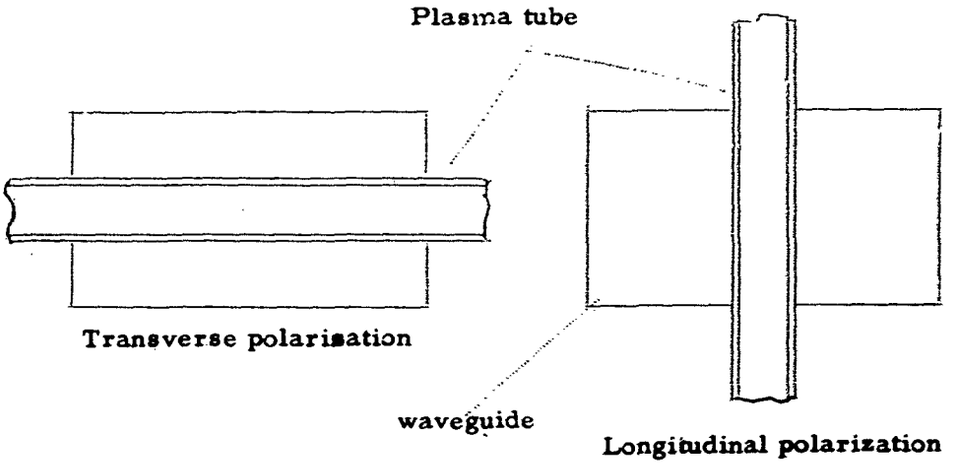
Plasma tube
Transverse polarisation
waveguide
Longitudinal polarization

Fig. 3.

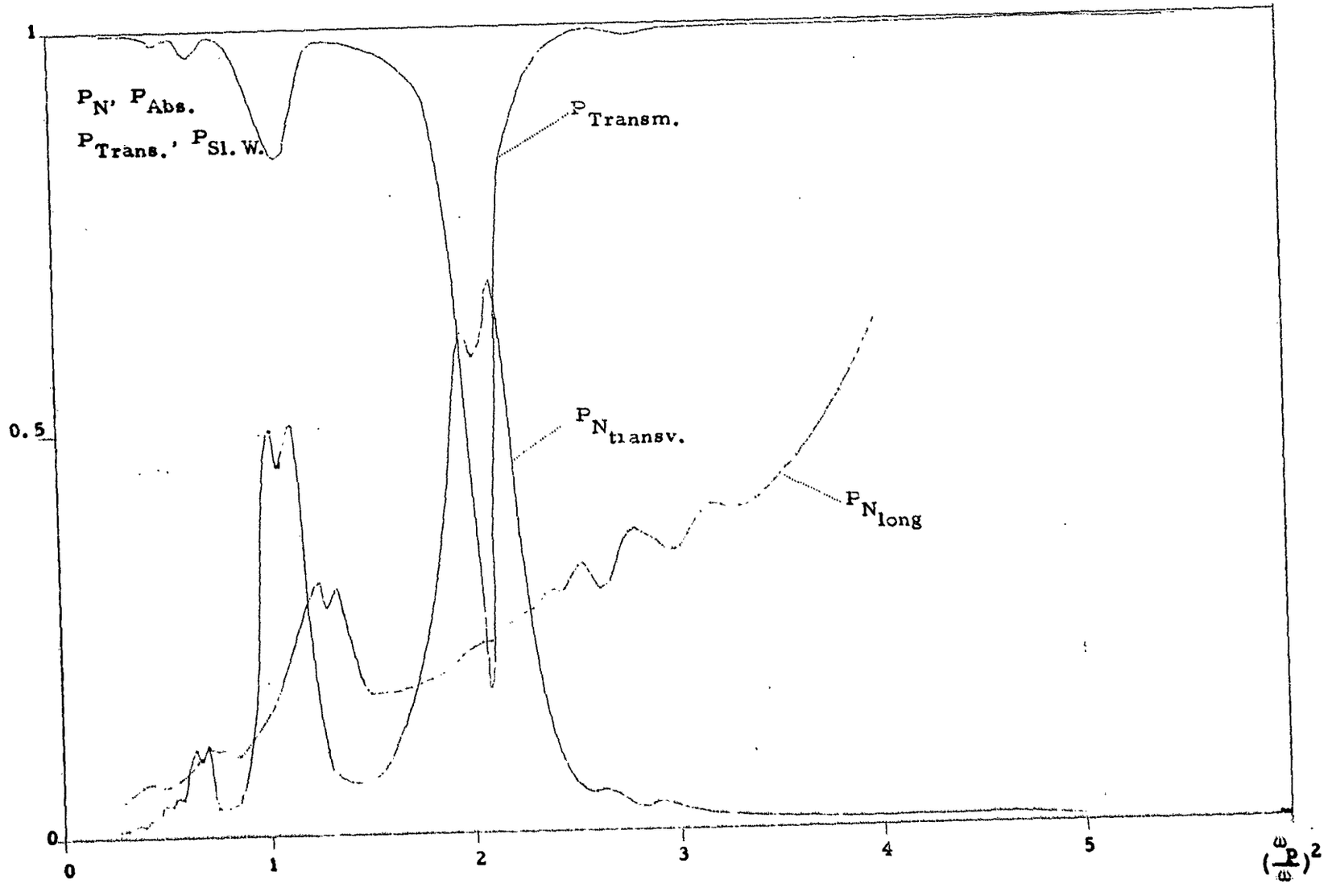
1
0.5
0
$P_{N'}$ $P_{Abs.}$
$P_{Trans.}$, $P_{Sl.W.}$
$P_{Transm.}$
$P_{N_{transv.}}$
$P_{N_{long}}$
0
1
2
3
4
5
$(\frac{p}{e})^2$

Fig. 4.

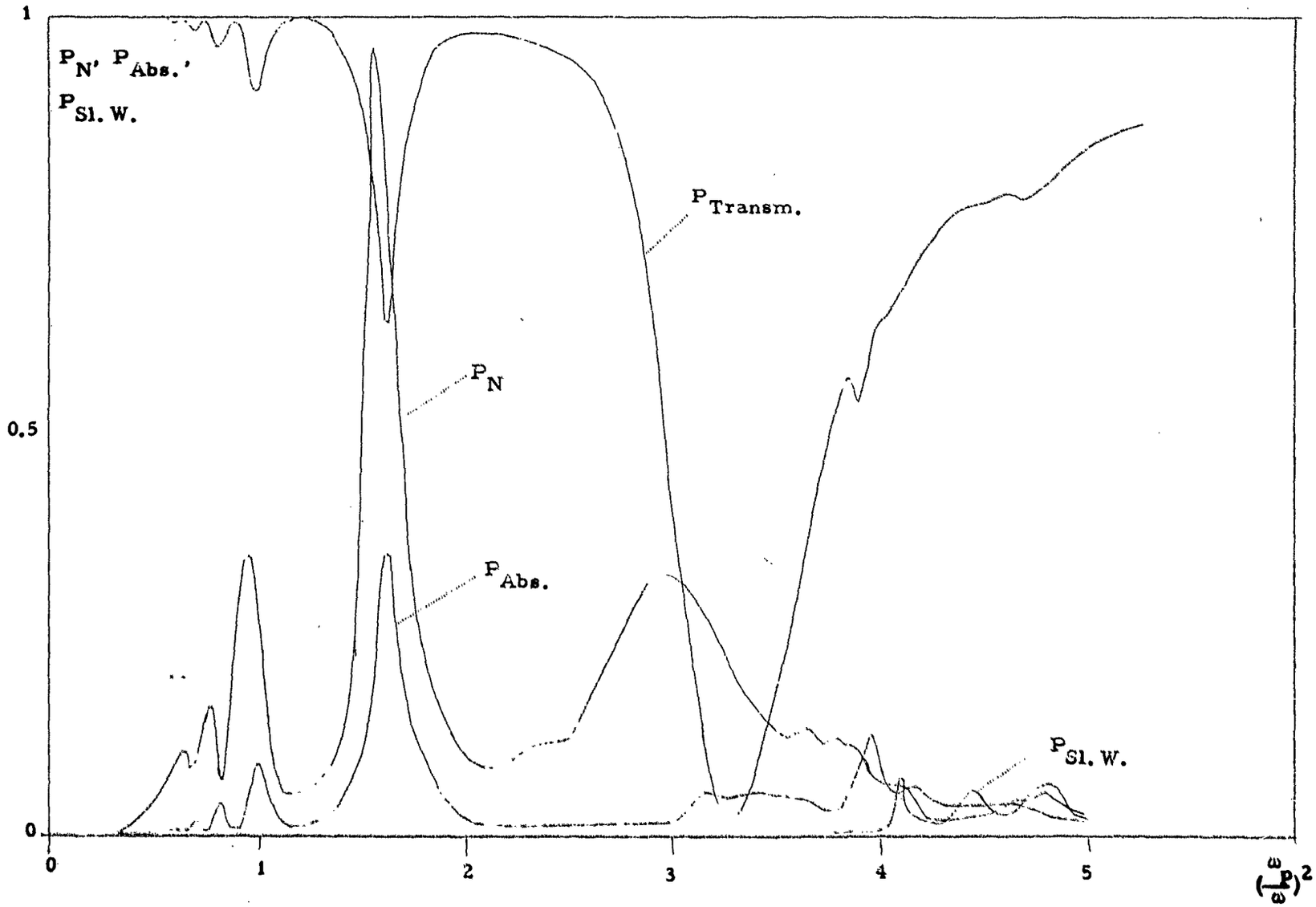
1
0.5
0
$P_{N'}$ $P_{Abs.}$ '
$P_{Sl.W.}$
$P_{Transm.}$
P_N
$P_{Abs.}$
$P_{Sl.W.}$
0
1
2
3
4
5
$(\frac{\omega}{\omega}P)^2$

Fig. 5.

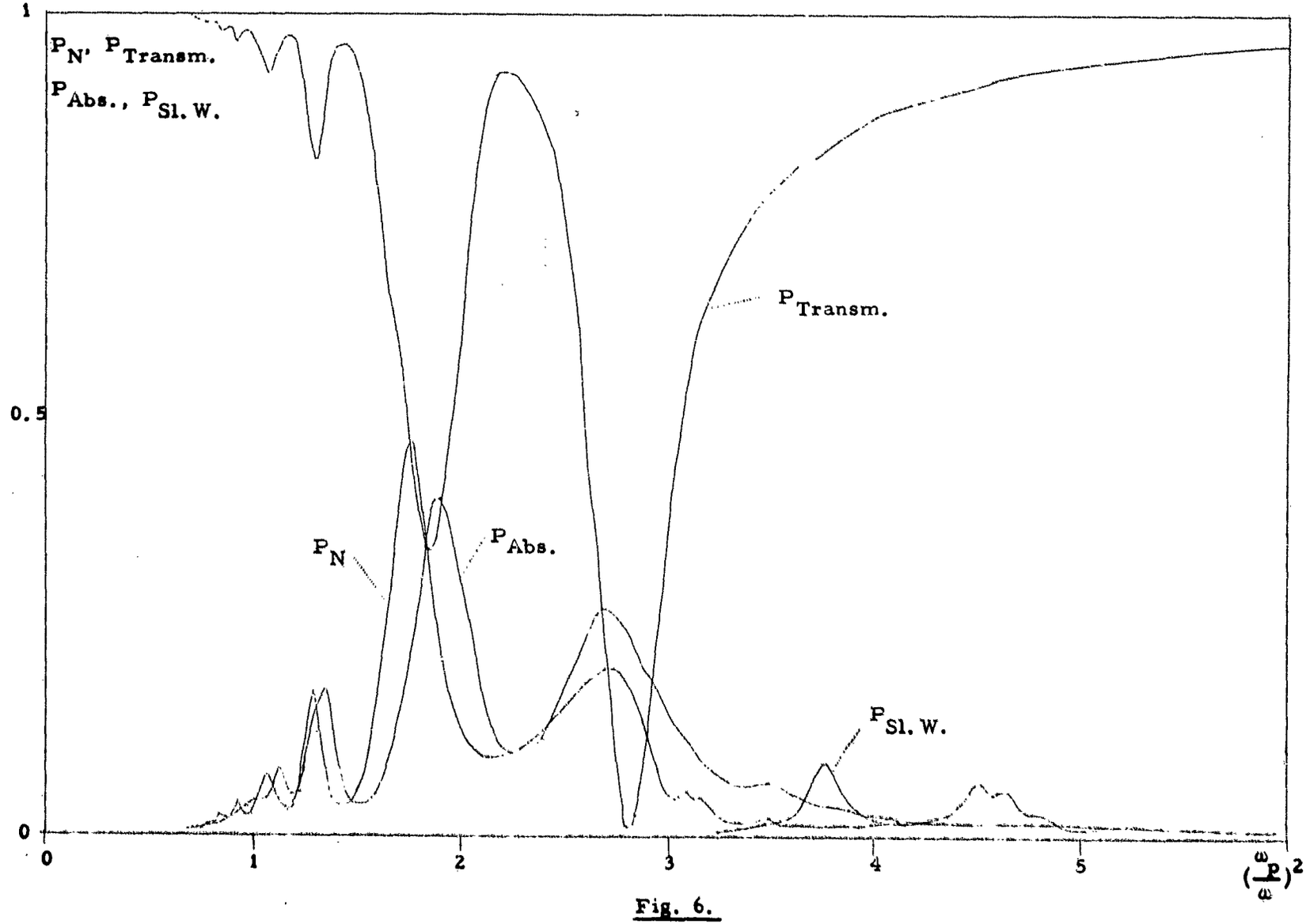
1
0.5
0
$P_{N'}$ $P_{Transm.}$
$P_{Abs.}$, $P_{Sl.W.}$
$P_{Transm.}$
P_N
$P_{Abs.}$
$P_{Sl.W.}$
0
1
2
3
4
5
$(\frac{\omega}{\omega_p})^2$

Fig. 6.

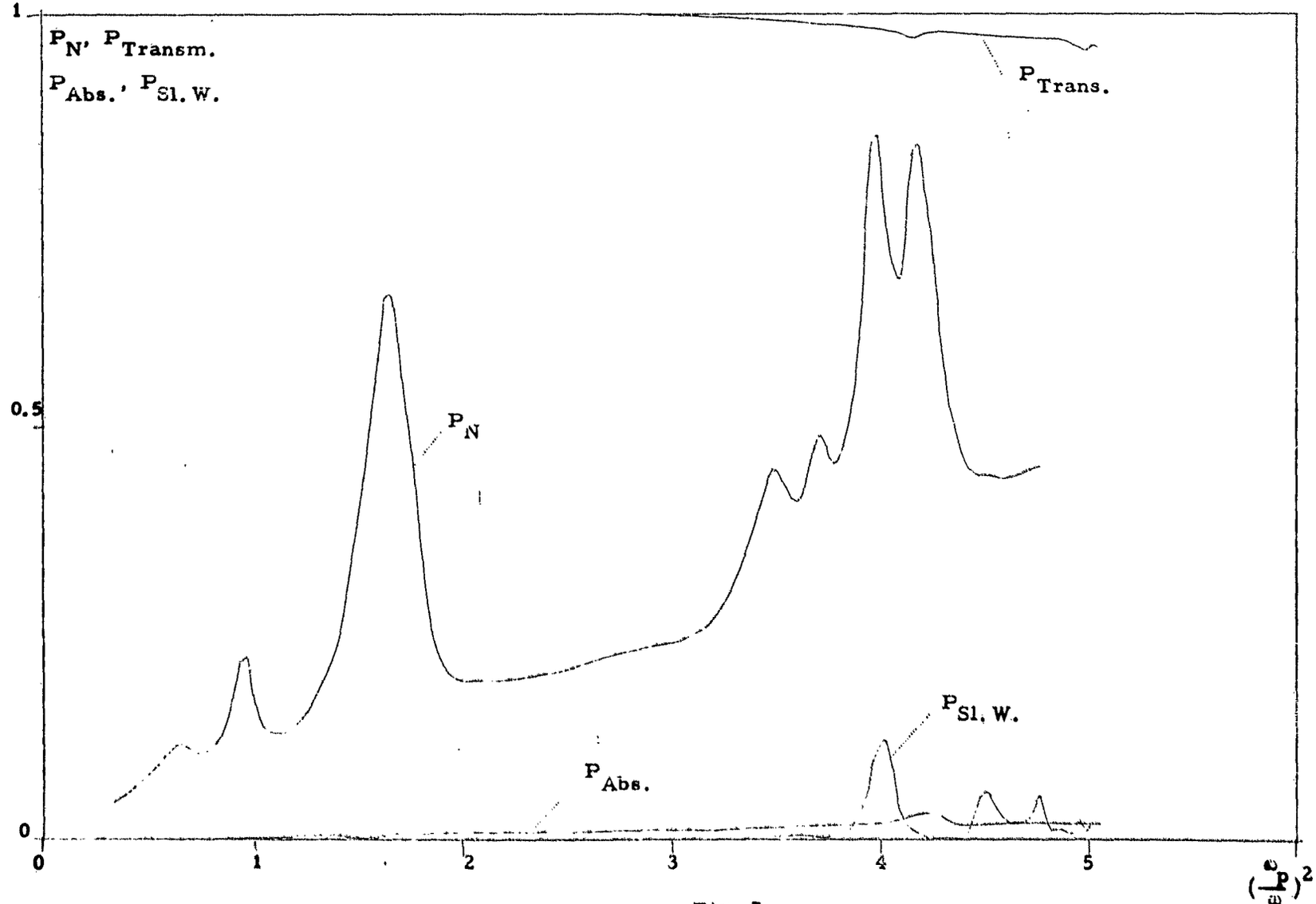
1
0.5
0
P_N, $P_{Transm.}$
$P_{Abs.}$, $P_{Sl.W.}$
$P_{Trans.}$
P_N
$P_{Sl.W.}$
$P_{Abs.}$
0
1
2
3
4
5
$(\frac{e}{\omega}P)^2$

Fig. 7.

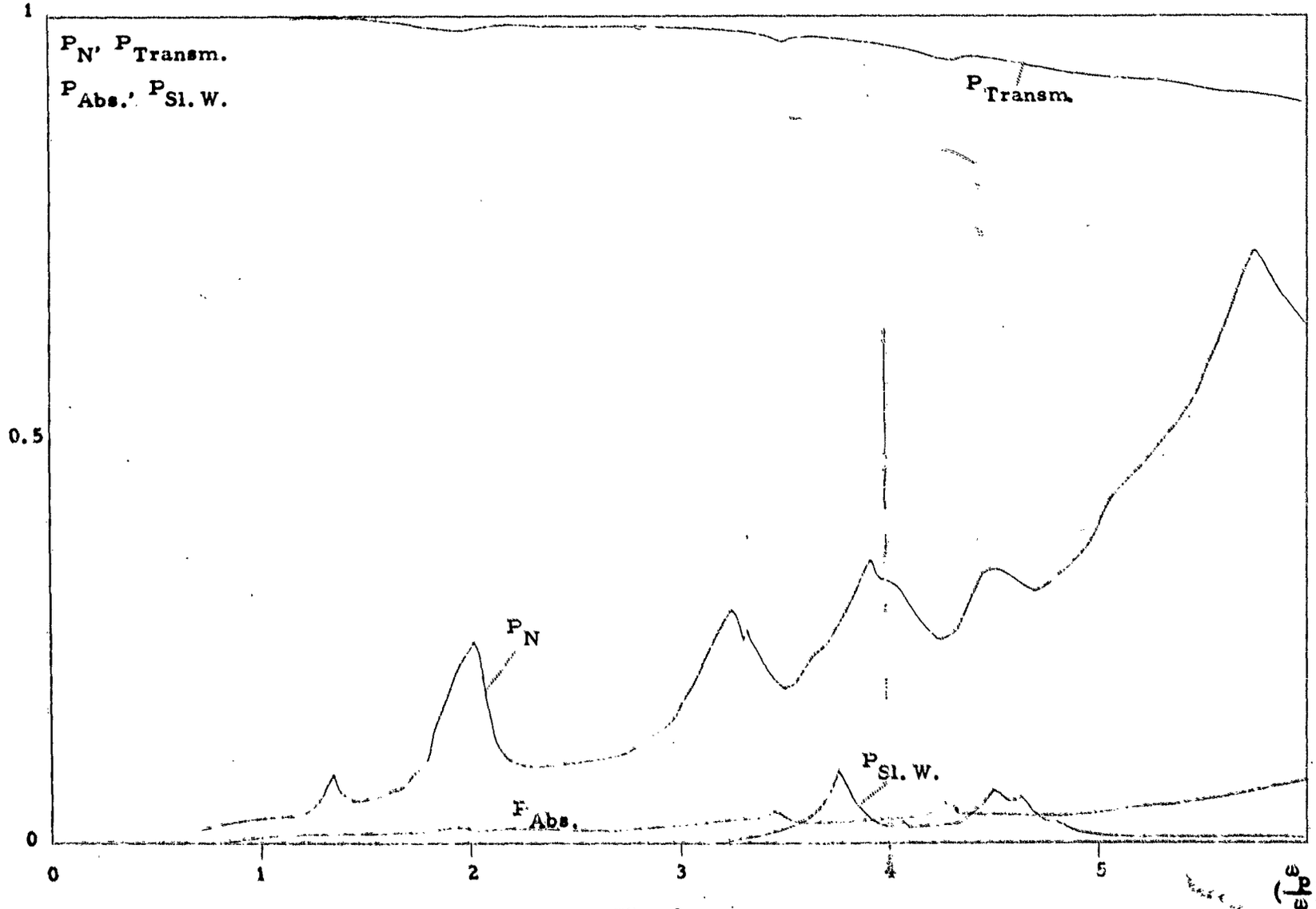
1
0.5
0
$P_{N'}$ $P_{Transm.}$
$P_{Abs.'}$ $P_{Sl.W.}$
$P_{Transm.}$
P_N
$P_{Sl.W.}$
$P_{Abs.}$
0
1
2
3
4
5
$(\frac{a}{\lambda}\frac{p}{\lambda})^2$

Fig. 8.

VIII MICROWAVE EMISSION FROM A CYLINDRICAL PLASMA

Introduction

The equipartition theorem ascribes an energy $\frac{kT}{2}$ to each degree of freedom in a medium in thermal equilibrium. In a gas of noninteracting particles the degrees of freedom are those associated with the individual particle motion. In contrast to this result Bohm and Pines[1] in one of their classic papers showed that in an electronic plasma some of the degrees of freedom are distributed in collective modes or plasma oscillations of a longitudinal character. As shown for instance by the present author[2] such longitudinal oscillations cannot exist in bounded plasma without coupling to external wave fields. In other words one would expect thermally excited collective modes to radiate. The basic assumption of the present work is that the radiation reaction has a small effect on the electronic motion and that the emitted power spectrum can be calculated assuming thermal equilibrium.

Experimental information on the emission spectrum has been published by Agdur et. al.[3] who measured the microwave noise radiation from a plasma cylinder as a function of frequency for polarization directions parallell and perpendicular to the axis. (Below we will refer to polarizations as TE and TM-modes respectively when the axial component of the electric or magnetic field is equal to zero.) Agdur et. al. measured a smooth spectrum for scattered TM waves and the wellknown resonance structure (see e.g. Dattner[4]) for scattered TE waves. TE-noise possessed an irregular spectrum with several small peaks whereas TM-noise was of much lower intensity and was not resolved into any particular structure. Later experiments by the same group which have given a more detailed information about these phenomenon have shown that both polarizations now appear to have spectra practically identical to that of scattered TE-radiation.

A first attempt to explain these results was made in[2]. As to the scattering spectrum the experimental results are now well explained[2, 6, 7]. The multiple resonances arise due to excitation of longitudinal waves perpendicular to the cylinder axis. The radially inhomogeneous density distribution of the electrons strongly modify the dispersion relation of these waves to give the observed spectrum. Assuming Rytov's[8] generalization of Kirchhoff's law to be valid, one should be able to use the same model, calculate the absorbtivity and predict the noise spectrum. This scheme was carried out in[2] for TE-waves emitted perpendicularly to the axis and lead to the same frequency spectrum as for scattered waves of the same kind. As the measurements give the total emitted TE Poynting flux which contains contributions from obliquely emitted TE-waves, we cannot immediately conclude that experimental and theoretical results agree. It seems likely, however, that the obliquely emitted TE-waves will be coupled to the longitudinal oscillations and have approximately the same frequency spectrum as the normally emitted ones. The purpose of the present paper is to show what may be less evident, that we will get obliquely emitted TM-waves with the same frequency spectrum thereby explaining the experimental results for this polarization direction. The basic idea is that thermal fluctuations will not only excite collective oscillations in phase along the column but also oscillations of arbitrary phase variation. In fact if the length of the cylinder is assumed to be infinite the result of Bohm and Pines is immediately applicable and we should have equally strong excitation for all axial wave numbers up to about one recipical Debye length after which the single particle degrees of freedom dominate. This argument suggests that fluctuating electric fields directed along the axis will be generated. The subsequent rather lengthy calculations will support this suggestion and show that a radiation field with nonzero electric vector along the axis is produced. Using Hughyens principle this result can easily be understood. If we pick out one single mode with axial wave number k_z of dipole character in the r-φ plane it is realized with reference to figure 1, that we will get a radiation field of waves propagating at an angle Θ to the normal of the cylinder axis.

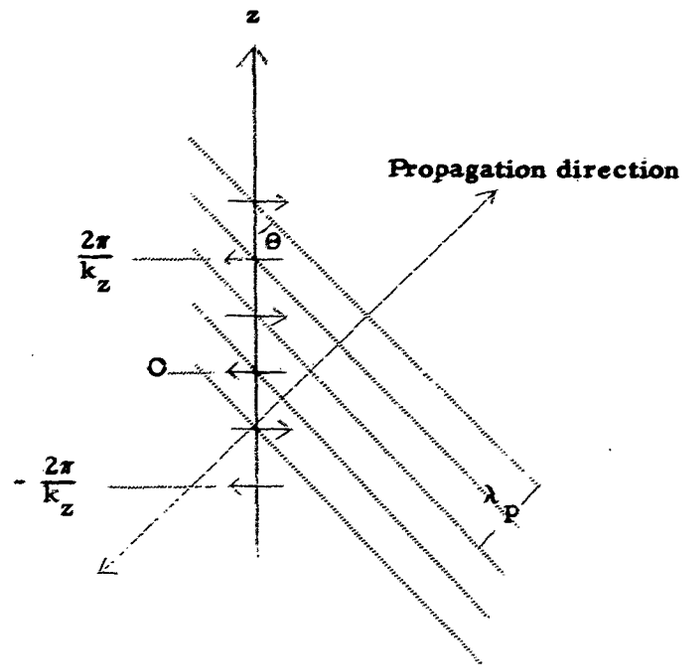

Fig. 1. Oblique emission from dipoles whose phase varies as $e^{iz \cdot k_z}$. $\cos\theta \approx \omega_p/c \cdot k_z = 2\pi/\lambda_p \cdot k_z$.

Description of the plasma

For our present purposes it is adequate to describe the plasma by means of hydrodynamic equations and to include the effect of the ions as a neutralizing background only. This model does not contain thermal fluctuations but is easy to handle when considering geometric complications.

As in[2] we will treat the scattering problem and then rely on Kirchhoff's law to give the fluctuation psectrum. After linearizing and assuming the plasma to be homogeneous and all perturbations to vary as $e^{-i\omega t}$ we get

1. $-i\omega N + N_0 \operatorname{div} \bar{v} = 0$
2. $-i\omega\bar{v} = -e\mathbf{E}/m - (w^2/N_0) \operatorname{grad} N$

In addition we have Maxwell's equations.

3. $\operatorname{curl} \mathbf{E} = i\omega\mathbf{B}$
4. $\operatorname{curl} \mathbf{H} = -N_0 e\bar{v} - i\omega\epsilon_0\mathbf{E}$

5. $\operatorname{div} \varepsilon_0 \mathbf{E} = -eN$

6. $\operatorname{div} \mathbf{B} = 0$

Eq. 1 is of course redundant but is convenient to keep explicitly. It was shown in[2] that Eq. 1 - 6 can be reduced to

7. $\nabla^2 \mathbf{B} + (\omega^2 \varepsilon / c^2) \mathbf{B} = 0$

and

8. $\nabla^2 N + (\omega^2 \varepsilon / w^2) N = 0$

with

9. $\varepsilon = 1 - \omega_p^2/\omega^2 = 1 - N_0 e^2/\varepsilon_0 m\omega^2$

and appropriate relations between $\mathbf{E}$, $\bar{v}$, $\mathbf{B}$ and N. In the present context we have found it more convenient to introduce the electromagnetic potentials $\mathbf{A}$ and Φ. As usual we put

10. $\mathbf{B} = \operatorname{curl} \mathbf{A}$

It turns out that by a suitable choice of gauge the resulting wave equations can be considerably simplified. The key to this simplification is that as seen from Eq. 4 the current $-N_0 e\bar{v}$ is composed of two parts, one due to electron motion caused by the average field and one caused by thermal motion and density gradients. The first part of this current is easy to include in a frequency dependent permittivity, the second is irrotational and can be removed from the source term by a suitable gauge transformation. Thus if we put

11. $\Phi = -(w^2 e/\omega^2 \varepsilon \varepsilon_0) N$

it is easy to show that the resulting wave equations are

12. $\nabla^2 \mathbf{A} + (\omega^2 \varepsilon / c^2)\ \mathbf{A} = 0$

13. $\nabla^2 \Phi + (\omega^2 \varepsilon / w^2)\ \Phi = 0$

14. $\operatorname{div} \mathbf{A} = 0$

15. $\mathbf{E} = -i\omega \mathbf{A} - \nabla \Phi$

The transversality condition 14 shows that eq. 12 represents transverse waves which in the absence of boundaries are uncoupled to the longitudinal waves represented by Eq. 13. Boundary conditions are as usual continuity of the tangential components of the $\mathbf{E}$ and $\mathbf{B}$ fields. In addition because of the presence of a longitudinal component we need a boundary condition on Φ. This is obtained from the requirement that the normal component of the particle current must vanish at the boundary. Expressing this current in terms of the potentials we get

16. $\bar{J} = -\varepsilon_0 (\omega_p^2 \mathbf{A} + i\omega \nabla \Phi)$

Oblique scattering of TM-waves

For oblique incidence of a TM wave we will get excitation of both TM and TE components. In order to derive suitable expressions for the TE waves we introduce the superpotential $\bar{\mu}$ defined by

17. $$\mathrm{I}\bar{A}^{TE} = \mathrm{curl}\ \bar{\mu}^{TE}$$

In addition to Eq:s 12 - 15, describing the fields in the plasma, we have the usual free space wave equation outside the cylinder. Decomposing the solutions into TM and TE components and choosing boundary conditions at infinity corresponding to an incoming plane wave and an outgoing scattered wave, we get in vacuum:

18.
$$\begin{cases} A_r^{TM} = \dfrac{ik_z}{a} \sum_n [J_n'(ar) + a_n H_n'(ar)]\, e^{i(n\varphi + k_z z)} \\ A^{TM} = -\dfrac{k_z}{a^2 r} \sum_n n\, [J_n(ar) + a_n H_n(ar)]\, e^{i(n\varphi + k_z z)} \\ A_z^{TM} = \sum_n [J_n(ar) + a_n H_n(ar)]\, e^{i(n\varphi + k_z z)} \end{cases}$$

19.
$$\begin{cases} \mu_r^{TE} = \dfrac{ik_z a}{} \sum_n b_n H_n'(ar)\, e^{i(n\varphi + k_z z)} \\ \mu^{TM} = -\dfrac{k_z a}{a^2 r} \sum_n n\, b_n H_n'(ar)\, e^{i(n\varphi + k_z z)} \\ \mu_z^{TM} = a \sum_n b_n H_n(ar)\, e^{i(n\varphi + k_z z)} \end{cases}$$

a denotes the cylinder radius and we have also introduced the abbreviations

20. $$a = \frac{\omega}{c}\cos\theta, \qquad k_z = \frac{\omega}{c}\sin\theta$$

and dropped the superscript $^{(1)}$ on the Hankel functions. a_n and b_n are arbitrary constants to be determined by the boundary conditions. Prime denotes derivative with respect to argument. To get the transverse fields in the plasma we use the same expression with the modification that new constants (d_n and f_n) are introduced, the Hankel functions are replaced by Bessel functions regular at the origin, the incoming wave term is omitted and a in the argument is replaced by a' defined by

21. $$a'^2 = \frac{\omega^2}{c^2}(\varepsilon - \sin^2\theta)$$

We also get for the scalar potential

22. $$\phi = \Sigma\, g_n\, J_n(\beta r)\, e^{i(n\varphi + k_z z)}$$

with

23. $$\beta^2 = \frac{\omega^2}{w^2}\left(\varepsilon - \frac{w^2}{c^2}\sin^2\theta\right)$$

Applying boundary conditions at $r = a$ we get the following set of equations for the determination of the constants a_n, b_n, d_n, f_n and g_n.

24.
$$\begin{cases}
-\frac{k_z n}{a^2}\left[J_n(\alpha a) + a_n H_n(\alpha a)\right] - \frac{\omega^2 a}{ac^2} b_n H_n'(\alpha a) = -\frac{k_z n}{\alpha' a} J_n(\alpha' a) d_n - \\
\quad - \frac{\omega^2 a \varepsilon}{\alpha' c^2} J_n'(\alpha' a) f_n - n J_n(\beta a) g_n \\
J_n(\alpha a) + a_n H_n(\alpha a) = J_n(\alpha' a) d_n - a k_z J_n(\beta a) g_n \\
-\frac{k_z n}{a^2} H_n(\alpha a) b_n - \frac{1}{a}\left[J_n'(\alpha a) + a_n H_n'(\alpha a)\right] = -\frac{\varepsilon}{\alpha'} J_n'(\alpha' a) d_n - \\
\quad - \frac{k_z}{\alpha'^2}\varepsilon n J_n(\alpha' a) f_n \\
\frac{\omega_p^2 k_z}{\alpha'} J_n'(\alpha' a) d_n + \frac{\omega_p^2 \omega^2 \varepsilon_n}{c^2 \alpha'^2} J_n(\alpha' a) f_n + \omega^2 \beta a g_n J_n'(\beta a) = 0 \\
b_n H_n(\alpha a) = \varepsilon f_n J_n(\alpha' a)
\end{cases}$$

Solving for b_n, the amplitude of the scattered TE-waves, we get

25. $$b_n = \frac{J_n(\alpha a)\, Q_n}{(k_z a) H_n(\alpha a)\left[P_n + \frac{\varepsilon}{1-\varepsilon} \cdot \frac{S_n T_n}{R_n} \cdot \frac{a^2}{k_z^2}\right]}$$

where

26. $$Q_n = \left[\frac{H_n'(\alpha a)}{H_n(\alpha a)} - \frac{J_n'(\alpha a)}{J_n(\alpha a)}\right]\frac{\alpha a}{n}$$

27. $$P_n = 1 - \frac{(\alpha a)^2}{n^2}\frac{H_n'(\alpha a)^2}{H_n(\alpha a)^2} - \frac{a^2}{\alpha'^2}\left[1 - \frac{\alpha \alpha' a^2}{n^2} \cdot \frac{J_n'(\alpha' a) H_n'(\alpha a)}{H_n(\alpha a) J_n(\alpha' a)}\right]$$

28. $$S_n = -\frac{\beta a J_n'(\beta a)}{n J_n(\beta a)}\left[\frac{J_n'(\alpha' a)}{J_n(\alpha' a)}\frac{\alpha' a}{n}\frac{a^2}{\alpha'^2} - \frac{\alpha a}{n}\frac{H_n'(\alpha a)}{H_n(\alpha a)}\right] + \frac{\omega_p^2 a^2}{c^2}\frac{1}{(\alpha' a)^2}$$

29. $$T_n = \frac{\alpha' a}{n} \frac{J_n'(\alpha' a)}{J_n(\alpha' a)} - \frac{\alpha a}{n} \frac{H_n'(\alpha a)}{H_n(\alpha a)}$$

30. $$R_n = \frac{\alpha' a}{n} \frac{J_n'(\alpha' a)}{J_n(\alpha' a)} - \frac{\beta a J_n'(\beta a)}{n J_n(\beta a)}$$

To find possible resonance conditions we now study the expression 25 in the limit $\omega a/c \ll 1$ i.e. when the vacuum wavelength becomes much larger than the plasma radius. From the Taylor expansions of the Bessel functions involved it is easily seen that unless the real part of the bracket in the denomination of 25 vanishes, b_n is of the order $(\omega a/c)^{2n}$. (We disregard the factor $(k_z a)^{-1}$ which originates from the fact that ab_n is the amplitude of $\bar{\mu}$ whereas the amplitude of IA in the incoming wave is put equal to unity) If, however,

31. $$\frac{nJ_n(\beta a)}{\beta a J_n'(\beta a)} = \frac{2\omega^2}{\omega_p^2} - 1$$

the real part of the bracket vanishes and b_n becomes of the order of unity. We observe that in the limit $\frac{\omega a}{c} \ll 1$ no dependence on the angle of incidence appears in equation 31. The resonance condition 31 coincides with the resonance condition obtained in[2] for perpendicularly incident TE-waves. This should not be surprising as the resonances are caused by longitudinal waves perpendicular to the cylinder axis. These waves are coupled to transverse fields only by a radial density discontinuity at the boundary. Keeping this physical picture in mind, one would not expect a phase difference along the cylinder axis to alter the resonance conditions. This lack of dependence on the angle of incidence is important to remember when discussing experimental results. As we will outline below the noise frequency spectrum will have peaks when 31 is satisfied. If there were a strong angular dependence, this would show up as a broadening of the peaks in the measured spectrum which is the $\cos\theta$-weighted sum of all waves emitted with a component of the electric vector along the cylinder axis. In the experiments of Kerzar there is no evidence of any additional broading in the noise spectra as compared to the scattering spectrum for normally incident TE-waves.

It should also be noted that for normally incident TM-waves the factor α^2/k_z^2 in the denominator of Eq. 25 will make b_n equal to zero even at frequencies when 31 is satisfied. For completeness we give the scattered TM amplitude for normal incidence

$$32. \quad a_n = \frac{J_n(\alpha a)}{H_n(\alpha a)} \cdot \frac{\left[\frac{\alpha a}{n}\frac{J_n'(\alpha a)}{J_n(\alpha a)} - \frac{\alpha' a}{n}\frac{J_n'(\alpha' a)}{J_n(\alpha' a)}\right]}{\left[\frac{\alpha' a}{n}\frac{J_n'(\alpha' a)}{J_n(\alpha' a)} - \frac{\alpha a}{n}\frac{H_n'(\alpha a)}{H_n(\alpha a)}\right]}$$

which is seen to possess no resonances and tend rapidly to zero with $\omega a/c$.

Noise spectrum

Assuming Rytov's result to apply*) we should now be able to calculate the spontaneously emitted energy per unit surface as frequency ω as

$$33. \quad P_\omega = \frac{kT}{2\pi\lambda^2} A\omega$$

with

$$34. \quad A_\omega = \frac{\int \mathrm{Re}\, \bar{j} \cdot \mathbf{E}^* \, dv}{\int \mathrm{Re}\, (\mathbf{E}_i \times \mathbf{H}_i) \cdot d\bar{S}}$$

where index i stands for incident radiation.

Now it was shown in[2] that for the present model we have

$$35. \quad A_\omega = \int \mathrm{Re}\, \bar{j} \cdot \mathbf{E}^* \, dv = \int \frac{|j|^2}{\sigma} \, dv$$

with

$$36. \quad \sigma = \frac{N_0 e^2}{m\nu_c}$$

---

*) This is an assumption to be verified by the results as Kirchhoff's law is derived either in the approximation of geometrical optics or by Rytov in media where the relation between $\mathbf{E}$ and $\mathbf{D}$ is local and linear. Our model is equivalent to a nonlocal linear relation.

The collision frequency, ν_c, is defined as the recipical momentum relaxation time. A term accounting for this dissipation must now be added to equation 2. Inserting 16 in 35 and using same simple vector identities we get

$$37. \quad A_\omega = \frac{\varepsilon_0^2 \omega_p^4}{\sigma} \int |IA|^2 \, dv + \frac{\omega^4 \varepsilon \varepsilon_0^2}{w^2} \int |\phi|^2 \, dv +$$

$$+ \frac{\omega^2 \varepsilon_0}{\sigma} \int \phi^* \nabla \phi \cdot d\bar{S} + \frac{i\varepsilon_0^2 \omega_p^2 \omega}{\sigma} \int (IA^* \phi - IA\phi^*) \, d\bar{S}$$

As was done in[2] we now assume that IA and ϕ can be obtained neglecting ν_c. It is then a straight forward, but tedious, procedure to insert IA and ϕ from 17, 18 and 22, carry out all integrations which turn out to be elementary and insert constants of integration from 24. We omit these calculations here and quote the main result only. The absorbtivity A_ω possesses sharp maxima at frequencies given by 31, if $\omega a/c \ll 1$. Consequently we have shown that in thermal equilibrium the noise radiation with the E-vector parallell to the cylinder axes should possess the same frequency spectrum as for instance scattered TE-waves. There also seems to be good reason to believe that the noise spectrum, as has been shown for the scattering spectrum, should be strongly modified by the non-homogeneous radial density distr. and then agree well with experimental results. The measured noise spectra therefore appears to give good evidence for the result of Bohm and Pines that part of the kinetic energy in a plasma is distributed over the collective degrees of freedom.

References

(1) Pines, D., Bohm, D., Phys. Rev. 85, 338 (1952).

(2) Weissglas, P., J. Nucl. En. Pt. C. In press.

(3) Agdur, B., Kerzar, B., Sellberg, F. Phys. Rev. 128.1(1963)

(4) Dattner, A. Ericsson Technics 1.1.(1963).

(5) Kerzar, B. Private communication.

(6) Nickel, J.C., Parker, J.V., Gould, R.W. Phys. Rev. Letters 11.183 (1963).

(7) Crawford, F.W. M.L. Report No. 1045. Stanford Univ.

(8) Rytov, S.M. Theory of Electrical Fluctuations and Thermal Radiation. Academy of Sciences Press, Moscow.

ROYAL INST. OF TECHN.
STOCKHOLM, SWEDEN
MICROWAVE DEPT.
31 Jan. 1964

AF 61(052) 552
TR-2
MICROWAVE
ELECTRONICS

INTERACTION BETWEEN MICROWAVES AND PLASMAS IN GASDISCHARGES AND SEMICONDUCTORS

B. Agdur

ABSTRACT: Theoretical and experimental investigations of 1) microwave propagation in gas discharge and semiconductor plasmas; 2) noise radiation from a low-pressure plasma; 3) variations of plasma properties along the positive column of a low-pressure Hg discharge.

ROYAL INST. OF TECHN.
STOCKHOLM, SWEDEN
MICROWAVE DEPT.
31 Jan. 1964

AF 61(052) 552
TR-2
MICROWAVE
ELECTRONICS

INTERACTION BETWEEN MICROWAVES AND PLASMAS IN GASDISCHARGES AND SEMICONDUCTORS

B. Agdur

ABSTRACT: Theoretical and experimental investigations of 1) microwave propagation in gas discharge and semiconductor plasmas; 2) noise radiation from a low-pressure plasma; 3) variations of plasma properties along the positive column of a low-pressure Hg discharge.

ROYAL INST. OF TECHN.
STOCKHOLM, SWEDEN
MICROWAVE DEPT.
31 Jan. 1964

AF 61(052) 552
TR-2
MICROWAVE
ELECTRONICS

INTERACTION BETWEEN MICROWAVES AND PLASMAS IN GASDISCHARGES AND SEMICONDUCTORS

B. Agdur

ABSTRACT: Theoretical and experimental investigations of 1) microwave propagation in gas discharge and semiconductor plasmas; 2) noise radiation from a low-pressure plasma; 3) variations of plasma properties along the positive column of a low-pressure Hg discharge.

ROYAL INST. OF TECHN.
STOCKHOLM, SWEDEN
MICROWAVE DEPT.
31 Jan. 1964

AF 61(052) 552
TR-2
MICROWAVE
ELECTRONICS

INTERACTION BETWEEN MICROWAVES AND PLASMAS IN GASDISCHARGES AND SEMICONDUCTORS

B. Agdur

ABSTRACT: Theoretical and experimental investigations of 1) microwave propagation in gas discharge and semiconductor plasmas; 2) noise radiation from a low-pressure plasma; 3) variations of plasma properties along the positive column of a low-pressure Hg discharge.